Synthesis and Characterisation of Biomimetic Immunostimulatory Lipid-Polymer Hybrid Nanoparticles

UNIVERSITY *of the*
WESTERN CAPE

Aime Fabius Irabin

A thesis submitted in partial fulfilment of the requirements for the degree of Magister Scientiae (Pharmaceutical Sciences) in the School of Pharmacy at the University of the Western Cape, Bellville, South Africa.

Supervisor: Prof. Admire Dube

October 2022

Table of contents

Keywords

Lipid-polymer hybrid nanoparticles; immunotherapy; biomimetic nanoparticles; tuberculosis; nanomedicine; immunostimulation; immunostimulatory biomimetic lipid polymer hybrid nanoparticles; mycolic acid; curdlan; macrophage.

Abstract

Purpose: Tuberculosis (TB), caused by *Mycobacterium tuberculosis (M. tuberculosis)*, remains a fatal infectious disease and one of the top ten leading causes of mortality, particularly in developing countries. Current drug therapy for TB is challenged by the poor physiochemical properties of the antibiotics used. These properties impact their bioavailability, toxicity, and treatment duration, thereby negatively impacting patient adherence. These factors also contribute to the emergence of the difficult to treat multi-drug resistant strains of *M. tuberculosis*. Recently, immunotherapy has emerged as a promising alternative treatment modality for TB. The primary host cells (macrophages) of *M. tuberculosis* could be activated to eradicate the intracellular resident bacterium. This could be enhanced by incorporating a biomimetic feature that mimics structural and/or functional aspects of the pathogen. In this study, nanoparticles (NPs) incorporating lipids and polymers were synthesized, i.e. lipid-polymer hybrid nanoparticles (LPHNPs), incorporating two immunomodulatory agents, namely mycolic acid (MA) from *M. tuberculosis* and curdlan from *Alcaligenes faecalis*. NPs were characterized and investigated for their capability to activate macrophages *in vitro*. This work lays the foundation for further studies into developing an immunostimulatory nanomedicine for the treatment of TB.

Methods: A polycaprolactone-curdlan copolymer (PCL-curdlan) was synthesized using carbodiimide chemical conjugation and characterized physiochemically by nuclear magnetic resonance (NMR), Fourier transform infrared spectroscopy (FTIR), thermogravimetric analysis (TGA), and hot stage microscopy (HSM) to confirm the conjugation. A panel of NPs (with varying curdlan from PCL-curdlan copolymer and MA) were then synthesized using a nanoprecipitation method. The LPHNPs were characterized physiochemically for size, polydispersity index, and zeta potential. Scanning electron microscopy (SEM) and transmission electron microscope (TEM) were used to characterize their morphology. The cytotoxicity of the NPs was assessed in RAW 264.7 macrophages using an MTT assay. The immunostimulatory effect of the NPs was determined in RAW 264.7 macrophages by quantifying TNF-α and IL-10 using an enzyme-linked immunosorbent assay (ELISA).

Results: Physiochemical characterizations indicated successful syntheses of the PCL-curdlan copolymer and the NPs. NPs synthesized from various ratios of lecithin/PCL ranged from 120 - 170 nm. 15 % w/w lecithin/PCL mass ratio was selected as the best ratio and used to synthesize NPs with various MA (0 – 8 % w/w) and curdlan (0 – 10 % w/w) densities.

Toxicity assays over 72 h indicated that 250 µg/mL of lecithin/PCL NPs (with a 94 ± 15.2 % viability), 50 µg/mL of 2 % w/w curdlan (84 ± 4.7 %) and 2 % w/w MA (85.8 ± 1.4 %) loaded NPs, and 25 µg/mL of 2 % w/w MA and 2 % w/w curdlan loaded NPs (100.1 ± 3.2 %) were the highest safe concentrations. ELISA assays indicated that the MA-curdlan loaded NPs stimulated the production of the highest levels of TNF-α (51.16 ± 6.60 pg/mL) which was statistically significant from the rest of NPs (lecithin/PCL produced 22.56 ± 1.65 pg/mL, lecithin/PCL-MA produced 25.76 ± 24.61 pg/mL, lecithin/PCL-curdlan did not stimulate TNF-α production. The positive control (Lipopolysaccharide) produced 68.10 ± 8.97 pg/mL, while the negative control (untreated cells) produced 17.00 ± 6.27 pg/mL), suggesting a synergistic effect when both MA and curdlan were loaded onto the LPHNPs. None of the NPs stimulated the production of IL-10.

Conclusion: A panel of biomimetic NPs having varying amounts of curdlan and MA were synthesized and characterized. The MA-curdlan loaded NPs exhibited an additive cellular toxicity when both MA and curdlan were loaded onto the LPHNPs. On the other hand, immunomodulatory studies indicated a synergistic effect on TNF-α production. This study demonstrates the possibility to synthesize biomimetic, immunostimulatory NPs of MA-curdlan. These NPs can be investigated for eradication of *M. tuberculosis* in future studies.

Declaration

I declare that *'**Synthesis and Characterisation of Biomimetic Immunostimulatory Lipid-Polymer Hybrid Nanoparticles**'* is my own work, that it has not been submitted for any degree or examination in any other university, and that all the sources I have used or quoted have been indicated and acknowledged by complete references.

Signed: 

Date: October 2022.

Dedication

To my family particularly my angelic mother in heaven who constantly watches out for me and the most-high God.

Acknowledgements

First and foremost, I would like to express my eternal gratitude to my supervisor, Professor Admire Dube, for giving me the opportunity, for his patience and continuous support (emotional, financial, academic, and encouragements) throughout this degree, I wouldn't have done it without you.

I would like to give a special appreciation to Dr. Sarah for her continued support throughout the degree. For introducing me to the lab, for her much-appreciated help with the synthesis of PCL-curdlan conjugation and for being a constant supply of help, academic support, and ensuring that the lab ran smoothly and everything we needed was there on time.

I would also like to thank all my brothers and sisters Infectious Disease Nanomedicine group. They welcomed, took under their wings, and made it all feel like family. With them we struggled, grinded, navigated through it and we overcame it all together.

I would also like to sincerely acknowledge the following:

- ✓ Mr. Yunus Kippie (UWC) for training and assistance with analytical techniques
- ✓ Mohamed Jaffer and Miranda Waldron (UCT) for assistance with TEM and SEM
- ✓ Prof. Edith Beukes (UWC) for assistance with NMR
- ✓ Ephraim Maphasa and Ooladipupo Moyinoluwa David (UWC) for training and assistance with tissue culture.

I would also like to acknowledge grant from NIAID (5R01AI152109) awarded to Prof. Admire Dube.

I can't forget to express my deepest gratitude to Dr. Jordan B. Peterson, Dr. Thomas Sowell, David Goggins, Dr. Myles Monroe, Ben Shapiro, Jim Rohn and the dry bar comedy and various comedians and YouTubers for being an ever-present great company in the lab and providing endless inspiration and growth.

Finally, I would like to extend my greatest appreciation and gratitude to my Family and friends. Your love, support and encouragement are what got me through it. I am eternally gratefully for your support. Special appreciation goes to my uncle Michael Bintu, Donath Musabyimana and my immediate family, especially my father.

Abbreviations

AG	Arabinogalactan
AIDS	Acquired immunodeficiency syndrome
APCs	presenting cells
ATP	Adenosine triphosphate
BBB	Blood-brain barrier
CFU	Colony forming unit
COVID	Coronavirus disease
CR	Complement receptor
CS	Chitosan
$dCDCl_3$	Deuterated chloroform
DCM	Dichloromethane
DCs	Dendritic cells
DESE	double emulsification solvent evaporation
DIEA	N,N-diisopropylethylamine
DLS	Dynamic light scattering
DMEM	Dulbecco's modified Eagle's medium
DMF	Dimethylformamide
DMSO	Dimethyl sulfoxide
DSC	Differential scanning calorimetry
EDC.HCL	1-Ethyl-3(3-dimethylaminopropyl) carbodiimide hydrochloride
EDS	Energy disperse spectroscopy
ELISA	Enzyme-linked immunoassay
ER	Endoplasmic reticulum

ESE	Emulsification-solvent evaporation
FBS	Foetal bovine serum
FDA	Food and Drug Administration
FTIR	Fourier Transform Infrared Spectroscopy
GTP	Guanosine triphosphate
HCA	Hydroxycaproic acid
HIV	Human immunodeficiency virus
HR	High resolution
HSM	Hot stage microscopy
IFN	Interferon
IL	Interleukin
LAM	Lipoarabinomannan
LM	Lipomannan
LPHNPs	Lipid-polymer hybrid nanoparticles
LPS	Lipopolysaccharide
MA	Mycolic acid
MDR	Multi-drug resistant
MRSA	Methicillin-resistant staphylococcus aureus
MTT	3-(4,5-dimethylthiazol-2-yl)-2,5-diphenyltetrazolium bromide) tetrazolium
NHS	N-hydroxysuccinimide
NIH	National institutes for Health
NMR	Nuclear magnetic resonance
NOS	Nitrogen oxide synthase

NP	Nanoparticle
OLM	Olmesartan medoxomil
PAMP	Pathogen associated molecular patterns
PBS	Phosphate-Buffered saline
PCL	Polycaprolactone
PDI	Polydispersity index
PEG	Polyethylene glycol
PLGA	Poly(lactic-co-glycolic acid
PRR	Pattern recognition receptors
RBC	Red blood cell
RILP	Rab7 interacting lysosomal protein
RNS	Reactive nitrogen species
ROS	Reactive oxygen species
SD	Standard deviation
SEM	Scanning electron microscopy
SLNs	Solid lipid nanoparticles
SPK	Sphingosine kinase
TACO	Tryptophan aspartate-containing coat
TB	Tuberculosis
TDM	Trehalose dimycolate
TEM	Transmission electron microscopy
TGA	Thermogravimetric analysis
THF	Tetrahydrofuran
TLR	Toll-like receptors

TMM	Trehalose monomycolate
TNF	Tumor necrosis factor
TNFR	Tumor necrosis factor receptor
UK	United Kingdom
USA	United States of America
UV	Ultraviolet light
WHO	World health organization
XDR	Extensive drug-resistant

List of figures

List of tables

CHAPTER 1: Introduction

Tuberculosis (TB) is one of the world's deadliest infectious diseases. In 2020, TB claimed approximately 1.5 million lives, including 214 000 deaths among human immunodeficiency virus (HIV) positive people (1). South Africa is one of eight countries whose TB infections account for two-thirds of all TB infections worldwide. In 2020 there were 301 000 new infections, of which 177 000 were co-infected with HIV (1). Advances made in reducing the global TB burden in recent years has been significantly impacted by the coronavirus disease-19 (COVID-19) pandemic, affecting diagnosis, access to treatment and consequently increase the TB mortality (1). The primary causative agent of TB in humans is *Mycobacterium tuberculosis* (*M. tuberculosis*) (2). There are two types of TB, namely pulmonary (TB affects the lungs) and extrapulmonary TB (TB affects organs other than the lungs such as bones and meninges), with pulmonary TB being the most prevalent type of TB (3)(4).

TB is an airborne disease transmitted by inhaling droplets containing *M. tuberculosis* (5). About a quarter of the world's population is infected with *M. tuberculosis*, however, only 5-10 % of those infected display symptoms of active TB (6)(7). Following the inhalation of *M. tuberculosis*, the bacteria are deposited in the lungs, where they are taken up by phagocytes, particularly alveolar macrophages, after being recognized as pathogens (8)(9). The uptake of *M. tuberculosis* by macrophages usually results in (i) complete destruction of *M. tuberculosis,* (ii) arrested growth of *M. tuberculosis* by host defence leading to latent infection, or (iii) severe suppression of the host defence by *M. tuberculosis* followed by active TB (10)(11)(12)(9).

TB is considered a curable disease with a therapeutic regimen consisting of a six-month combination therapy of four drugs, namely rifampicin, isoniazid, ethambutol and pyrazinamide, taken daily for the first two months of an intensive treatment phase, followed by a four-month continuation phase, in which rifampicin and isoniazid are taken daily (13). Side effects, frequent drug administration, and long treatment durations challenge the currently available therapeutic regimen and severely impact patients adherence, leading to treatment failure and treatment resistance (14). Aside from adherence issues, other factors such as pharmacokinetic properties and degradation of drugs such as rifampicin in acidic environments, can significantly reduce the quantity of drug reaching the targeted site of action following oral administration, thereby predisposing them to resistance

(15)(16)(17)(18). The emergence of drug resistant strains of *M. tuberculosis* has necessitated new approaches to treating TB (19).

M. tuberculosis is an intracellular organism that resides primarily in macrophages. One strategy proposed to eradicate *M. tuberculosis* is to stimulate macrophages to self-eradicate this pathogen. This approach, also known as immunotherapy or host-directed therapy, involves the use of immunomodulatory agents to alter the host's response to the pathogen (20)(21)(22). Nanoparticles have shown great potential to deliver a variety of therapeutic materials to cells, including immunomodulatory agents (23)(24). Through their effective delivery of various therapeutic materials, nanoparticle drug delivery systems are a promising approach to address drug resistance, toxicity, and to improve the physiochemical properties of existing drugs.

It was hypothesized that two immunostimulatory compounds, namely curdlan (from the bacterium *Alcaligenes faecalis*) and mycolic acid (from the *M. tuberculosis* cell wall), could be loaded onto lipid-polymer hybrid nanoparticles (LPHNPs). It was further hypothesized that these LPHNPs would be non-toxic and possess macrophage stimulating capacity dependent on functionalization with MA and curdlan. Therefore, the aim of this study was to synthesize and characterize LPHNPs incorporating both immunostimulatory compounds and to investigate them for their cytotoxicity and their ability to stimulate RAW264.7 macrophages *in vitro*. Further studies can explore the biomimetic and immunotherapeutic effects of these LPHNPs in *in vivo* and *in vitro* models of *M. tuberculosis* infection.

Chapter 2: Literature review

2.1. The epidemiology and treatment of TB

In 2020 alone, TB claimed 1.5 million lives globally, i.e. approximately 4148 deaths every day, and of those 1.5 million deaths, nearly 15 % of deaths occurred in persons co-infected with HIV (1). TB is among the top 10 leading causes of death globally and since 2007 until the outbreak of the COVID-19 pandemic, TB was ranked as the number one leading cause of death from a single infectious agent, ranking above HIV/AIDS (1). The emergence of COVID-19 has significantly impacted and reversed years of progress made in reducing the global TB burden by affecting TB diagnosis, treatment, and prevention. This is due to the severe disruption of services including access to diagnosis, medicines and preventative therapies. This is evidenced by an approximately 18 % drop in TB diagnoses between 2019 and 2020, with an increase in TB mortality, highlighting the impact of COVID-19 on TB. The WHO reported an estimated 9.9 million new TB cases worldwide in 2020, a relatively constant figure in recent years, and of the newly reported cases, people living with HIV accounted for 8 % (1). Although the incidence in 2020 was approximately 1.9 % lower than in 2019, it is expected to worsen in 2021 and 2022 as a result of COVID-19 related impacts. TB mortality and morbidity usually accelerated by HIV co-infection, the emergence of drug resistant TB strains, chronic diseases such diabetes and immunosuppressive diseases or chemicals, have been significantly increased by COVID-19 (1)(25).

TB is an airborne communicable disease transmitted by inhaling aerosols containing *M. tuberculosis* (5). There are two types of TB, the most prevalent being pulmonary TB, which occurs when TB infects the lungs, and extra-pulmonary TB, which occurs when TB infects other sites (3)(26). The intensity of exposure and the immune status of the infected person determine the severity of the infection. *M. tuberculosis* replication is often forestalled by a strong immune response, however, viable *M. tuberculosis* cells can persist for a long time in a dormant state leading to latent TB infection (5).

About a quarter of the world's population is infected with latent TB (27)(28). Latent TB infection is asymptomatic and non-infectious. However, upon exposure to a new infection or reactivation, latent TB can progress to active TB (5). Approximately 5 -10 % of latently

infected individuals develop active TB and show symptoms of TB with the remaining individuals being reservoirs for potential future active TB infections (25)(29). As previously mentioned, a six-month combination therapy of rifampicin, isoniazid, ethambutol, and pyrazinamide taken orally daily in two phases, namely intensive and continuation phase. In the first two months (intensive phase) all four drugs are taken as a combination, while in the continuation phase two drugs (rifampicin and isoniazid) are taken for four months (13). However, frequent administration and duration of treatment severely impact the adherence to this therapy resulting in treatment failure and resistance (14). In addition to adherence issues, other factors such as degradation and pharmacokinetic properties including poor and variable solubility, drug degradation in gastrointestinal tract, drug instability when administered in a combination, and variable half-lives of these drugs contribute to *M. tuberculosis* resistance to treatment (15)(16)(31)(32). All of the listed factors can significantly reduce the quantity of drug reaching the target site of action, thus predisposing them to resistance (16)(17)(31)(32). In addition to multidrug-resistant (MDR), the emergence of extensive drug-resistant (XDR), totally drug-resistant TB, the endemic spread of AIDS, and the recent emergence of the COVID-19 pandemic has made the situation even more alarming (5)(1). This scenario calls for new approaches to enhance the effectiveness of the currently available treatments and the development of new treatment regimens to address this situation (33).

2.2. The bacteriology of *M. tuberculosis*

2.2.1. *M. tuberculosis* cell wall

M. tuberculosis is a slow-growing intracellular Gram-variable acid-fast bacterium of the *Mycobacterium* species with a slow generation time of 15-20 hours, a physiological trait that can contribute to its virulence. Successfully identified and isolated as the etiological agent of TB by Robert Koch in 1882, *M. tuberculosis* is an aerobic to facultative anaerobe that is a highly adaptable pathogen that can switch from a carbohydrate-based to a fat-based diet depending on the conditional requirements (34)(35)(36)(37). *M. tuberculosis* is rod-shaped with a length and width of 2-4 μm and 0.2-0.5 μm respectively (37). *M. tuberculosis* possesses a thick waxy cell envelope composed of interconnected polymers of mycolic acids (MAs), arabinogalactan (AG), and peptidoglycan (PG) (38). The envelope is responsible for the drug resistance of *M. tuberculosis* as it acts as a barrier to both hydrophobic and hydrophilic materials, making *M. tuberculosis* poorly permeable to many antimicrobial agents and thus inherently resistant to most antibiotics (39). This envelope is also responsible

for the interaction of *M. tuberculosis* with the host immune system, resulting in facilitated uptake of *M. tuberculosis* by macrophages (40). Some components of the *M. tuberculosis* envelope are responsible for suppressing immune responses, while others are instrumental in activating them (5).

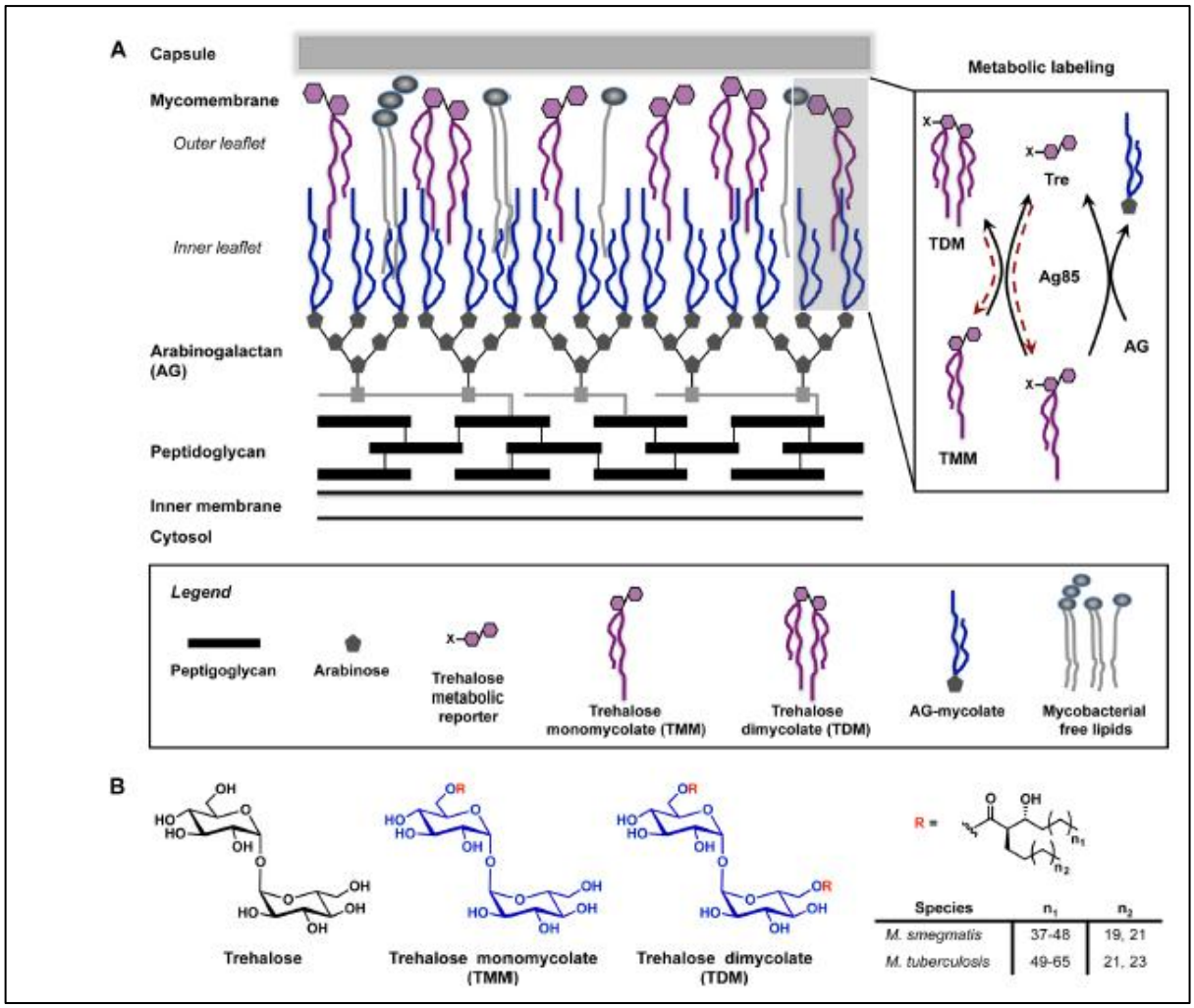

Fig. 2.1. Mycobacterial cell envelope and trehalose mycolate structures. (A) Mycobacterial cell envelope constituents and mycolylation of arabinogalactan from the TMM (trehalose monomycolate) donor mediated by Antigen 85, in which two TMM molecules are used to create TDM (trehalose dimycolate), releasing one molecule of trehalose. (B) shows chemical structures of MA constituents and lists the number of carbons (n1, n2) in linear mycolate chains for *M. smegmatis* and *M. tuberculosis*. Image obtained from (38).

M. tuberculosis requires both activation and suppression of immune cells for its survival, as activation increases uptake into macrophages, while suppression allows survival within macrophages (5)(41). For instance, lipoarabinomannan may play a role in preventing

phagosome maturation but also in secretion of pro-inflammatory cytokines, and MAs can induce secretion of inflammatory cytokines (41).

2.3. Host defence and intracellular survival of *M. tuberculosis*

2.3.1. Cellular uptake of *M. tuberculosis*

Upon deposition of *M. tuberculosis* in the lung following inhalation, bacilli are recognized by the resident immune cells such as alveolar macrophages, dendritic cells (DCs) and neutrophils (42)(43)(44). An innate immune response is triggered by the interaction of pathogen associated molecular patterns (PAMP) and pattern recognition receptors (PRR) such as toll-like receptors (TLRs), C-type lectin receptors, and Nod-like receptors (NLRs) (45)(46)(47)(48). PAMPs are highly conserved smaller molecular products with polysaccharide-like structures that are recognized by PRR (49)(50). Through their selective binding, PAMPs on *M. tuberculosis,* specifically mannosylated-lipoarabinomannan (MAN-LAM), lipomannan, and phosphatidylinositol mannoside (PIM) interact with PRRs and initiate immune response, which in turn triggers the uptake of *M. tuberculosis.* The fate of *M. tuberculosis* within the macrophage is (i) complete eradication of *M. tuberculosis* cells, (ii) arrested growth of *M. tuberculosis* leading to latent TB infection, or (iii) severe suppression of the immune system (host-defence) by *M. tuberculosis* followed by active TB (10)(11)(12).

2.3.2. Phagosome maturation and phagolysosome formation

Phagocytosis is a crucial mechanism of innate immunity by which antigens are detected, engulfed, degraded, and subsequently presented to T cells, resulting in adaptive immune activation (51). Phagocytosis is initiated by the interaction between PAMP and PRRs resulting in phagocytic uptake of antigens by macrophages (52). The engulfed *M. tuberculosis* is confined into a phagosome, an intracellular vesicle (51)(53). Phagosomes mature by interacting with various endosomes and lysosomes that modify their enzymatic activities, resulting in a mature phagolysosome with desired antimicrobial activities (51). However, *M. tuberculosis* has evolved numerous strategies to suppress immune responses, including arresting phagosome maturation and phagolysosome formation, allowing them to persist in macrophages and establish infection (54).

M. tuberculosis can arrest phagosomal maturation by interfering with Rab molecules. Rab molecules are members of the RAS protein superfamily and are located in the intracellular

membrane (55)(56). Rab molecules are functionally related to membrane fusion, a fundamental process in eukaryotic cells, and vesicular transport in humans (56). Generally, Rab molecules have a guanosine triphosphate (GTP) hydrolase (GTPase) fold, low molecular weight, and are considered markers of phagosomal maturation. Under normal conditions, Rab5 is found in early phagosomes, which is replaced by Rab7 in late phagosomes hence Rab7 marks late phagosomes (55)(57)(58)(59). The active form of Rab7 (aRbab7) reportedly binds to Rab7 interacting lysosomal protein (RILP), an intra-phagosomal membrane, and form aRAb7/RILP complex that promotes phagosomal maturation and Rab5 dissociation (56)(58)(60). Matured phagosomes fuse with lysosomal vesicles to form phagolysosomes (56). However, *M. tuberculosis* containing phagosomes, can obviate this process by amassing Rab22, a late endosomal regulator, and consequently preventing the involvement of Rab7 (61). Additionally, *M. tuberculosis* can release a factor that catalyzes the Rab7 GTP/GDP conversion, resulting in a mutant aRab7 isoform that is unable to bind to RILP (57)(56).

Following phagocytic uptake of *M. tuberculosis* by macrophages, vacuolar ATPase (V-APTase) is rapidly recruited to the phagosomal membrane. V-ATPase pumps protons (H^+) into the phagosome, gradually acidifying the intra-phagosomal compartment (51). Although the mechanism by which *M. tuberculosis* excludes V-ATPase is a subject of ongoing debate, it is known that *M. tuberculosis* arrests the internal acidification process by selectively excluding of V-ATPase from the phagosomal membrane (62)(63). Consequently, the internal acidification process is arrested at a pH of approximately 6.4 which is much higher than the desired pH (≤5), thereby suppressing phagosomal proteases and lysosomal enzyme activities that require low pH for optimal functioning (63).

Calcium (Ca^{2+}) mobilization is associated with pathogen uptake, membrane fusion and phagosome maturation (64)(65). Sphingosine kinase (SPK) induces Ca^{2+} mobilization through phosphorylation of sphingosine to sphingosine-1-phosphate which stimulates the release of Ca^{2+} from endoplasmic reticulum stores (64). Ca^{2+} increase in the cytosol leads to the binding of Ca^{2+} with calmodulin (CaM), which activates CaMKII (64)(65). This pathway leads to increased production of PI3P upon activation of hVPS34 which catalyzes PI3P (65). Binding of early endosomal antigen 1 to PI3P promotes membrane fusion and phagosome maturation (65). However, viable *M. tuberculosis* can suppress Ca^{2+} mobilization and signalling by inhibiting of SPK. Interestingly, the uptake of inactivated *M. tuberculosis* activates SPK (64). Viable *M. tuberculosis* can also release SapM, a lipid phosphatase that

hydrolyses PI3P and promotes the continuous removal of PI3P in *M. tuberculosis* containing phagosomes (66).

It has also been reported that *M. tuberculosis* exploits the increase in Ca^{2+} promoted by the retention of tryptophan aspartate-containing coat (TACO) protein, resulting in Ca^{2+} dependent activation of calcineurin, a calcium-dependent phosphate directly involved in preventing phagolysosomal fusion (67). The TACO protein, also known as Coronin 1, COROA1A or P57, is involved in various F-actin dependent cellular processes and keeps extra-cellular signals integrated with F-actin remodelling (67)(68). TACO protein is normally present on the phagosome surface, however, detachment of this protein from phagosomes leads to phagosome maturation and delivery of phagosomes to lysosomes (67)(69). It has been reported that incubation of viable *M. tuberculosis* with macrophages resulted in TACO retention in 90 % of phagosomes, while incubation with dead bacilli resulted in TACO release within 2 h (69)._Jayachandran *et al.* (2007) reported that TACO promotes high intracellular Ca^{2+} influx, resulting in SPK independent Ca^{2+} mobilization that activates calcineurin which in turn prevents phagolysosomal fusion (67). On the other hand, Vergne *et al.* (2003) reported that *M. tuberculosis* releases LAM, which inhibits the increase in intracellular Ca^{2+} influx and thus inhibits calmodulin-dependant PI3P production and thereby affects Ca^{2+} dependent phagosome maturation (70).

The formation of phagolysosome marks a final and critical stage in microbial eradication, and this stage is accompanied by acquisition of various enzymes and the production of ROS (reactive oxygen species) or NOS (nitrogen oxide synthase),which further enhance the antimicrobial activity of the phagolysosome (51)(71). Various soluble N-ethylmaleimide sensitive factor (NSF) NSF attachment protein receptors (SNAREs) mediate the fusion of phagosomes and lysosomes into phagolysosomes (51). In addition to acidifying the formed phagolysosomes to a lower pH (4.5), the acquisition of various hydrolytic enzymes such as cathepsins potentiates the degradative capacity of the formed phagolysosomes (51)(71). Furthermore, the antimicrobial effect is further enhanced by an increased production of ROS/NOS by the NADPH oxidase (NOX) complex and the inducible nitric oxide synthase (iNOS) (72). NOX-mediated electron transfer from NADPH to intra-phagosomal oxygen yields superoxide anions, which dismutate and produce hydrogen superoxide and other degradative ROS (72). In addition, iNOS generates nitrate and nitrite, which react with nitrous acid at low pH to produce nitric oxide and nitrogen dioxide. The nitric oxides produced react with superoxide to form peroxynitrite, an extremely toxic substance that is

crucial for eradicating pathogens (72). However, to obviate toxicity, *M. tuberculosis* can produce proteins involved in detoxification and damage repair (72). *M. tuberculosis* secretes a catalase-peroxidase KatG that catabolises hydrogen peroxide into oxygen and water (72)(73). In addition, *M. tuberculosis* LAM can scavenge free oxygen radicals and thus further suppress oxidative stress (72). *M. tuberculosis* can also secrete PknG, a eukaryotic-like serine/threonine kinase protein, into the cytosol of macrophages. PknG plays an essential role in repressing phagosome-lysosome fusion by phosphorylation of a currently unknown host factor involved in membrane fusion. Thereby suppressing the lysosomal delivery of the phagosome by the host factor (73).

2.3.3. Cytokine mobilization and granuloma formation

Macrophage uptake of *M. tuberculosis* triggers the release of various cytokines and chemokines, which act jointly to increase vascular permeability, increase local inflammatory cell recruitment, and mediate systematic effects such as fever (74). The macrophage cytokine profile consists of pro-inflammatory cytokines such as IFN-γ, TNF-α, IL-2, IL-6, IL-12, IL-18, IL-23, and anti-inflammatory cytokines such as IL-27, IL-4, IL-10, IL-13, and TGF-β (74)(75). Pro-inflammatory cytokines activate macrophages for effective bactericidal effects. However, to avoid host cytotoxicity, these cytokines must be produced in appropriate amount and this should be taken into account when designing immunotherapies (76)(77)(78)(79). *M. tuberculosis* inhibits macrophage activation by inhibiting pro-inflammatory cytokine production or by inducing anti-inflammatory cytokines (80)(81)(82)(83)(84)(85). For instance, *M. tuberculosis* LAM inhibits IFN-γ secretion, a key macrophage activating cytokine, while the uptake of *M. tuberculosis* stimulates the release of IL-10, an anti-inflammatory cytokine whose increased secretion is associated with reduced secretion of IFN-γ as well as reduced recruitment of other pro-inflammatory cytokines (79)(86). O'Leary *et al*. (2011) reported about twice as much IL-10 in live *M. tuberculosis* infected macrophages compared to inactivated *M. tuberculosis*-infected macrophages, and the authors reported enhanced phagosome maturation following the addition of anti-IL-10 antibodies, highlighting an important role IL-10 plays in *M. tuberculosis* pathogenesis and survival (86). On the other hand, MA has been shown to induce pro-inflammatory cytokines such as IFN-γ which plays a crucial role in protective immunity against *M. tuberculosis,* while also inhibiting the production of IL-10, an anti-inflammatory cytokine crucial for *M. tuberculosis* survival (41).

2.3.3.1. Granuloma formation

The granuloma is the hallmark of *M. tuberculosis* infection and creates an environment that allows the host defence to control *M. tuberculosis* replication (87). Phagocyte/macrophage PRR and *M. tuberculosis* antigen interactions result in the secretion of various cytokines and chemokines that recruit other innate and adaptive immune cells including epithelioid cells, Langerhans giant cells, mononuclear phagocytes, fibroblasts, and T and B lymphocytes (72)(87). The accumulation of these immune-regulating cells in response to secreted cytokines and chemokines forms a highly organized structure known as a granuloma, a hallmark of *M. tuberculosis* infection (87)(88)(89). The granuloma is an acidic, hypoxic environment that is less conducive to *M. tuberculosis* replication, allowing the host to control the infection (87)(90). A delicate balance of pro- and anti-inflammatory cytokines is required to maintain granuloma structure and functionality. TNF-α and IFN-γ are highly involved in granuloma formation and function, while IL-10 is one of the major anti-inflammatory cytokines (87). About 90-95 % of infected individuals develop latent TB i.e., immune cells effectively contain *M. tuberculosis* by forming a granuloma. At this stage, *M. tuberculosis* enters a non-replicating persistent (NRP) state, resulting in latent infection. However, when the balance between pro- and anti-inflammatory cytokines is tampered, which is more likely in immunocompromised patients such as HIV patients, this facilitates the reactivation of bacilli and forms caseous lesions that can cause the granuloma to cavitate and its subsequent collapse releasing *M. tuberculosis* into the lungs and eventually causing active TB (72)(87)(90).

2.4. Stimulation of macrophages as a strategy to eradicate intracellular *M. tuberculosis*

The process of infection development involves an interaction between invading pathogens and the host defence system. Following the pathogen invasion, the host's immune system is activated, and various mediators are released in response to the invading pathogen. This initial response aims to eliminate the invading pathogen and prevent subsequent infections. Inadequate immune response fails to eliminate the pathogen, resulting in an infection, while over-exuberant immune response results in detrimental effects to the host such as cytokine storm (76)(77)(78)(91). A delicate balance is therefore required and this should be an important consideration when designing immunotherapies (76)(77)(79).

Once infection is established, treatment usually consists of antimicrobial chemotherapy, which kills the invading pathogen. However, the rise in antimicrobial resistant pathogens such multi-drug resistant (MDR-) and totally drug resistant (XDR-) *M. tuberculosis*, as well

as the increasing prevalence of immunocompromised patients, have led to an increased interest in modulating the innate immune response to achieve desirable health and treatment outcomes (20)(21)(22).

Immunotherapy is the use of small molecules or biologics that modulate the immune response to a particular pathogen to control the disease and eradicate the pathogen. For infectious diseases, immunotherapy can be used with or without antibiotics to achieve better control of the infection (92). As previously mentioned, latent TB infections is the most common outcome (90-95 %) of *M. tuberculosis* infections and these infections progress to active TB infection when *M. tuberculosis*, a pathogen that typically reside within macrophages, severely suppresses or evades the immune system (93). This highlights the crucial role of the immune system in *M. tuberculosis* infection control, as well as the inherent ability of host defence to control *M. tuberculosis* replication and prevent active TB development (94).

Immunotherapy provides antimicrobial effects by (i) interfering with host mechanisms that the pathogen uses to persist or replicate in host tissues, (ii) potentiating the host immune defences against the invading pathogen, (iii) targeting pathways that may contribute to disease progression such as classically hyperinflammation and finally (iv) modulating host factors at local level that are involved in pathogenic responses (90). Antibiotic resistance to current treatment is a major global health problem. In fact, it is estimated that approximately 10 million people will succumb to antimicrobial resistance annually by the year 2050 (95)(96). However, unlike antibiotics, which target pathogen functions, immunotherapy targets host functions, making it unlikely that pathogens will develop resistance to this form of therapy. Therefore, with fewer new anti-TB drugs in the pipeline in the near future, immunotherapy offers a promising alternative treatment strategy for TB (90). One of the strategies that could be used is to stimulate macrophages to self-eradicate *M. tuberculosis* (20)(21)(22)(97). Biological functions of activated microphages such as ROS/RNS secretion and autophagy, supported by the subsequent adaptive immune response, lead to phagolysosome formation and potentially enhance the antimicrobial response (71)(90). As previously mentioned, *M. tuberculosis* survives by suppressing some macrophage responses, therefore, by stimulating the microphage, self-eradication of *M. tuberculosis* could be achieved by immune response of the stimulated pathways.

2.5. Mycolic acid (MA)

MA is a major lipid component of the *M. tuberculosis* cell wall and is a long-chain(α-alkyl-β-hydroxyl) fatty acid lipophilic compound with a carbon range of 60 to 90 and constitutes about 40-60 % of the total dry weight of the *M. tuberculosis* envelope (41)(98)(99)(100)(101). In *M. tuberculosis*, MA is present either covalently bound to the cell wall or non-covalently bound to sugar esters in the form of the glycosylated derivative such as TMM, TDM, glucose monomycolate or as secreted free MAs (41). MAs can vary by composition and source; thus, it is important to indicate the type used. MA can act as a PAMP and is therefore associated with triggering immune responses (41)(102).

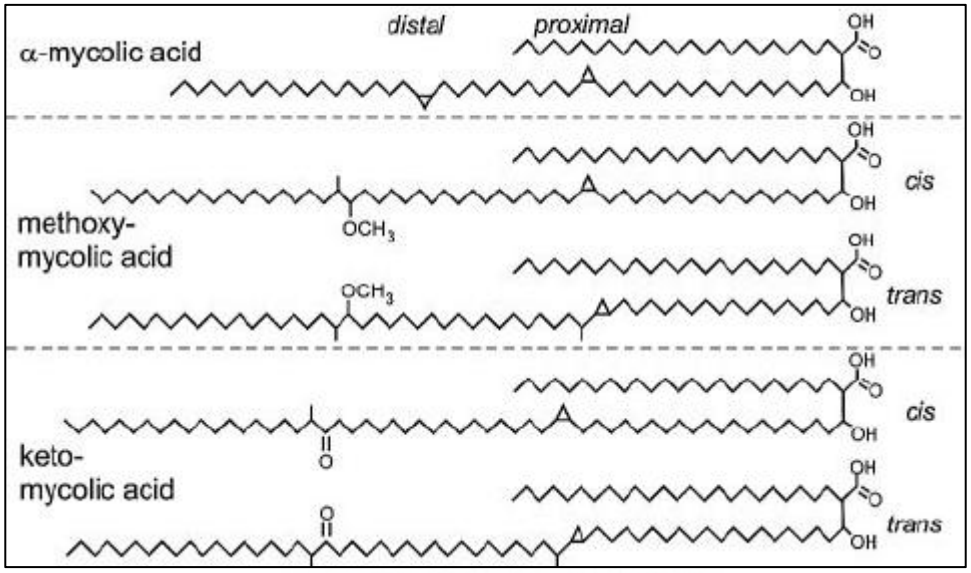

Fig. 2.2. The chemical structure of MAs of *M. tuberculosis* (103).

MA is one of lipids of *M. tuberculosis* whose interaction with macrophages leads to macrophage activation (104). MA is also one of the *M. tuberculosis* lipids presented to T cells by CD1 molecules (particularly CD1b). CD1 molecules, membrane proteins, are antigen presenting molecules on professional APCs and functionally present microbial lipids to T cells. CD1-restricted T cells have been shown to provide antimycobacterial immunity. CD1-restricted T cells from both infected and uninfected individuals have been shown to be cytotoxic and produce TNF-α and IFN-γ and these T cells have been found to be more abundant in individuals exposed to *M. tuberculosis* than in non-exposed individuals,

suggesting macrophage activation following *M. tuberculosis* infection (104). Zhao *et al.* (2015) reported that human mycolic acid-specified CD1b-restricted T cells were polyfunctional in a transgenic mouse; they were cytotoxic, implicated in granulomas and in reducing the bacterial load of *M. tuberculosis* in the lungs, spleen and liver, and provided protection against *M. tuberculosis* infection (104). Korf *et al.* (2005) using liposomes as carriers of MA, reported that MA induced some of the key features of M. *tuberculosis* infection to some extent. The author reported that MA induced formation of foamy macrophages (which are involved in granuloma formation), production of myeloperoxidase, an enzyme involved in the generation of reactive oxidants and production of local inflammatory responses, followed by the production of IL-12, IL-6 and IFN-γ. Compared to TDM, MA was effective in inducing IL-6 and IL-12 production, however, only TDM could induce TNF-α. It was also interesting to note that upon secondary exposure to inflammatory triggers such as LPS, the cells (*ex vivo*) showed a reduced production of IL-10 and an increase in IFN-γ production. The authors also reported that MA colocalized in acidic phagosomes, indicating that MA is not involved in disrupting phagosome maturation (41). Lemmer *et al.* (2015) formulated isoniazid-loaded PLGA (isoniazid-PLGA) NPs with MA as a targeting ligand. The authors reported that these NPs showed increased phagocytic uptake compared to isoniazid-PLGA NPs without MA. Phagosomes containing isoniazid-PLGA NPs with or without MA were localized into murine microphage phagolysosomes and remained there for approximately nine days (105).

2.6. Natural polysaccharides and curdlan

Natural polysaccharides are among the most abundant biomaterials in the world (106). Polysaccharides are made by animals and plants to serve various functions such as energy storage and structural support (106)(107)(108). Natural polysaccharides, like all other polymers, are made up of long chains of monomers of the same or different types. Owing to their biocompatibility, biodegradability, and versatility, natural polysaccharides are used in various industries such as packaging, biomedical, food and pharmaceutical industries (107)(109)(110)(111). Natural polysaccharides have recently found increased application in biomaterial science due to their ability to be handled at the nanoscale, with uses in biomedical delivery, tissue repair and immunotherapy (109)(112). Natural polysaccharides have been found to possess immunomodulatory responses (113)(114)(115). While some polysaccharides such as cellulose and curdlan enhance and stimulate immune responses,

others have been found to reduce or inhibit immune response, which is also helpful in controlling and regulating the immune response, which in excess can cause diseases such as allergies and cytokine storm in extreme cases (114)(115)(116)(117).

In disease control, the ability of the innate immune system to identify and respond to pathogens is paramount (118). Curdlan, a 1,3-β -glucan, is a glucose polysaccharide known to possess immunomodulatory effects that stimulate innate immune responses and activate complement (119)(120). Curdlan, a major component of fungal cell wall, is also found in bacteria such as *Alcaligenes faecalis*, yeast and some foods such as cereal oats, mushrooms and seaweed (121)(122). Curdlan exerts its immunomodulatory effect on macrophages mainly through interacting with Dectin-1 receptors (123)(124)(125)(126).

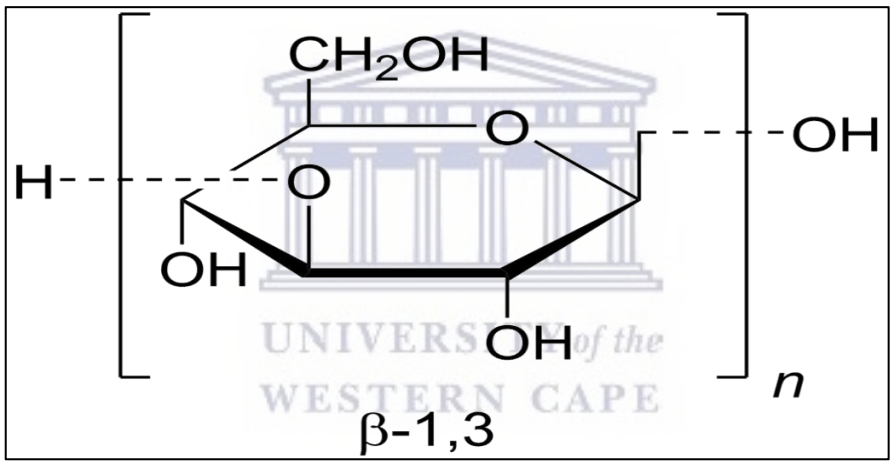

Fig. 2.3. The chemical structure of β-glucan linked through 1,3-linkage (β-1,3-glucan otherwise known as curdlan)(127)(128).

Dectin-1 is a type 2 transmembrane protein receptor that can activate and regulate the innate immune response, and this protein interacts with β-1,3-glucan (122). Interaction of curdlan with Dectin-1 receptors, which are widely expressed by immune cells, particularly macrophages, results in increased phagocytosis, which in turn increases uptake of the curdlan-containing cargo into the macrophages (126). This interaction also results in the stimulation and initiation of the immune response (121), induction of reactive oxygen species (ROS) or reactive nitrogen species (RNS), enhanced TNF-α and lysosomal enzymes production as well as pro-inflammatory cytokines, chemokines such as IL-12 and inflammatory lipid mediators that recruit other immune cells and control their activation

(119)(122)(126). It is also know that dectin-1 activation enhances intracellular calcium, which is suppressed by *M. tuberculosis* (129)(130). Intracellular calcium has been associated with microbial ingestion, phagosomal maturation, and autophagy (130)(131). Since Dectin-1 is expressed on other innate immune response cells such as neutrophils and dendritic cells (118), its activation also leads to immune responses from other cells such as dendritic cells and neutrophils. An examples of these responses is neutrophil degranulation (122). Besides dectin-1, curdlan can also activate macrophages by interacting with complement receptor 3 CR3 (CD11b/CD18) which is also expressed on polymorphonuclear leukocytes, mononuclear phagocytes and natural killer cells (119). Hetland *et al.* (2002) reported the interaction of glucan with the lectin-binding site in the complementary receptor 3 CR3 (CD11b/CD18), which is also one of the entry routes of *M. tuberculosis* inside the macrophage. Entry of *M. tuberculosis* through CR3 avoids a toxic oxidative burst due to the lack of this response when CR3 is engaged. Their results suggest that β-1,3-D-glucan can competitively inhibit *M. tuberculosis* entry via this route (119). Mansour *et al.* (2013) reported that 1,3-β-glucan activation of dectin-1 facilitated phagosomal phagocytosis of polystyrene-1,3-β-glucan beads. The authors also reported that dectin-1 activation promoted dectin-1-dependent spleen tyrosine kinase (Sky) activation which is critical for 1,3-β-containing phagosome acidification and Sky-dependant phagosomal maturation (132).

Tukulula *et al.* (2015) successfully formulated a 1,3-β-glucan conjugated PLGA (poly (lactic-co-glycolic acid) (C-PLGA) NPs that were also loaded with rifampicin. C-PLGA and PLGA NPs possessed a characteristic biphasic drug release with an initial burst phase that released up to 30 % of rifampicin within 1 h, followed by a sustained release phase of the payload until 6 h when tracking drug release was terminated. The authors reported that C-PLGA NPs released less drug at both 1 h and 6 h, suggesting that curdlan incorporation enhanced the sustained release properties of PLGA NPs. It was also reported that both C-PLGA and PLGA NPs exhibit lower flux across intestinal model of Caco-2 cells (Rif had 3.2 and 2.3-fold greater flux than C-PLGA and PLGA respectively (120). Compared to PLGA, C-PLGA NPs showed increased production of ERK, an upstream mediator of ROS, which was as much as curdlan-only treated cells, indicating immunostimulatory activity of curdlan and C-PLGA NPs. The MTT assay indicated that C-PLGA (0.13-200 μg/mL) was non-toxic over the 72 h period evaluated. Although their impedance data did not correlate with their MTT results, their impedance data suggested a calcium signalling associated with NPs uptake (120). Soto *et al*. (2010) successfully formulated rifampicin-loaded alginate-sealed glucan particles.

Alginate-sealed glucan particles exhibited a slow-release kinetics of rifampicin over 24-72 h, assessed. Although rifampicin-loaded alginate-sealed glucan particles (10 % w/w rifampicin/glucan) released a sub-minimum inhibitory concentration of rifampicin, that these particles were shown to significantly enhance the reduction in *M. tuberculosis* burden in infected bone marrow-derived macrophages compared to free rifampicin at the same concentration and empty glucan particles, demonstrating the role of glucan in macrophage targeted drug delivery and in optimizing the current therapy while potentially reducing side effects (133).

2.7. Nanoparticles and nanomedicine

NPs have recently emerged as excellent carriers of various therapeutic agents, including immunomodulatory agents (21)(22). A nanomaterial is a material that contains at least 50 % of particles with one or more external size dimension in the nanoscale range (1 - 100 nm)(134). Due to their smaller particle size and larger surface area to volume ratio, NPs may exhibit pronounced differences compared to the same material at a larger scale. These differences include changes in biochemical, magnetic, optical, and electronic properties (135)(136). These new and unique properties associated with NPs have recently gained the interest of the scientific community, and there are currently over 50 nanomedicines registered by the United States Food and Drug Administration (FDA) for disease therapy (137)(138). The unique properties noted above enable these drugs or drug carriers to provide controlled drug release and targeted drug delivery with improved drug absorption, safety and effectiveness. (139)(140). NPs have also proven to be good carriers for various therapeutics, including small molecules, genes, and proteins (141)(142)(143). Therefore, NPs represent a valuable delivery system for various therapeutic compounds to treat a plethora of diseases, including TB (139). NPs that have been widely utilised in drug delivery include lipid NPs, polymeric NPs, carbon nanotubes, quantum dots, dendrimers, metal and metal oxide NPs, graphene derivatives, and nanoporous materials (144).

Of all the nanocarriers, lipid and polymeric polymers have been the most frequently used. This is proven by a large body of research, reports, clinical trials and approved medicines containing these particles (137)(145). In fact, the majority of the FDA-approved nanomedicines are lipidic and polymeric nanomedicines (137)(139)(146)(147)(148)(149). Some of the lipid-based nanomedicines currently on the market include Doxil®, a liposomal doxorubicin for Karposi's sarcoma, ovarian cancer and multiple myeloma; Abelcet® and AmBisome®, liposomal amphotericin B for fungal infections; and Vyxeos®, a synergistic

combination of daunorubicin and cytarabine, the first approved cancer drug that synergistically delivers two drugs, for acute myeloid leukaemia; and Patisiran/ONPATTRO, the first RNAi approved therapeutic is a siRNA for gene silencing of a specific gene that express transthyretin that is responsible for hereditary transthyretin amyloidosis (148)(150). From 2016 to late 2019, 12 of the 18 new nanoparticle-based drugs that entered clinical trials were lipid-based and 17 of these were for cancer therapy (148)(150). In 2013, two of the top 10 bestselling drugs in the United States were polymer based nanomedicines Copaxone® (a glatiramer acetate for treatment of multiple sclerosis) and Neulasta® (a PEGylated recombinant granulocyte colony-stimulating factor for minimizing chemotherapy-induced neutropenia for cancer patients) (151). Other polymer based medicines include Adynovate®, an antihemophilic factor VIII used to treat haemophilia; Adagen®, a PEGylated adenosine deaminase enzyme for severe combined immunodeficiency disease; Mircera®, a chemically synthesized erythropoiesis-stimulating agent for anaemia associated with chronic kidney disease (148)(150). However, to advance the clinical translation of lipid and polymeric NPs, a new generation of a combination of both lipidic and polymeric NPs, known as lipid-polymer hybrid nanoparticles (LPHNPs), has emerged as an effective delivery system that combines both the advantages of both lipidic and polymeric NPs while minimizing their shortcomings (see section **2.7.5**).

2.7.1. Lipid NPs

Lipids are used in a variety of drug delivery systems such as lipids, solid lipid NPs, lipid drug conjugates and others (137)(145)(147). Lipid NPs have been used extensively to deliver therapeutic materials. Liposomes are of one the types of_NPs that have been heavily used (137)(145). Liposomes are spherical lipid vesicles consisting of single or multiple lipid layers that encapsulate drugs and act as carriers of a variety of pharmaceutical products (152).

Liposomes are drug carriers made from phospholipids, which are analogues of biological membranes and can fuse with cell membranes, enhancing internalization of liposomes (153)(154). Liposomes are prepared from both natural and synthetic amphiphilic lipids. They are generally biocompatible, biodegradable with little or no toxicity, flexible and non-immunogenic for systematic and non-systematic use (147)(155)(156). Due to the similarities between liposomes and mononuclear phagocytes, liposomes are readily taken up by mononuclear phagocytes, particularly macrophages, which is a positive attribute when macrophages are the target of interest (157). However, liposomes suffer from several

limitations such as relative poor bioavailability due to higher clearance, lack of structural integrity leading to leakage of contents (156)(158). Liposomes also exhibit fast release, issues related to physical and chemical instability during storage and higher cost, and scale up issues (152).

Solid lipid NPs (SLNs), on the other hand, are NPs developed as an alternative to liposomes. SLNs are a class of colloidal particles composed of solid lipids at room and physiological temperatures, incorporating therapeutic molecules (144). Solid lipids provide a better controlled drug released compared to liquid oils due to a considerable reduction in mobility of the embedded drug in the solid lipid matrix (159)(160). SLNs are submicron in size and consist of physiologically tolerable solid lipids dispersed in an aqueous surfactant phase (144). SLN production involves the use of lipids and surfactants that are either FDA approved or generally recognized as safe (GRAS) (144)(161). SLNs exhibit desirable attributes such as surface modification, increased permeation through biological barriers, resistance to chemical degradation, ability to simultaneously deliver various therapeutic agents, and stimuli-responsiveness. All of these attributes help SLNs to overcome various biological barriers, provide increased bioavailability, provide enhanced drug protection, and allow SLNs to provide targeted drug delivery while minimizing their acute or chronic toxicity (144)(161). SLNs have found applications in diverse areas such as cosmetics, biologically active food components and particularly in drug delivery. SLNs can be administered via different routes such as intravenous, oral, intranasal, ocular, dermal, rectal, subcutaneous and intramuscular administration (144)(161). Nooli *et al*. (2017) successfully formulated an Olmesartan medoxomil (OLM) loaded SLN consisting of soy phosphatidylcholine, glyceryl monostearate, and Tween 80. The average particle size of SLN was about 80 nm with a loading efficiency of about 78 %. OLM-SLN showed improved pharmacokinetic properties such as a 2.32-fold increase in bioavailability following oral administration of free OLM suspension and OLM-SLN in male Sprague Dawley rats. The OLM-SLN suspension also showed a 1.95-fold increase in the maximum concentration (C_{max}). However, upon storage, OLM-SLN was only stable for 10 days at room temperature, turning creamy within 30 days. Storage at refrigerated temperatures showed a significant increase in stability as the formulation remained stable for 30 days without significant change in particle size (162). Neves *et al*. (2016) developed a resveratrol-loaded SLN functionalized with apolipoprotein E (ApoE) which can be recognized by the low-density lipoprotein receptors overexpressed on the blood-brain barrier (BBB). MTT and lactate dehydrogenase (LDH) assay results revealed no statistically

significant toxicity, indicating the safety of the ApoE-functionalized resveratrol SLN. A 1.8 fold increase in permeability in the hCMEC/D3 monolayer, mimicking *in vivo* BBB permeability, was observed in ApoE-functionalized resveratrol SLN compared to non-functionalized resveratrol SLN (163). Sandri *et al.* (2017) successfully prepared chitosan associated SLN (CS-SLN) for ocular drug delivery. The authors aimed at exploiting the mucoadhesive nature of chitosan to address retention time issue of most ophthalmic formulations. The authors reported a significant increase in mucoadhesion of CS-SLN (161). The above studies indicate the flexibility and diversity of SLN. However, in addition to their sensitivity to temperature and light that adversely affect their stability, SLNs still suffer from major drawbacks such as polymorphic transition during storage that result in drug expulsion, low loading efficiency, relatively low circulation time, agglomeration polydispersity, high operative temperatures, initial burst release effect the of embedded drug and refrigerated storage conditions (144). Therefore, LPHNPs, a delivery system that overcomes the limitations of lipid NPs while retaining their advantages, have been proposed (see section **2.7.5**).

2.7.2. Polymeric NPs

Polymeric NPs are another class of NPs that are widely used (137)(145). These particles have gained attention due to their structural integrity, storage stability, controlled drug release ability and their facile synthesis and functionalization (164). These NPs are prepared from natural, pseudosynthetic or synthetic, biodegradable and biocompatible polymers (148)(156). Polymeric NPs are generally classified as nanocapsule or nanosphere and they differ in their morphological structure. Nanocapsules are polymeric NPs with an oily inner layer to encapsulate drugs and a polymeric outer layer to control drug release. These NPs are typically used for lipophilic drugs (165)(166). On the other hand, the nanosphere lack the oil layer, they are a continuous polymeric matrix in which the drug can be encapsulated or adsorbed. Nanospheres are typically used for hydrophilic drugs (166)(167). However, poor encapsulation for hydrophilic drugs, use of toxic organic solvents during preparation, drug leakage, polymer degradation, scale up challenges and safety issues are some of the drawbacks associated with polymeric NPs (168)(169). To overcome the limitations of each (lipid and polymer NPs) while combining their advantages, LPHNPs have been developed (see section **2.7.5**).

2.7.3 Biomimetic NPs

Drawing from the knowledge of cellular and viral biology; NPs can be designed to mimic important cellular or viral aspects such as surface features that can replicate the natural and biological properties of cells and viruses such as surface protein presentation, chemical composition, and membrane fluidity (170)(171). The term biomimetic originated from two Greek words bios, meaning life, and mimesis, meaning to imitate (172). In biomedicine, biomimetic NPs are NPs rationally designed to mimic biological properties and/or functions of various cells for therapeutic purposes of different diseases (170)(173). Due to the nature of biomimetic NPs, they can be used to provide enhanced targeted drug delivery, to promote tissue generation and to modulate cellular functions, among others (174)(175)(176). Cell-based interactions are crucial for information exchange that often triggers different pathways. Cell-based interactions could take the form of interaction between cell and endogenous biomolecules, between cell and surrounding extracellular matrix, or between cell and cell (170)(174). Tipped to be the next generation particle-based therapeutics, biomimetic NPs intend to recreate features of biological systems and surfaces they are designed from, in a way that naturally resembles those features to induce the desired outcome and thus potentiating therapeutic effect of these NPs (170). Because these NPs can possess features of bacteria or viruses, they can adopt the same mechanism and elicit some of the responses elicited by bacteria such as increased intracellular uptake. These NPs can also elicit immune responses depending on the component of the cells they carry hence they have been studied not only as potential immunotherapies but also as potential vaccine candidates or vaccine carriers (177)(178)(179). Additional benefits of this design include increasing the stealth property of these NPs, physiological tolerance and physiological barrier permeability, provide targeted delivery (177)(178)(179).

In designing biomimetic NPs, size, shape, and surface properties are of utmost importance. This is because biomimetic NPs are designed to interact with biological membranes, which are highly selective and require a high degree of specificity. For instance, when designing a biomimetic NP for cellular mimicry, its size and shape should match cellular size and shape as possible for more potent therapeutic outcomes (170)(174). Besides mimicking the physical properties of the cells, other strategies are used to achieve biomimicry such as the use of soluble mediators which mimic secretory functions of cells and the mimicry of surface chemistry that mimics cell-to-cell interactions through surface-bound ligand to surface-bound receptors (180)(181)(182).

Bottom-up and top-bottom approaches are used to achieve surface chemistry mimicry. Bottom-up approaches involve the use cellular components such as lipids or surface proteins to functionalize the NP. These components are presented to various cells, including immune cells, to trigger an immune response to the presented components. On the other hand, top-bottom involves using the macromolecule such as an entire cell membrane that encapsulates the particle core (183)(184). Wang *et al.* (2016) formulated red blood cell (RBC) membrane-coated PLGA biomimetic NPs that were later conjugated with toxoid α-hemolysin (Hla), a major methicillin-resistant staphylococcus aureus (MRSA) virulence factor. A 95 % retention of Hla on the NPs was reported. The efficacy of these Hla biomimetic NPs as a (MRSA) antivirulence vaccines was investigated in murine studies. Normally, MRSA bacteria engage Hla to help colonize the site of challenge, resulting in significant skin lesion formation and systematic invasiveness. The authors reported the formation of germinal centers, which are critical for potentiating the humoral immune response, and following the administration of the Hla biomimetic NPs in mice at day 0 and a booster dose on day 14, a significant amount of anti-Hla titers was detected in serum at day 14 and a further increase in anti-Hla titers was noted at day 35. Over the course of the study, administration of toxoid-negative biomimetic NPs and PBS showed no detectable anti-Hla titers. The authors' findings have also shown a significant reduction in skin lesion formation in mice within the treatment group compared to the control group (Hla negative particles and PBS), following subcutaneous challenge of mice with live MRSA on day 35, on day 6 post-challenge, mice in the treatment group showed a fivefold reduction in dermonecrotic area compared to the control group and upon the conclusion of the study, mice in treatment group showed a 11.3-14.7 fold reduction in serum bacterial burden compared to mice in the control groups. In most analyzed organs, a reduction in bacterial burden in the treatment group compared to the control group and an approximately a two-fold reduction in bacterial burden in spleen and kidney were also observed on day 6 post challenge (185). In another study, Thamphiwatana *et al.* (2017) evaluated the use of macrophage-coated NPs in sepsis treatment. under normal conditions, endotoxins play an important role in Gram-negative bacterial sepsis. Bacteria release lipopolysaccharides (LPS) endotoxins. LPS form a complex that acts like PAMP and triggers dose-dependent nitric oxide (NO) production of potent pro-inflammatory cytokines, both of which are deleterious to the host at high levels. The authors synthesized biomimetic NPs consisting of a PLGA core coated with a cell membrane derived from macrophages (Mϕ-NPs). The authors reported that Mϕ-NPs bind and neutralize LPS and inhibit its induction of cytokine production, effects not observed in control groups using RBC-coated PLGA (RBC-

NPs) and PEGylated PLGA (PEG-NPs). In mice studies, following the injection of LPS, Mϕ-NPs were administered in the treatment group and RBC-NPs and PEG-NPs were immediately administered in the control group. The results showed no increased cytokine production in the treatment group, while cytokine levels in the control group followed the same kinetics as in the LPS-only group. Upon the administration of a lethal dose of LPS, followed by administration of Mϕ-NPs and RBC-NPs and PEG-NPs, there was a 60 % survival rate in the treatment group, while there was no significant improvement in survival rate in the control group. Finally, the efficacy of Mϕ-NPs was tested in a live infection model of gram-negative bacterial sepsis in which mice were challenged with lethal dose of *E. coli*. In the treatment group ,4 out of 10 mice survived for 60 h, while all mice in the control group were killed (186). The above studies show the role of biomimetic NP in the treatment and prevention of disease.

2.7.4. Lipid-polymer hybrid nanoparticles (LPHNPs)

LPHNPs are a novel drug delivery system that combines the advantages of lipid and polymeric NPs while overcoming the limitations of each. LPHNPs are polymeric NPs coated by a lipid layer (155)(187)(188). They possess the potential to be a robust drug delivery system as LPHNPs exhibit positive attributes of both lipid and polymeric NPs such as structural integrity, controlled drug release, high encapsulation efficiency, targeted drug delivery among other advantages of these NPs while overcoming their limitations (187)(188)(187). LPHNPs consist of three structural components: (i) the inner polymer core, which is used to encapsulate therapeutic substances, (ii) the middle lipid layer that envelopes the polymer core. The middle layer controls water permeation into the polymer core, which in turn controls polymer degradation and thereby controls drug release kinetics. Drug release depends on polymer erosion or hydrolytic polymer degradation, therefore, by controlling water permeation, the middle layer controls the drug release kinetics of the loaded drug. The middle layer also prevents drug leakage by acting as a molecular barrier that holds the encapsulated material interiorly. Lastly, the functionalization layer/ligand, which is the outermost layer, is either a polymer or a lipid whose role is to functionalize the NPs. Functionalization of NPs results in many advantages such as biomimicry, increased circulation period, target specificity and immune modulation (152)(190).

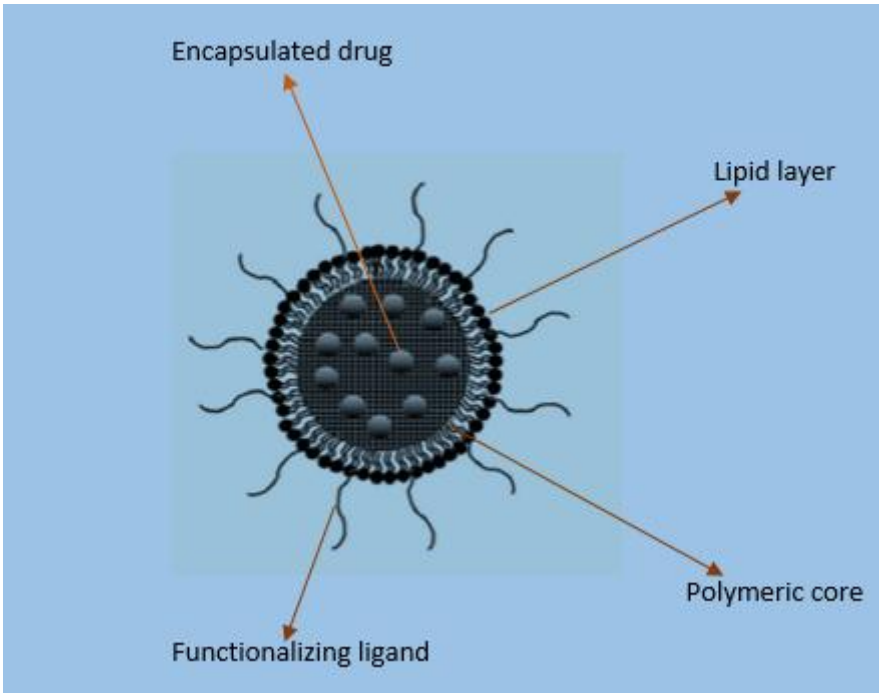

Fig. 2.4. Structure of lipid–polymer hybrid nanoparticles (LPHNPs), which comprise a polymeric core and a lipid layer, a functionalizing ligand, and the encapsulated drug. Adapted from (156).

The lipid to polymer ratio has a profound effect on the properties of LPHNPs such as particle size, colloidal stability, release kinetics, encapsulation efficiency (156). Therefore, the L/P ratio must be carefully monitored. Higher lipid concentrations lead to the formation of empty lipid vesicles that affect the consistency of the formulation, while insufficient lipid quantity results in inadequate coating of the polymer, leading to particle agglomeration (146)(149). Guo *et al.* (2020) formulated linezolid loaded LPHNPs of PLGA (polymer) and lecithin, cholesterol and DSPE-mPGE (lipids) of approximately 110 nm. Compared to linezolid solution, the authors reported that LPHNPs were significantly superior. The intracellular activities of linezolid solution and LPHNPs at three different concentrations, namely 2, 4 and 8 µg/mL, were compared against a highly virulent intracellular MRSA (methicillin-resistant *Staphylococcus aureus*). The results showed significant differences in CFU/mL between linezolid solution and the LPHNPs. At 2 µg/mL, the result showed an 87.0-fold difference in CFU/mL between linezolid solution and LPHNPs. A12.3-fold and 12.6-fold differences in CFU/mL were also observed with 4 and 8 µg/mL of linezolid solution and LPHNPs. The LPHNPs also suppressed the biofilm at lower drug concentrations (35 – 60 %) than required for free linezolid. Furthermore, the LPHNPs were reported to increase linezolid bone levels by more than four-fold compared to the free linezolid group. The authors also reported a controlled drug release profile with about 25 % release within initial 4 h followed by a

gradual release of the remaining payload over 120 h, compared to 70 % of the drug release of PLGA only NPs within initial 12 h and 90 % release of linezolid from free drug solution. The LPHNPs were generally stable in environments that stimulated blood plasma with minimal toxicity as indicated by the MTT assay after 16h incubation with osteoblast cells (191).

2.7.4.1. LPHNP constituents

2.7.4.1.1 Lecithin

Lipids have been used extensively in drug delivery systems (137)(145). This is because of their biological properties, stability, biodegradability, and biocompatibility (192). They are diverse and versatile in nature, which enables them to provide drug release via different routes of administration, such as oral, pulmonary and topical drug delivery, and to provide different release kinetics (193)(194). According to their components, lipids used in drug delivery can be classified into three types, namely homolipids, heterolipids and complex lipids. Homolipids, also known as simple lipids, are made up of only carbon, hydrogen, and oxygen. Examples of simple homolipids are wax and triacylglycerols (195). In addition to Carbon, Hydrogen and Oxygen, heterolipids are made up of nitrogen and phosphorus. Example of heterolipids include phospholipids and sphingolipids (195). Finally, complex lipids, which are lipids closely associated with proteins, examples of which include lipoproteins and chylomicrons (196). The choice of lipid used is highly dependent on the desired properties of the drug delivery system. This is because drug release from lipids is highly dependent on properties such as polymorphism, crystallinity of lipids and melting point (M.P) of lipids (197)(198). These properties affect the stability of the lipids on storage, and they affect their loading capacity as well as the release kinetics of encapsulated drugs (199)(200). For instance, amorphous lipids tend to provide high loading capacity compared to crystalline lipids, but lipids with a crystalline structure have been found to provide good sustained release due to low drug diffusion in the crystal structure (201). It has also been shown that β-polymorphs of lipids provide better stability of the lipids upon drug storage (202)(203). The melting point (M.P) of lipids is also of paramount importance, particularly depending on the route of administration. This is because M.P affects the plasticity and drug release properties of lipids. For instance, lipids with a M.P higher than that of the body temperature provide a better controlled drug release (196). Emulsifiers can be used in lipidic drug delivery systems to impart stability and prevent their aggregation, and sometimes they can provide a synergistic effect (196)(204).

Lecithin is a mixture of phospholipids; the main component of which is phosphatidylcholine (205). Phospholipids are amphiphilic lipids that contain phosphorus, a polar portion and a non-polar portion in their structure. Phospholipids consist of a hydrophobic head and a hydrophilic tail, linked together by alcohol. Depending on the alcohol they contain, they are classified as glycerophospholipids or sphingomyelins (206). Glycerophospholipids contain a glycerol backbone and naturally possess L-configuration and α-structure. Lecithin, a glycerophospholipid, is the main phospholipid in eukaryotic cell membranes (206)(207). On the other hand, sphingomyelins contain a sphingosine backbone and are an important component of the animal cell membrane (206)(208)(209). Phospholipids are derived from natural and synthetic sources. Phospholipids from natural sources, including lecithin, are widely distributed in plants, particularly in vegetable oils such as soybean, cottonseeds, sunflower, and they are also distributed in animal tissues such as egg yolk and bovine brain (206)(209)(210). The two main sources of natural phospholipids in drug delivery are egg yolk and soybean (210). Phospholipids from soybean and egg yolk differ in content, such as high phosphatidylcholine content in egg yolk compared to soybean and high degree of saturation in egg yolk than soybean, which makes soybean more susceptible to oxidative reactions, thus egg yolk possesses a superior oxidative stability than soybean lecithin (206). Furthermore, it is more challenging to obtain a quality controlled liposome product using soybean lecithin compared to egg yolk due to the higher content of unsaturated fatty acids in soybean (211).The encapsulation efficacy of egg yolk lecithin liposomes was also shown to be lower while their leakage rate was higher compared to egg yolk lecithin (206). The amphiphilic nature of phospholipids makes them excellent emulsifiers, wetting agents with self-assembly characteristics (212)(213). Lecithin-containing formulations such as Myocet®, a doxorubicin coated with egg yolk lecithin, are currently available on the market (206). Yanasarn *et al.* (2010) prepared a docetaxel PEGylated NPs encapsulated with soy lecithin. The authors reported that the NPs were approximately 270 nm in size with almost 100 % docetaxel loading efficiency. In tumour cell culture, docetaxel NPs exhibited a significantly higher tumour cell killing efficiency than free docetaxel. In mice studies, compared to free docetaxel, docetaxel NPs did not cause any significant red blood cell lysis, platelet aggregation, or significant liver injury and these NPs showed higher (4.5-fold) accumulation in a model tumour in mice (214).

2.7.4.1.2. Polycaprolactone (PCL)

PCL is a hydrophobic semi-crystalline synthetic polymer composed of caprolactone units linked together through ring-opening polymerization of ε-caprolactone preparation method (215)(216). This aliphatic linear polyester possesses several desirable features such as biocompatibility, biodegradability, high permeability, good stability under ambient conditions that make it suitable for NP formulations (217)(218). In addition, PCL is a bioresorbable, non-toxic, Food and Drug Administration (FDA) approved polymer for biomedical applications (217)(219). PCL is enzymatically degraded by lipases and esterases of microorganisms such as bacteria and fungi, but not those of humans (217). PCL undergo hydrolysis *in vivo* due to the hydrolyzable ester linkage of its backbone, yielding 6-hydroxycaproic acid (6-HCA) (220). An intermediate of 6-HCA and acetyl coenzyme is formed and enters the citric acid cycle and is ultimately eliminated from the body (221). However, the rate of hydrolysis is very slow, lasting about 3-4 years (219). This slow degradation in humans makes PCL a good candidate for prolonged drug delivery and it is widely utilized in biomedicine for drug delivery and tissue engineering (219).

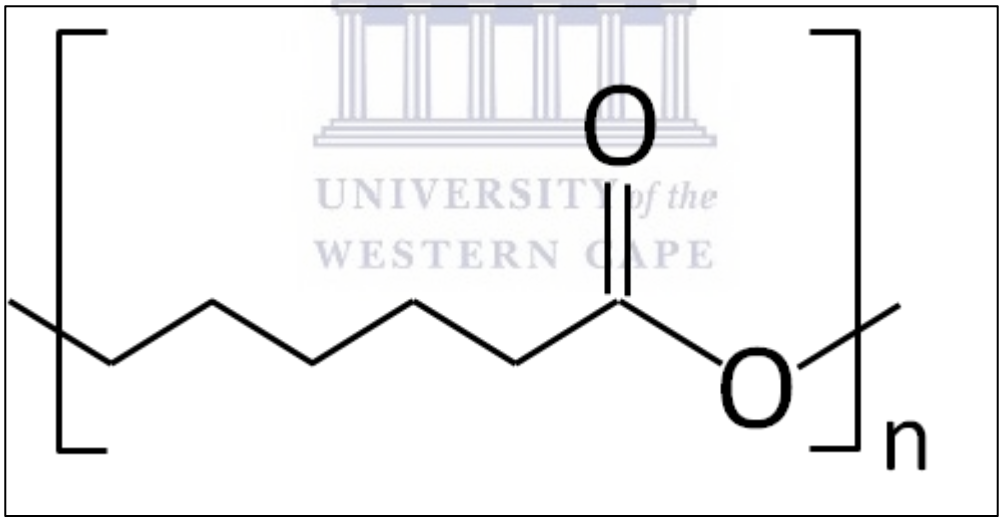

Fig. 2.5. The chemical structure of polycaprolactone (PCL), an aliphatic linear polyester produced via ring-opening polymerization of ε-caprolactone.

The molecular weight and degree of crystallinity of PCL determine its physical, thermal and mechanical properties (217). At room temperature, PCL is soluble in a number of solvents such as dichloromethane (DCM), cyclohexane, tetrahydrofuran (THF), carbon tetrachloride, benzene, toluene, chloroform. PCL is partially soluble in acetone, ethyl acetate, dimethylformamide (DMF), 2-butanone, and acetonitrile and it is insoluble in water, alcohols, diethyl ether and petroleum ether (217). This thermoplastic polymer attains a rubbery state at

physiological temperatures, resulting in higher toughness and superior mechanical properties (217)(222). In addition, PCL has desirable rheological properties with a glass transition temperature of 60 °C as well as a relatively low M.P temperature (-60 °C) (217)(219). PCL is also miscible with lipids and other polymers, forming mechanically compatible composites (217). Owing to its solubility and facile processability due to its low M.P and blend compatibility, PCL has attracted interest for various applications (217)(219). Like other biodegradable polymers, PCL has few drawbacks such as low encapsulation efficiency, burst release, and poor mechanical properties (218)(219). The combination of PCL with lipids and/or other polymers can prove to be an important strategy to overcome these drawbacks and to adjust their properties (mechanical and degradation kinetics) to achieve the desired release profile of therapeutic agents (219).

2.7.4.2. LPHNPs Synthesis

2.7.4.2.1. Two-step method of synthesis of LPHNPs

In the early days of development, the two-step method was frequently used in the preparation of LPHNPs (156). Conventional two-step method and the non-conventional two-step method are two subtypes of two-step method. In the conventional two-step method, preformed lipid vesicles are mixed with preformed polymer NPs. Electrostatic forces are responsible for the adsorption of lipid vesicles onto the preformed polymeric NPs (152)(156). Polymeric NPs are usually prepared by nanoprecipitation, emulsification-solvent evaporation (ESE), or high-pressure homogenization, and these formed polymeric NPs are then added either directly to dried lipid or to preformed vesicles obtained by hydration of a thin lipid film. Either way, LPHNPs are formed by the application of external energy through vortexing or ultra-sonication at a temperature higher than the phase transition temperature of the lipid component of LPHNP. The LPHNPs are then separated from free lipid vesicles by differential centrifugation (156)(223).

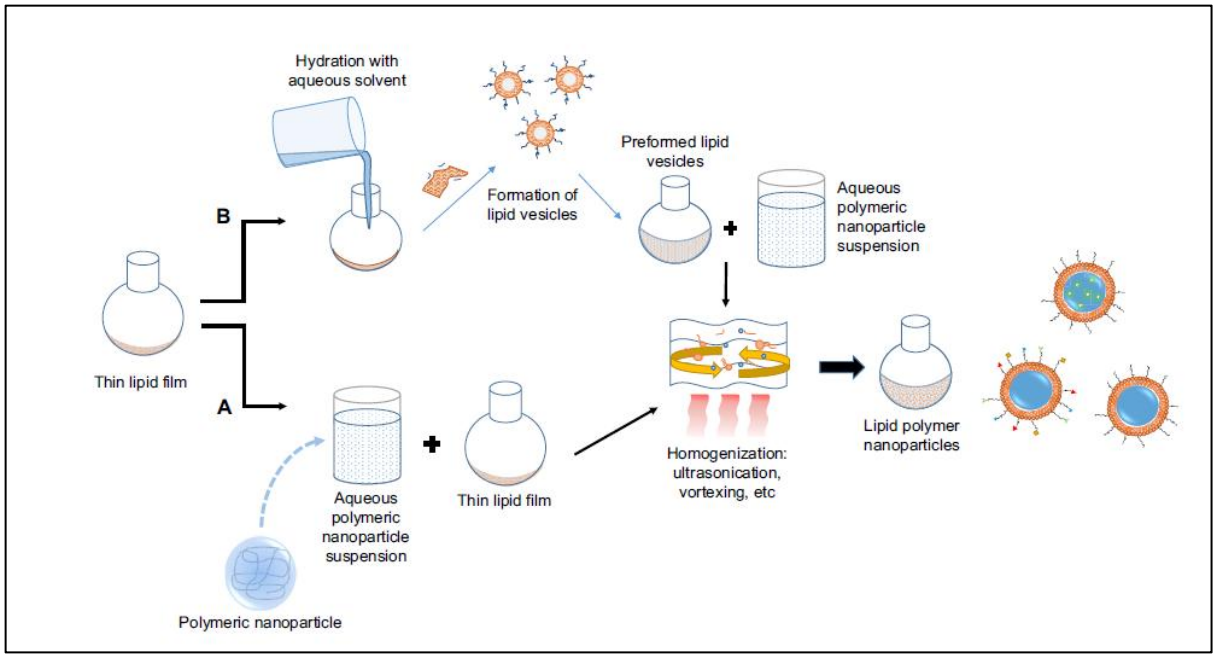

Fig. 2.6. Schematic representation of a two-way version of the LPHNP preparation via the two-step method. (A) The aqueous polymeric NP suspension is directly added to the dried lipid film. (B) The aqueous solvent is firstly used to hydrate the thin lipid film to allow facile formation of lipid vesicles, followed by the addition of polymeric NP suspension (223).

2.7.4.2.2. One-step method of synthesis of LPHNPs

Shortcomings of the two-step method such as time and energy consumption, batch-to-batch inconsistency, as well as low encapsulation efficiency (a result of drug leakage from the inner core during the second step) have led to the search for a more efficient method that would overcome the stated shortcomings such as reproducibility and content uniformity (152).

The one-step method is the alternative method to the two-step method that minimizes its shortcomings. Instead of having preformed polymeric NPs and preformed vesicles, this method involves mixing together the solution containing polymer and lipid. The lipids and polymer will self-assemble to form LPHNPs, either by nanoprecipitation or emulsification-solvent evaporation (152)(156). One-step preparation is generally achieved by nanoprecipitation, emulsification-solvent evaporation, which are further discussed in this section (152).

2.7.4.2.2.1. Nanoprecipitation method of synthesis of LPHNPs

Nanoprecipitation, also known as salting out, is a well-known method for the formulating of NPs of less than 100 nm in size (152). In this method, two miscible solvents with different

solubilizing powers for the polymer are used. The one with higher solubility (good solvent) for the polymer is usually an organic solvent, while the one with lower solubility (poor solvent) for the polymer is usually water (152). The polymer and drug (if there is one to be encapsulated) are firstly dissolved in the good (organic) solvent (such as acetone, acetronitrile, or ethanol) which is miscible with water. At the same time, the lipids (membrane-forming and functionalizing lipid, in our case lecithin and MA respectively) are dispersed in water. Usually, the dispersion of the lipids in water is carried out at 65-70 °C so as to form a homogeneous dispersion. The mixture containing the polymer is then added dropwise to the aqueous lipid dispersion under constant stirring, leading to the precipitation of the polymer into NPs. Simultaneously with the precipitation of the polymer, the lipids self-assemble around the polymer core and NPs are formed as a result of hydrophobic interactions. The tail of the lipids is attached to the polymer core while the hydrophilic head points outwards towards the aqueous phase. This leads to the formation of LPHNPs, which are stabilized by the lipids. Following solvent evaporation, the resulting LPHNPs are then recovered by centrifugation (223)(156).

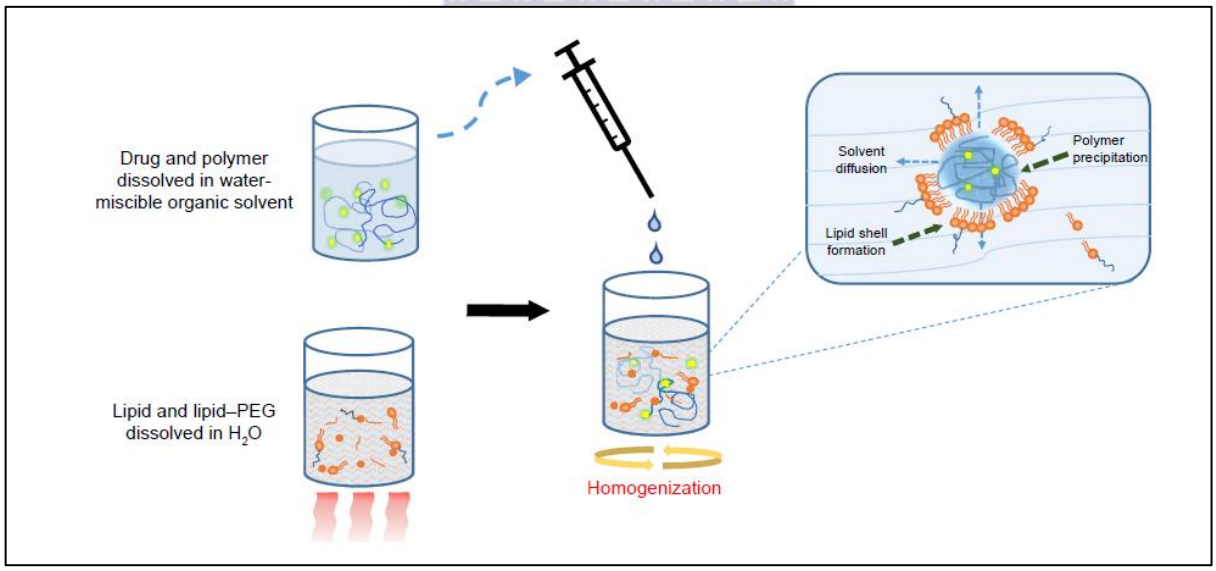

Fig. 2.7. The nanoprecipitation method for preparing LPHNPs. Polymer phase is added dropwise to the aqueous phase at 65-70 °C under constant stirring, resulting in the precipitation of the polymer into NPs. Simultaneously the lipids self-assemble around the polymer core and form LPHNPs (223).

2.7.4.2.2.2. Emulsification-solvent evaporation method of synthesis of LPHNPs

The emulsification-solvent evaporation (ESE) method is the most commonly used one-step method to synthesis LPHNPs (152). This method is divided into two types, namely a single

and a double emulsification solvent evaporation method. Each method is used depending on the lipophilicity of drug to be loaded into the NPs. The single ESE method is used when the drug to be loaded is a hydrophobic drug, while the double emulsification solvent evaporation (DESE) method is used for hydrophilic drugs (223). In the single ESE method, an oil in water (O/W) emulsion is formed. The oil phase is formed when the polymer and drug (if present) are mixed with a water immiscible solvent, while the aqueous phase is formed when the lipid is dissolved in water with constant stirring. (223). Subsequent to the emulsion formation, is the removal of the oil phase by evaporation which leads to formation of the polymer core and simultaneous, the self-assembly of the lipid around the polymer core (the same as in nanoprecipitation), resulting in the formation of LPHNPs with the tail of the lipids bonded to the polymer core while the hydrophilic head points outward towards the aqueous phase (152)(156).

In the DESE method, the aqueous phase is prepared by dissolving the drug (hydrophilic drug), while the oil phase is formed by the lipid and polymer dissolved in an organic solvent. After emulsifying the aqueous phase in the oil phase, the water in oil in water emulsion is formed by adding the formed emulsion to an aqueous solution containing lipids. Then LPHNPs are formed by removing the organic solvent (152). However, this method tend to result in larger sized NPs compared to other methods due to the formation of a multilayered shell around the polymer core following solvent evaporation (152).

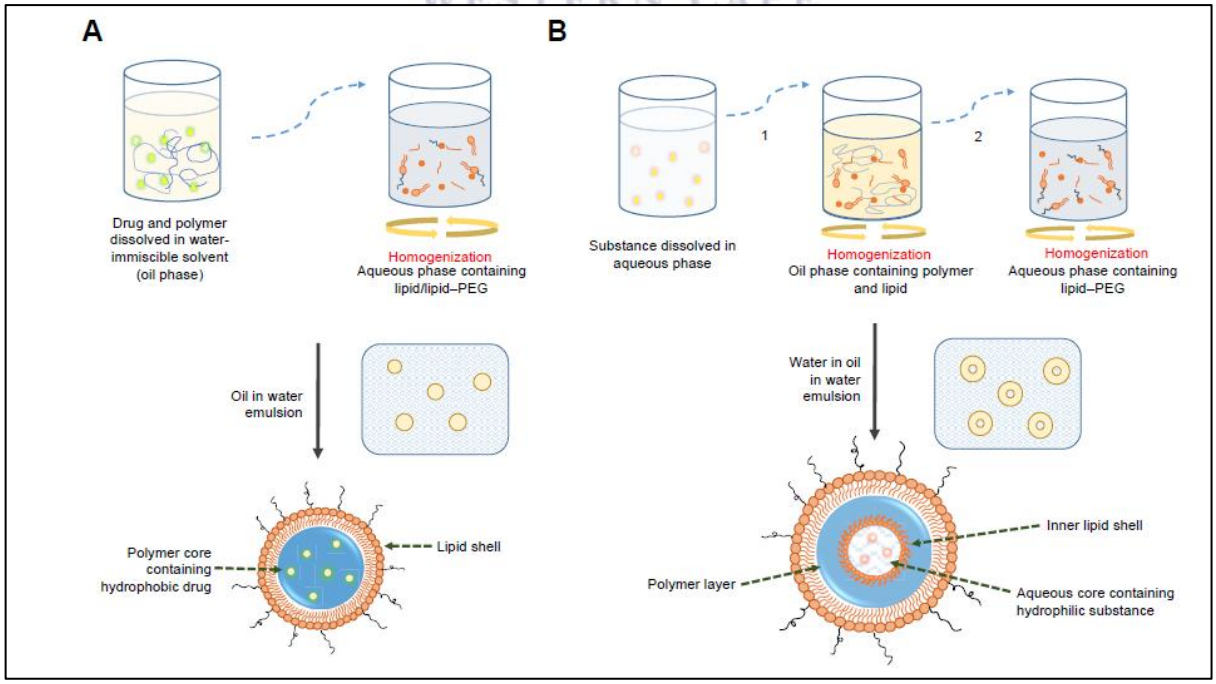

Fig. 2.8. LPHNP preparation method by emulsion solvent evaporation. A: Emulsification Solvent Evaporation preparation method. B: Double Emulsification Solvent Evaporation technique preparation method (223).

2.7.4.2.3. Non-conventional methods

Besides the conventional two-step method described above, two-steps non-conventional methods such as spray drying and soft lithography particle molding have been used to formulate LPHNPs (224)(225)(226)(227). Two-step non-conventional methods are usually used for large scale production of LPHNPs (228). Hitzman *et al.* (2006) used spray drying to formulate core-shell LPHNPs. Spray drying was used to prepare a polymeric core, which was thereafter mixed with a lipidic solution and spray dried to yield LPHNPs of 900-1200 nm (224). The large size of the NPs was associated with a spray dryer that was unsuitable for NPs synthesis, and the use of a suitable spray dryer has yielded NPs with a smaller, controlled size (224)(229). Hasan *et al*. (2012) used a soft lithography particle molding method to prepare lipid coated PLGA LPHNPs for gene delivery. The method yielded LPHNPs of about 200 nm. The size and shape of the NPs obtained depends on the mold used, hence this technique offers the possibility to control the size and shape of the LPHNPs obtained (225). Limitations such as technical complications due to mechanical problems and relatively low processing efficiency limit the widespread use of these methods (228).

2.8. Characterisation of polymers and NPs

2.8.1. Polymer characterization

Nuclear magnetic resonance (NMR) spectroscopy is an analytical technique that can be used for structure elucidation and quantification of polymers (230)(231). Proton (H^1) nuclear magnetic resonance (^{1}H NMR) spectroscopy was used to evaluate the formation of carboxyl-terminated PCL and to characterize and quantify the PCL-curdlan conjugate/copolymer.

Thermogravimetric analysis (TGA) is a thermal analysis technique that uses weight change and the rate of weight change as a function of temperature, time, and atmosphere to determine thermal stability and other physical processes such as desorption and adsorption, and also chemical processes such as solid-gas reaction and oxidation (232).

Hot stage microscopy (HSM) is another thermal analysis technique that was used. HSM combines thermal analysis and microscopy to study changes in physicochemical properties as a function of time and temperature. HSM allows the user to visualize physiochemical

transitions in real time during a thermal experiment (233). HSM analysis/results are coupled with TGA or differential scanning calorimetry (DSC) results and could potentially detect small changes TGA or DSC could miss (233).

2.8.2. Physiochemical characterisation of NPs

Dynamic light scattering (DLS) was used to characterize NPs for hydrodynamic size and PDI. Since small particles in a suspension are always undergoing Brownian motion, an instrument is used to measure Brownian motion at a certain temperature and scattering angle of 90 °C and correlates it with particle size (234)(235). This is achieved using the Stokes-Einstein equation, where the instrument calculates the intensity of the scattered light as a function of particle size (235). Using the same instrument, the zeta potential is characterized by laser dropper micro-electrophoresis to measure the surface charge of the NPs (235)(236). This technique applies an electric field to NPs in a suspension. The charged NPs move as a result of the applied electric field. The resultant velocity, which is a function of particle charge, suspending medium and electric field strength, is measured by a laser and used to determine the electrophoresis, which is then used to determine zeta potential (237). zeta potential, which represents the degree of repulsion between like-charged particles, is used to predict the stability of NPs on storage (238).

Although DLS provides size and PDI of NPs, advanced microscopic techniques such as scanning electron microscopy (SEM) and transmission electron microscopy (TEM) are used to specifically determine surface morphology and shape properties (239)(240). This is because of their high resolution, which generates clear images of the NP surface which can be used to determine size, surface morphology, and shape properties. For the SEM analysis, a suspension sample is mounted on a sample holder and allowed to dry completely. After drying, the sample is coated with a conductive metal such as gold using a sputter coater to make it electrically conductive. The sample is then scanned by a fine-focus beam of accelerated electrons, which interact with the sample surface to generate signals that are detected and used to create high-resolution SEM images (239)(241). For TEM, the images are obtained when a beam of accelerated electrons is transmitted through a layer of an ultra-thin sample placed on a metal grid, and the electrons interact with the sample as they pass through it (240) . To withstand vacuum and facilitate sample handling of NPs such as polymeric NPs, samples can be fixed with negative staining materials such as uranyl acetate

(240). The aim of performing these tests was to examine and analyze the size and morphology of NPs in the solid state.

2.8.3. Cytotoxicity and immune modulation characterization

2.8.3.1. Cytotoxicity assessment

The MTT (3-(4,5-dimethylthiazol-2-yl)-2,5-diphenyltetrazolium bromide) tetrazolium assay has long been used to assess metabolic activity in living cells and toxicity of NPs in the cellular environment (242)(243). Among all tetrazolium salts, MTT is the most used for cytotoxicity assessment and is considered the gold standard as it can be used as a unique method or in combination with other methods to assess toxicity (243)(244)(245). The assay is based on the enzymatic reduction of coloured MTT to its purple formazan salt crystals by viable cells (246). The water-insoluble formazan, which is spectrophotometrically quantifiable, is dissolved in DMSO and its absorbance is used to determine the percentage viability of treated cells compared to untreated cells, giving the ratio of viable cells (246)(247). choice of growth media, MTT concentration, pH, spectroscopic absorption wavelength as well as NP properties or the presence of other chemicals such as reducing agents or enzyme inhibitors can affect MTT results, therefore their consideration is of great importance to ensure optimal results when performing MTT assays (248)(249)(250)(251)(252).

2.8.3.2. Immune modulation assessment

2.8.3.2.1. Cytokine production

Cytokines are messengers that play an important role in regulating both the innate and acquired immune systems (78). Over 130 cytokines have been discovered. They play a role not only in the development, maturation and localization of cellular components of the immune system, but also in the initiation, execution, and suppression of both innate and acquired immunity against invading pathogens (80)(81)(253). Different cytokines perform various functions ranging from immunosuppression to immune stimulation i.e., while some cytokines are heavily involved in the elimination of invading pathogens or other triggering stimuli, others are responsible for preventing damage and restoring homeostasis after the elimination of the triggering stimulus (77)(254)(255). However, in some cases, the triggering stimulus cannot be effectively removed, leading to chronic cytokine secretion or excessive production of cytokines, resulting in tissue damage (78). Therefore, a fine balance should be struck when administering immunomodulators to avoid excessive cytokine production, as this

can lead to a cytokine storm or, as in the case of anti-inflammatory cytokine, immune suppression (76)(77)(78).

In response to a pathogen/stimulus, macrophages secrete tumor necrosis factor (TNF-α), followed by a release of potent pro-inflammatory cytokines (interleukin-1β (IL-1β), IL-6, IL-8, IL-17A, IL-18 and interferon-γ (IFN-γ)). This release of pro-inflammatory cytokines is then followed by the production of anti-inflammatory IlL-10 (77). Two cytokines, namely TNF-α and IL-10, were evaluated in this study.

2.8.3.2.1.1. Cellular effect of TNF-α

Activated macrophages are known to produce TNF-α, in fact most TNF-α is produced by activated macrophages, T-lymphocytes and natural killer cells (256). TNF-α produced by macrophages plays a role in orchestrating pro-inflammatory cytokines and mediating cytotoxic activities of macrophages. In addition, TNF-α regulates proliferation, differentiation and viability, apoptosis, as well as activation of macrophages (80)(81)(253). TNF-α exerts its activity by binding to two transmembrane receptors namely TNFR1 and TNFR2. While TNFR1 is expressed on the surfaces of numerous cells throughout the body, TNFR2 is mainly found in immune cells (256)(257). Due to the presence of death domain in TNFR1, binding to it may lead to apoptosis, while binding to TNFR2, which is mainly present in immune cells, orchestrates the release of pro-inflammatory responses (256)(257).

TNF-α also plays a crucial role in the pathogenesis of TB (258). This is because TNF-α is critically involved in granuloma formation and maintenance, and its suppression by IL-10 or other inhibitors has been shown to either disrupt granuloma formation or cause granuloma dissolution and TB dissemination (80)(259). TNF-α also plays a critical role in apoptosis of *M. tuberculosis* infected macrophages, which is essential for *M. tuberculosis* elimination, and its suppression by IL-10 reduces apoptosis, thereby increasing susceptibility to *M. tuberculosis* infection (80)(81).

2.8.3.2.1.2. Cellular effect of IL-10

IL-10 family is heavily involved in the immune response to diseases. The IL-10 family consists of IL-10, IL-20 subfamily IL-19, IL-20, IL-22, IL-24 and IL-26; and the distantly related cytokines IL-28A, IL-28B, and IL-29, more commonly classified as type III interferons (IFNs) and termed IFN-l2, IFN-l3, and IFN-11, respectively (260). The IL-10 family has a diverse biological function ranging from immunosuppression to immune

activation (261). IL-10 is one of cytokines from the IL-10 family involved in immune suppression (261). This cytokine is heavily involved in immune tolerance and dampening the immune response following the release of pro-inflammatory cytokines against a triggering stimulus (260)(262). IL-10 helps protect the host from the deleterious effects of pro-inflammatory cytokines, aids in tissue repair and healing or regeneration, and helps maintain homeostasis (260). As with any other cytokine, controlled release of this cytokine is required. Too little IL-10 can lead to cytokine storm and tissue damage, while excessive IL-10 levels lead to immunosuppression and chronic infection or inflammation as well as autoimmune diseases (76)(77)(78)(254)(255).

As mentioned in the literature review (see Section 2.2.1), *M. tuberculosis* uses a combination of immune stimulation and immunosuppression to invade the host, hence *M. tuberculosis* exploits IL-10 immunosuppression (85). *M. tuberculosis* upregulates the synthesis of IL-10, which in turn contributes to its survival, persistence and evasion of the immune system (82)(83)(84)(85). This is because IL-10 arrests phagosomal maturation, disrupts pathogen presentation and has been shown to reduce Th1-type responses and block other cytokines such as TNF-α, IL-12 and IFN-γ which are heavily involved in the immune response to TB (80)(81) (84)(263)(264)(265)(266)(267). In fact, a study by Redford *et al*. (2010) indicated that IL-10 knockout mice showed a significant reduction in *M. tuberculosis* bacterial load in the lungs and spleen and showed better control of *M. tuberculosis* infection compared to the control group (85). In another study, IL-10 transgenic mice failed to clear *M. tuberculosis* and suffered severe infections, resulting in death, compared to the control group (268). Elevated serum levels of IL-10 have also been observed in individuals infected with active TB (269). Therefore, the role of IL-10 in TB pathogenesis cannot be overemphasized, which is why it was evaluated in this study because of its ability to suppress both innate and acquired immune responses to *M. tuberculosis*.

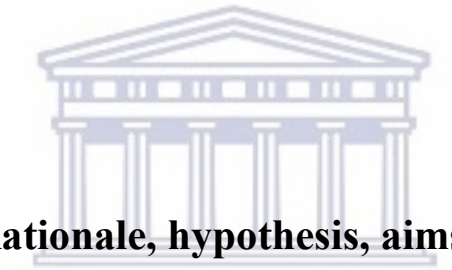

CHAPTER 3: Rationale, hypothesis, aims and objectives

3.1. Study rationale

TB remains one the world's deadliest infectious diseases from a single infectious agent, ranking above HIV, claiming approximately 1.4 million people every year. This disease is the leading cause of morbidity and mortality globally particularly in poor countries. TB is usually treated with a four-drug cocktail taken daily for a period of six months in two phases, namely a 2-month intensive phase of taking four drugs (isoniazid, rifampicin, ethambutol and pyrazinamide) followed by a four-month continuation phase of taking two drugs (isoniazid and rifampicin) daily. The prevalence of immunocompromised patients, especially HIV patients in African countries, particularly in South Africa, the outbreak of COVID-19 and the emergence of *M. tuberculosis* resistant strains such as M-DR and X-DR *M. tuberculosis* with few new drugs for TB treatment in the pipeline has made the situation alarming. Therefore, there is an unmet need for TB treatments, which calls for new and innovative treatments with new mechanisms of action. *M. tuberculosis,* the causative agent of TB, is an obligate intracellular organism that resides within immune cells, particularly macrophages, which normally represent the first line of defense against this pathogen. Through immune responses,

immune cells, including macrophages, either eradicate or halt the replication of *M. tuberculosis* by forming granulomas. However, in immunocompromised patients, *M. tuberculosis* survives within macrophages by suppressing the macrophage response. This study has proposed an approach to modulate immune responses (also known as immunotherapy) by stimulating immune macrophages to self-eradicate the *M. tuberculosis* using two immune modulatory compounds, namely MA and curdlan. Unlike current TB treatments, that target the pathogen, immunotherapeutic drugs target immune cells therefore, *M. tuberculosis* is unlikely to develop resistance mechanisms against these drugs. In this study, macrophage stimulation will be achieved through the use of curdlan, an immunomodulatory agent that has shown the ability to stimulate macrophages, and MA, a major lipid of the *M. tuberculosis* envelope, which is known to stimulate innate and acquired immune response due to its ability to act as a PAMP along with its ability to be presented to T cells by CD-1 molecules. NPs of the LPHNP type will be used to deliver curdlan and MA to macrophages. Therefore, the incorporation of MA and curdlan will impart biomimetic and immunostimulatory functionality to the LPHNPs. There are various types of NPs that can be used in delivery. However, LPHNPs are used in this project due to their ability to combine the advantages of the two mostly used and relatively safe drug delivery system, namely lipid and polymeric NPs, while overcoming their shortcomings.

The nanoprecipitation method will be used in the synthesis of LPHNPs due to its facile synthesis and its ability to produce smaller sized particles. This study focuses on the synthesis and characterization of LPHNPs functionalized with immunostimulatory biomimetic compounds. The result of this study provides a foundation for further studies to explore the use of biomimetic immunotherapeutic NPs in *in vitro* and *in vivo* models of *M. tuberculosis* infection.

3.2. Hypothesis

It was hypothesized that curdlan could be conjugated to PCL and the resulting copolymer could be used to formulate curdlan and MA loaded LPHNPs. It was further hypothesized that these LPHNPs are non-cytotoxic and possess macrophage stimulating capacity that depends on functionalization with curdlan and MA.

3.3. Aims

1. Synthesize and characterize PCL-curdlan copolymer.
2. Synthesize and characterize LPHNPs containing curdlan and MA.

3. Evaluate the cytotoxicity of the LPHNPs against RAW 264.7 macrophages.
4. Evaluate the immunomodulatory capability of the LPHNPs on RAW 264.7 macrophages.

3.4. Objectives

- To synthesize PCL-curdlan copolymer by conjugation of curdlan and PCL and to characterize the PCL-curdlan polymer.
- To synthesize LPHNPs containing curdlan and MA
- To determine the size, PDI, zeta potential and morphology of the NPs.
- To determine the cytotoxicity of the NPs against macrophages
- To determine the immunomodulatory capability of the NPs in macrophages

Chapter 4: PCL-curdlan copolymer synthesis and characterisation

4.1. Introduction

This chapter describes the polymerization of PCL and curdlan and the characterization of the resulting PCL-curdlan copolymer. To achieve the copolymerization of the polymers, an intermediate polymer, i.e. PCL-COOH was first synthesized using a ring opening synthesis method. The resulting PCL-COOH was then characterized and conjugated to curdlan to produce a PCL-curdlan copolymer. Polymers and the copolymer were physiochemical characterized to confirm the polymerization. After characterization, the copolymer was used in the synthesis and characterization of LPHNPs (see Chapter 5 for LPHNPs).

4.1.1. Aim and objectives

The aim for this part of the study was to synthesize and characterize PCL-curdlan copolymer. The objective was to synthesize PCL-COOH using different methods, to select the best synthesis method and to characterize PCL-COOH. A further objective was to conjugate PCL

and curdlan using the carbodiimide conjugation method and to characterize the resulting copolymer to confirm the copolymerization of both polymers.

4.2. Copolymer synthesis

4.2.1. Materials

ε-caprolactone (97 %), Glycolic (99 %), N,N-diisopropylethylamine (DIEA), N-hydroxysuccinimide (NHS), 1-Ethyl-3(3-dimethylaminopropyl)carbodiimide hydrochloride (EDC.HCl) and curdlan from *Alcaligenes faecalis* were purchased from Sigma-Aldrich (St Louis, MO). Dimethyl sulfoxide (DMSO) was purchased from Merck KGaA laboratory supplies (Darmstadt, Germany). Tetrahydrofuran (THF) was purchased from Riedel-De Haën AG (Honeywell specialty chemicals Seelze, Seelze, Germany). Unless otherwise indicated, all reagents were of analytical grade or higher and were used as received without further purification. Deionised water was used throughout the study and was obtained from a Barnstead EasyPure (II) UV-ultrapure water system (Thermo Fisher Scientific, USA).

The equipment used in this study included a bruker avance spectrometer (Bruker Avance IIID Nanobay, Bruker BioSpin GmbH, Rheinstetten, Germany), PerkinElmer 400 FTIR spectrophotometer (Perkin Elmer, Waltham, USA), PerkinElmer TGA 4000 instrument (PerkinElmer Waltham, USA), Linkam hot stage (Surrey, England) mounted on an Olympus SZX7 microscope (Nikon, Japan), Upright ultralow -86 °C freezer (NU-9668E, NuAire, USA), Centrifuge (Digicen 21, Orto Alresa, United Scientific), Vacuum pump (Rocker, Singhla Scientific, Haryana, India).

4.2.2. PCL-COOH synthesis by ring opening of ε-caprolactone using glycolic acid as the initiator

The procedure followed for the synthesis of PCL-COOH was adapted from Liu *et al.* (2010) with some modifications (270). Briefly, 33.3 mg of glycolic acid was added to a reaction vessel containing 1 g of ε-Caprolactone. The vessel was degassed using a vacuum pump for 1 min and then placed into an oil bath at 120 °C for 24 h under constant magnetic stirring (400 rpm). After 24 h, the reaction vessel was placed in ice for 10 min to stop the reaction. Tetrahydrofuran (THF) (10 mL) was slowly added to the reaction vessel (1 mL apart until the product was completely dissolved). Thereafter, PCL-COOH was precipitated by adding 50 mL of methanol (5: 1 ratio to THF). To extract PCL-COOH, the product was centrifuged at

10000 rpm for 10 min. The collected PCL-COOH was stored in a desiccator to allow complete drying.

4.2.3. PCL-diol and dioxane syntheses of PCL-COOH

The procedure followed during PCL-COOH synthesis was adapted from (271) with some modifications. Briefly, 80 mg of PCL-diol was added to 800 µl of dichloromethane (DCM) under nitrogen gas. 12 mg of succinic acid was added followed by the addition of 14.7 mg of 4-dimethylaminopyridine (DMAP) under constant stirring at 500 rpm. The reaction was allowed to take place for 24 h at room temperature. Sodium bicarbonate was added to neutralize unreacted succinic acid followed by the removal of the aqueous phase. DMAP was washed off at least 3 times by adding deionized water followed by the centrifugation of the solution for 10 min at 8 720 x *g*. The resulting product was dissolved in dDMSO and sent for NMR analysis. Dioxane synthesis followed synthesis of PCL terminated with carboxyl group as described in (271).

4.2.4. Conjugation of curdlan to PCL-COOH

The procedure followed for PCL-COOH conjugation was adapted from Tukulula *et al.* (2015) with some modifications (97). Briefly, 587 mg of PCL-COOH and 68.2 mg of curdlan were added to 6.8 mL of anhydrous dimethylformamide (DMF) and 6.8 mL of dimethyl sulfoxide (DMSO), respectively, at 60 °C under nitrogen gas and left to dissolve for 24 h under constant stirring (900 rpm). After 24 h, the PCL-COOH solution was placed in water at room temperature. To activate PCL-COOH, N-hydroxysuccinimide (NHS) (14.50 mg) was then added to PCL-COOH at 400 rpm until complete dissolution. Then N,N-Diisopropylethylamine (DIEA) (21.23 µl) and 1-ethyl-3-(3-dimethylaminopropyl) carbodiimide (EDC) (32.18 mg) were subsequently added and allowed to react for 3 h. After 3 h, the activated PCL-COOH (the solution containing PCL-COOH, NHS, DIEA, and EDC) was added dropwise to the dissolved curdlan and allowed to react at 60 °C for 48 h under nitrogen gas. After 48 h, the copolymer (PCL-curdlan) was precipitated by adding excess ice-cold deionized water and washed several times. The product was then collected, lyophilized over 3 days, and stored in a desiccator at room temperature.

4.3. PCL-curdlan copolymer characterization

Polymers (PCL, curdlan and PCL-curdlan) were characterized using ^{1}H NMR on a Bruker Avance spectrometer (Bruker, Massachusetts, USA) at 400 MHz. Deuterated DMSO

(DMSO-d_6) and/or deuterated chloroform ($dCDCl_3$) were used as internal standards. Data were analyzed using Bruker Topspin 4.1.1 software (Bruker, Massachusetts, USA).

Fourier transform infrared spectroscopy (FTIR) was used to investigate the PCL-COOH and curdlan interaction to form PCL-curdlan. The FTIR spectrum was performed using a PerkinElmer 400 FTIR spectrophotometer (Perkin Elmer, Waltham, USA). Pressing at 15000 psig, the solid powder samples were scanned in the spectral range of 4000 to 650 cm^{-1}. Data were analyzed using Spectrum GX series model software (Perkin Elmer, Waltham, USA).

Thermal analysis was carried out using Thermogravimetric analysis (TGA) and hot stage microscopy (HSM). TGA was used to determine changes in thermal stability as a result of the copolymerization of PCL-COOH and curdlan. The observed changes were compared to individual polymers and a 50:50 physical mixture of curdlan and PCL-COOH. A PerkinElmer TGA 4000 instrument (PerkinElmer Waltham, USA) was used to perform TGA on samples with a heating rate of 10 °C/ min from ambient temperature to 600 °C under nitrogen. Data were analyzed using Pyris 6 TGA software (PerkinElmer Waltham, USA). HSM was used to observe thermal transitions of the polymers. A Linkam hot stage (Surrey, England) mounted on an Olympus SZX7 microscope camera (Nikon, Japan) was used to analyze the samples. The samples were heated from ambient temperature to 600 °C in silicone oil at a heating rate of 10 °C/min.

4.4. Results and discussion

4.4.1. Synthesis and characterisation of PCL-curdlan copolymer

4.4.1.1. PCL-COOH characterisation

To synthesize curdlan containing NPs, it is essential to synthesize PCL-COOH which is thereafter conjugated to curdlan to produce a PCL-curdlan copolymer for use in the synthesis of the NPs. Therefore, it was imperative to first synthesize and characterize PCL-COOH. To synthesize PCL-COOH, three methods were attempted (Fig. 4.1.) (270)(271)(272). ^{1}H NMR was used to select the best synthesis route and to determine if PCL-COOH was being produced. This is because ^{1}H NMR can be used to analyze polymers quantitatively and qualitatively (230)(231)(273)(274). Proton (^{1}H) NMR analysis of PCL-COOH was performed using a Bruker 400 REM instrument (400 MHZ) (Bruker, Massachusetts, USA) and the analysis was carried out using Bruker Topspin 4.1.1 software (Bruker, Massachusetts, USA).

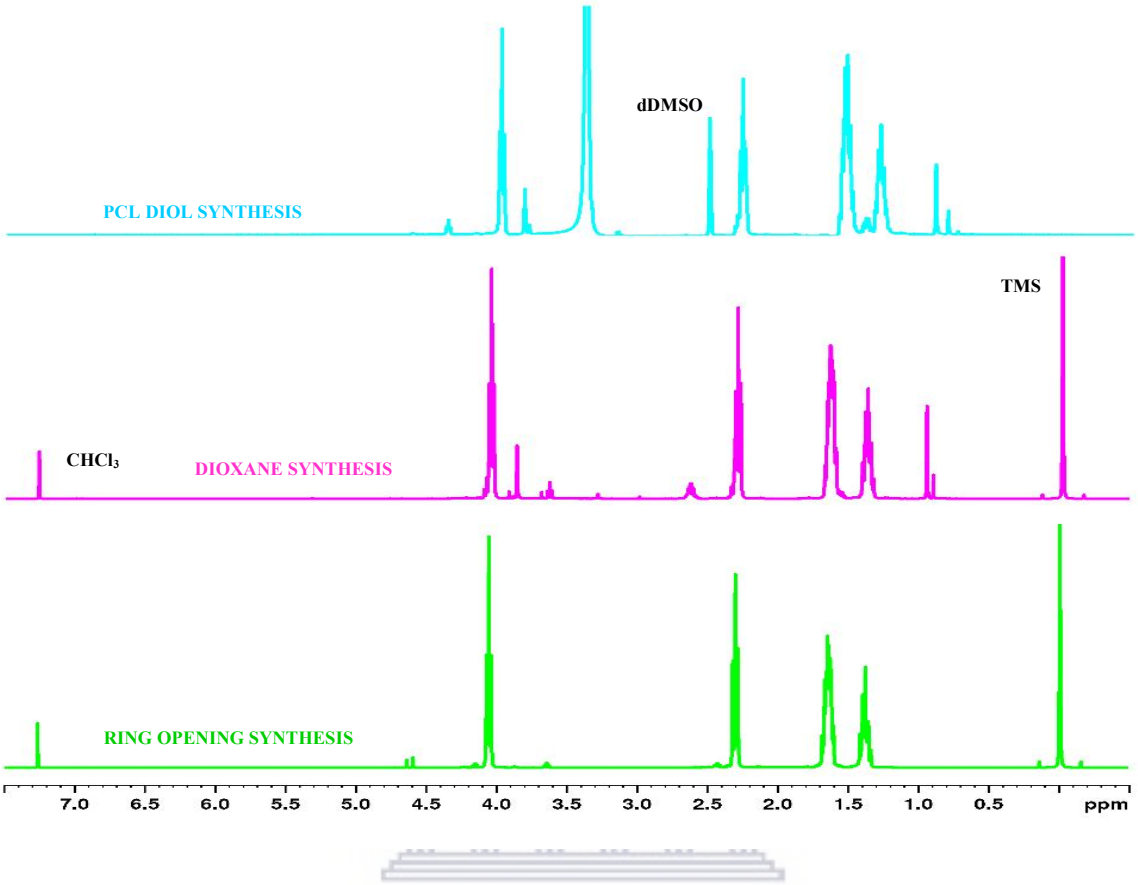

Fig. 4.1. The three synthetic routes attempted to produce the PCL-COOH polymer. The ring opening method was chosen as the method of choice for synthesis because of the following reasons: (i). Starting material are less toxic, (ii) simpler reaction and clean up and (iii), the NMR showed the 'cleanest' spectrum.

From the NMR results obtained as seen in Fig. 4.1., it was clear that the ring opening synthesis produced the cleanest spectrum while retaining the peak of interest as shown in Fig. 4.2. The starting material used in this synthesis were less toxic compared to those used in other methods such as dioxane and the synthesis reaction and clean up were the simplest. Thus, ring-opening method was selected as the method of choice for PCL-COOH synthesis.

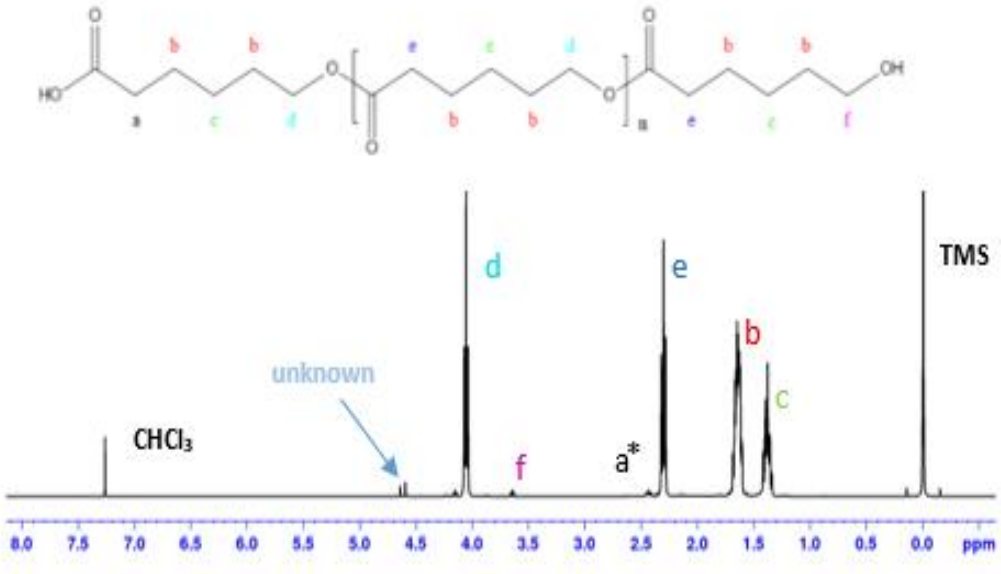

Fig. 4.2. ^{1}H NMR spectra of PCL-COOH obtained from ring opening synthesis. The spectra show a new peak at about 2.4 ppm (marked a*) attributed to the presence of -COOH group.

The NMR spectra of PCL-COOH (Fig. 4.2.) obtained from ring-opening synthesis showed a new peak at about 2.4 ppm (marked a*). This peak indicates the methylene group bonded to the carboxyl group of the newly formed PCL-COOH (275). The obtained PCL-COOH was carried forward for PCL-curdlan copolymer synthesis as indicated in Fig. 4.3.

4.4.1.2. PCL-curdlan copolymer characterisation

4.4.1.2.1. NMR spectroscopy PCL-curdlan copolymer

Carbodiimide conjugation method was used in the synthesis of PCL-curdlan. It is the most commonly used conjugation method in polymer based drug delivery (276). Essentially, this method works by adding NHS and carbodiimide compounds to activate carboxyl groups and form NHS-ester intermediates which are then conjugated to primary amines via an amide bond (276). Following COOH synthesis, PCL-curdlan copolymer was synthesized by carbodiimide chemistry. ^{1}H NMR, FTIR, TGA and HSM to characterize the obtained product. The ^{1}H NMR results of the PCL-curdlan copolymer are presented in Fig. 4.3.

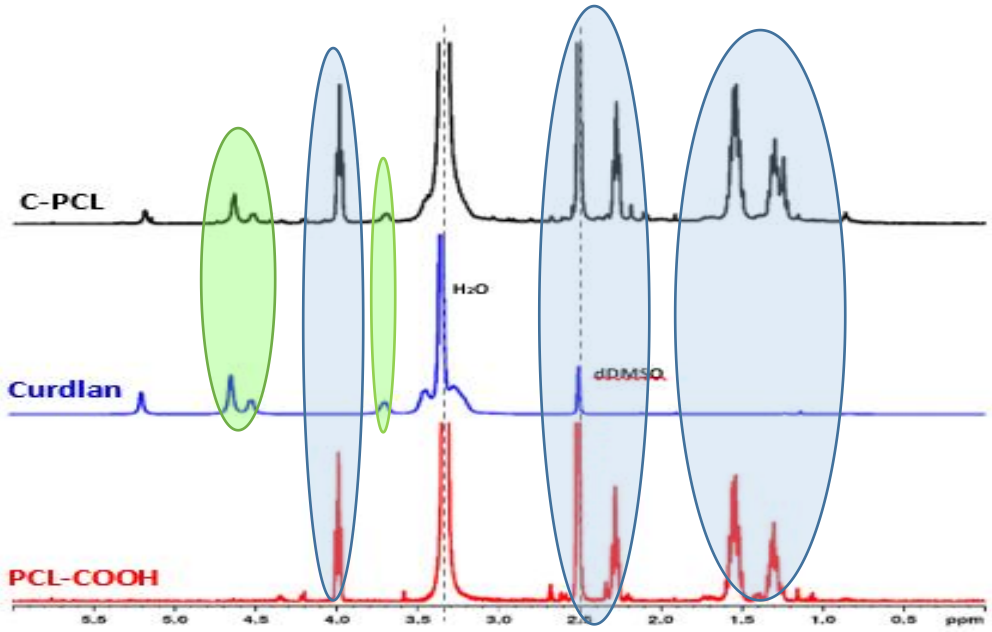

Fig. 4.3. Overlay of ^{1}H NMR spectra of PCL-COOH, curdlan, and PCL-curdlan copolymer. The shadings highlight some of the common peaks in the polymers and the newly synthesized PCL-curdlan copolymer.

The PCL-curdlan NMR spectrum (Fig. 4.3.) shows peaks from both the curdlan and PCL-COOH spectra, indicating the presence of both polymers in the newly formed product (PCL-curdlan). However, the presence of both PCL-COOH and curdlan does not guarantee the conjugation of the two polymers; thus, further characterizations were required to prove the copolymerization of both curdlan and PCL-COOH through carbodiimide chemical conjugation, which has also been used to conjugate other polymers such as PLGA and curdlan (97). Topspin 4.1.1 software (Bruker, Massachusetts, USA) was used to integrate the PCL-curdlan spectra to determine the ratio and percentage concentration of both curdlan and PCL-COOH in the newly formed product. The integral values of peaks resonating at about 3.6 ppm for curdlan and that at about 1.5 ppm for PCL-COOH were used. About 15 % of curdlan was found to be present in the product, the rest was PCL. FTIR and various thermal analysis methods were used to investigate the conjugation of curdlan and PCL in the products.

4.4.1.2.2. FTIR spectroscopy PCL-curdlan copolymer

FTIR was used to study the interaction between curdlan and PCL-COOH. The interaction would be proven by the presence of typical characteristic functional groups of both polymers in the formed product (PCL-curdlan).

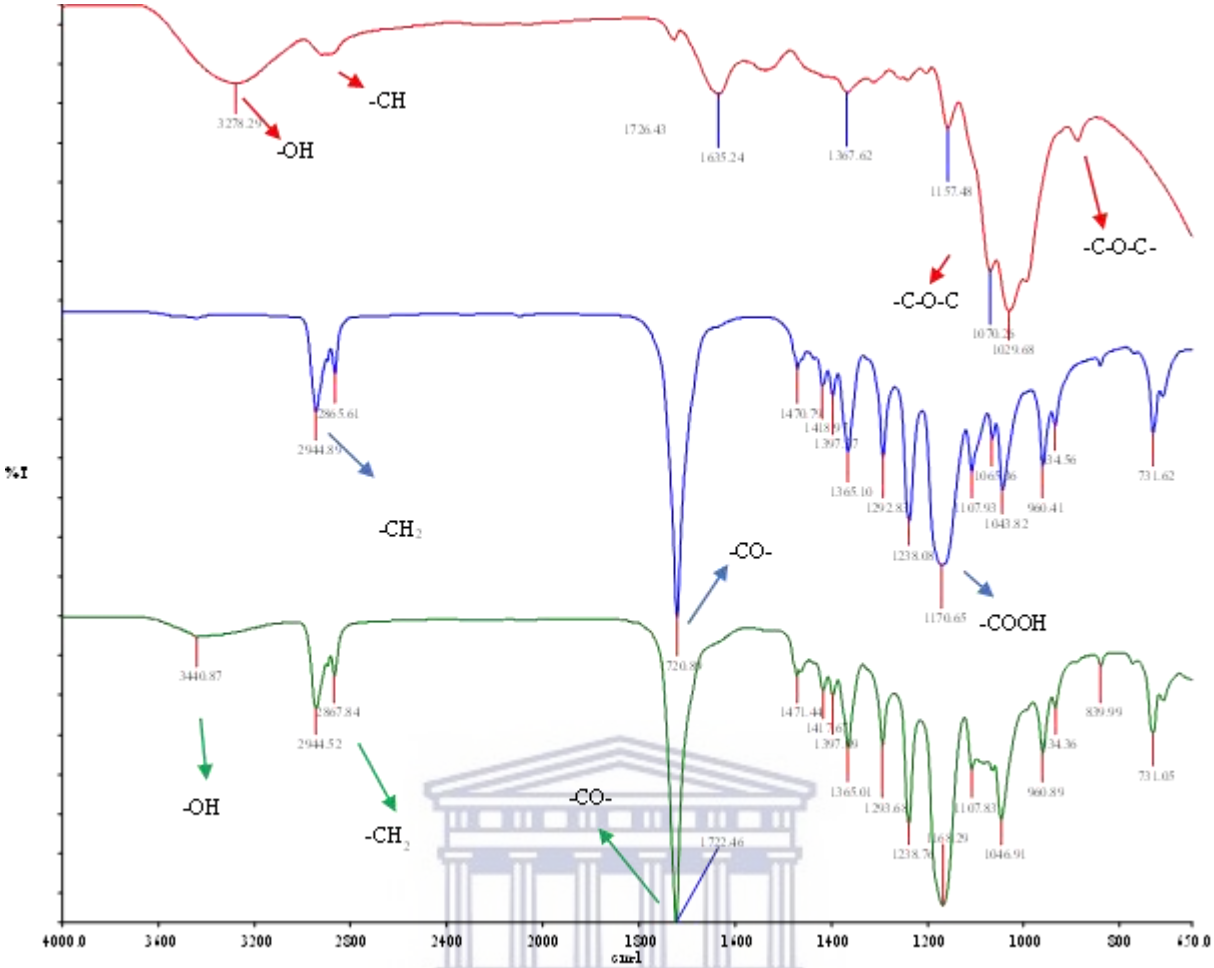

Fig. 4.4. Overlay of FTIR spectra of curdlan (red), PCL-COOH (blue), and PCL-curdlan (green)

The FTIR overlays of curdlan, PCL-COOH and C-PLGA are presented in Fig. 4.4. The curdlan spectrum exhibits a strong peak at 3278 cm^{-1} which was assigned to the -OH (hydroxide) bond, while those at 2920 cm^{-1}, 1100-1190 cm^{-1} and 892 cm^{-1} were assigned to -CH stretching, C-O-C bonds and the β-linked glycosidic bridges found in polysaccharides (97). PCL-COOH exhibits absorption peaks at 2945 cm^{-1} and 2866 cm^{-1} that were attributed methylene groups (-CH_2-) stretching and peaks at 1721 cm^{-1} and 1170 cm^{-1} that were attributed to the vibrations of -CO- and COOH groups (275)(277). PCL-curdlan shows some combination of peaks from both compounds, which could be indicative of their conjugation. However, additional tests were required to prove the conjugation. Thermal analytical methods were used for this purpose.

4.4.1.2.3. TGA analysis of PCL-curdlan copolymer

TGA was used to study the thermal behaviour of curdlan, PCL-COOH, their physical mixture, and the resulting carbodiimide conjugation product.

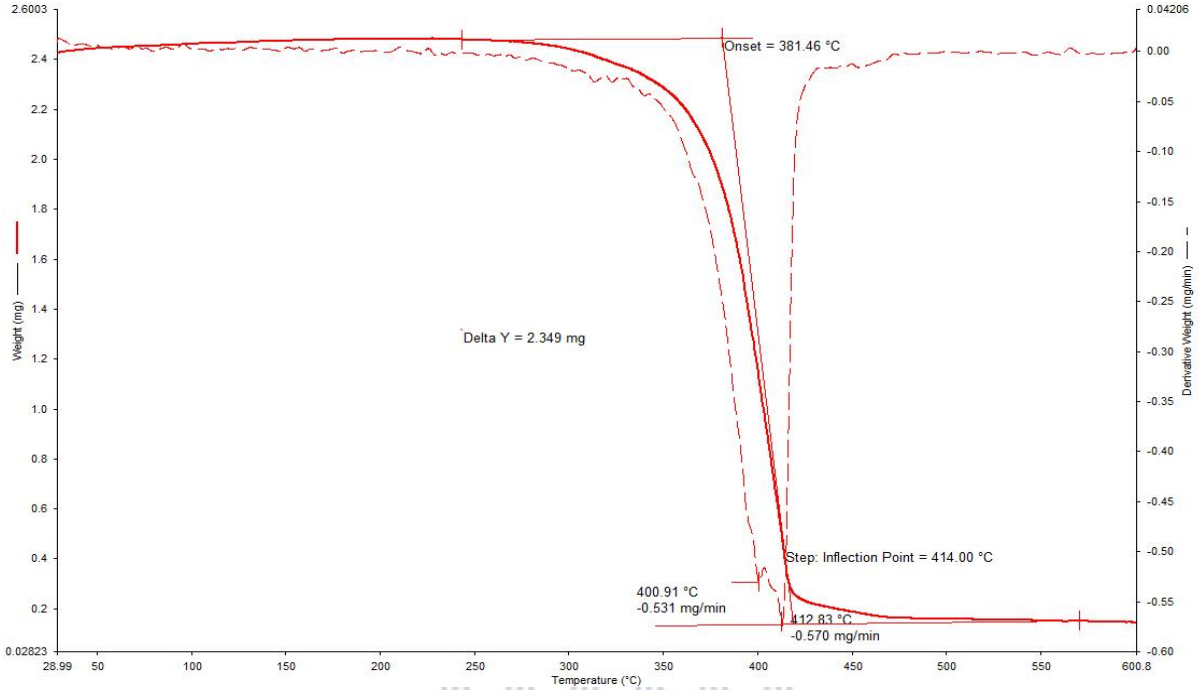

Fig. 4.5. TGA thermogram curves of PCL-COOH revealing two inflection points.

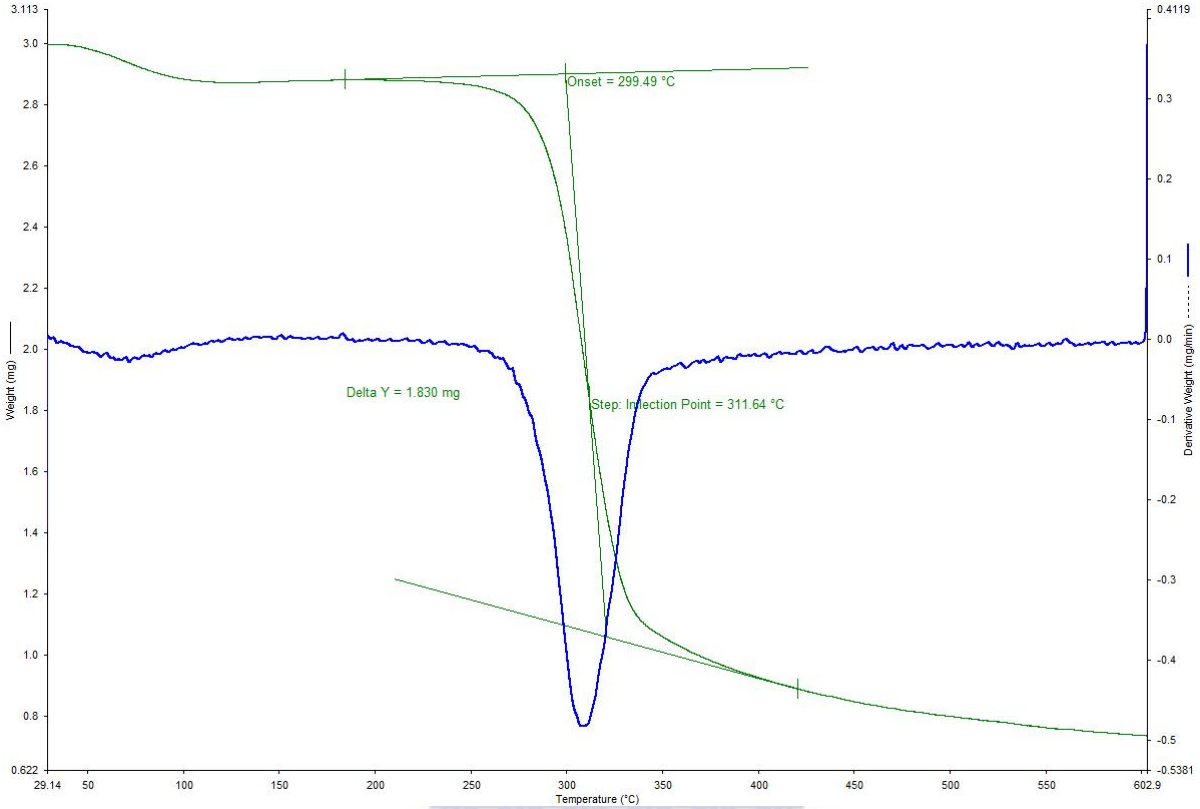

Fig. 4.6. TGA thermogram curve of curdlan indicating two weight losses. The first weight loss from 50-150 °C was attributed to desorption and water loss, while the second weight loss from 250-400 °C was associated with curdlan decomposition.

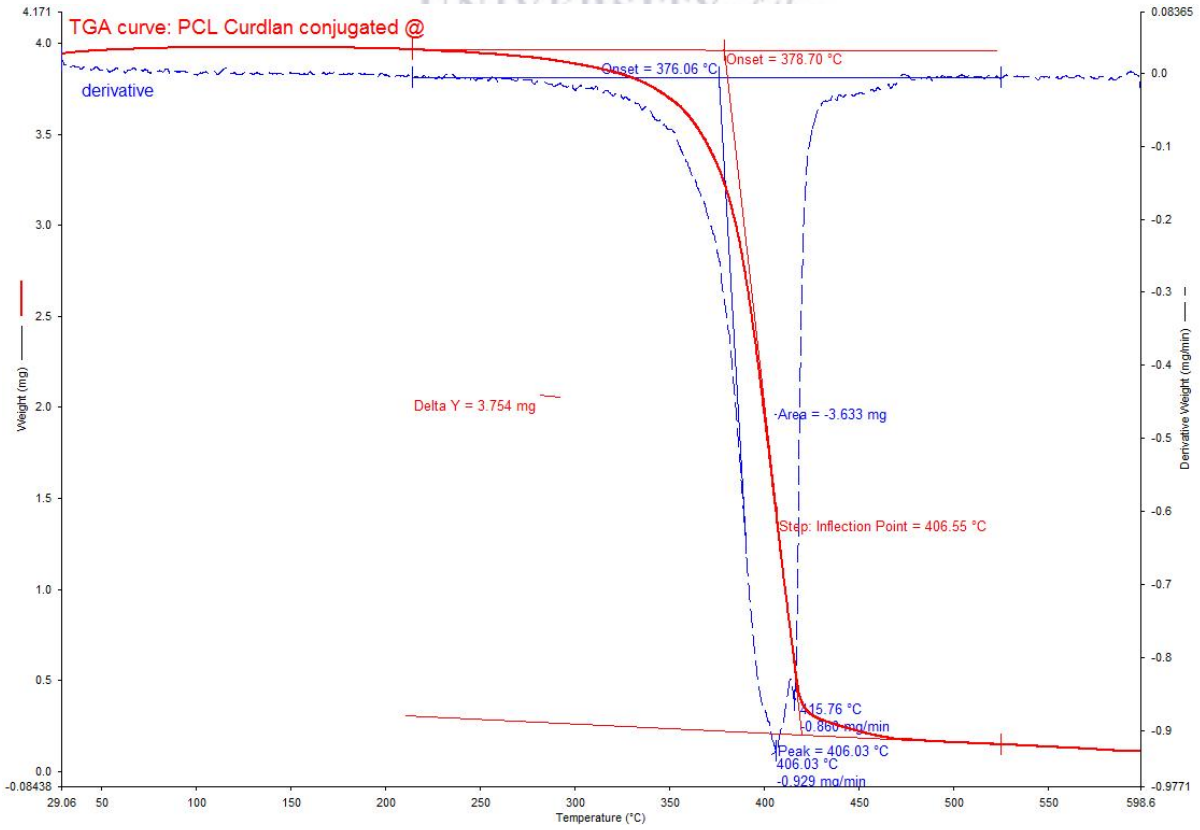

Fig. 4.7. TGA thermogram curves of the physical mixture of curdlan and PCL-COOH physical mixture indicating the two infection points as observed on the PCL-COOH thermogram

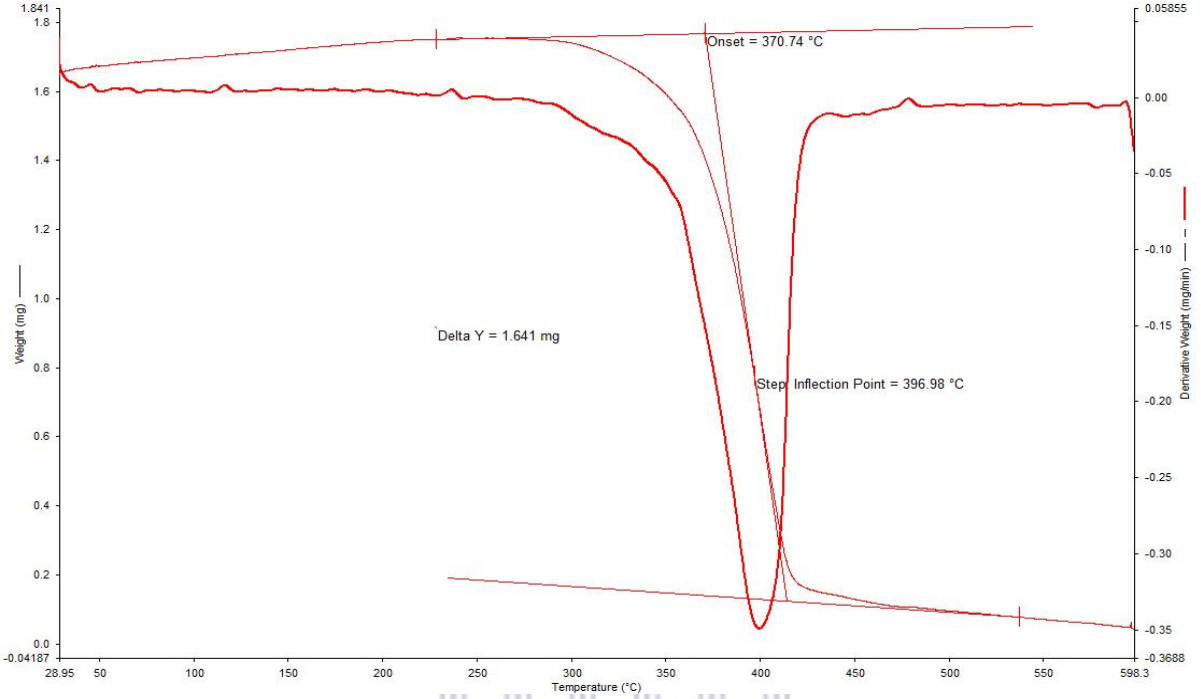

Fig. 4.8. TGA thermogram curve of PCL-curdlan showing one infection point as opposed to two infection points shown in Fig.4.7 of the physical mixture.

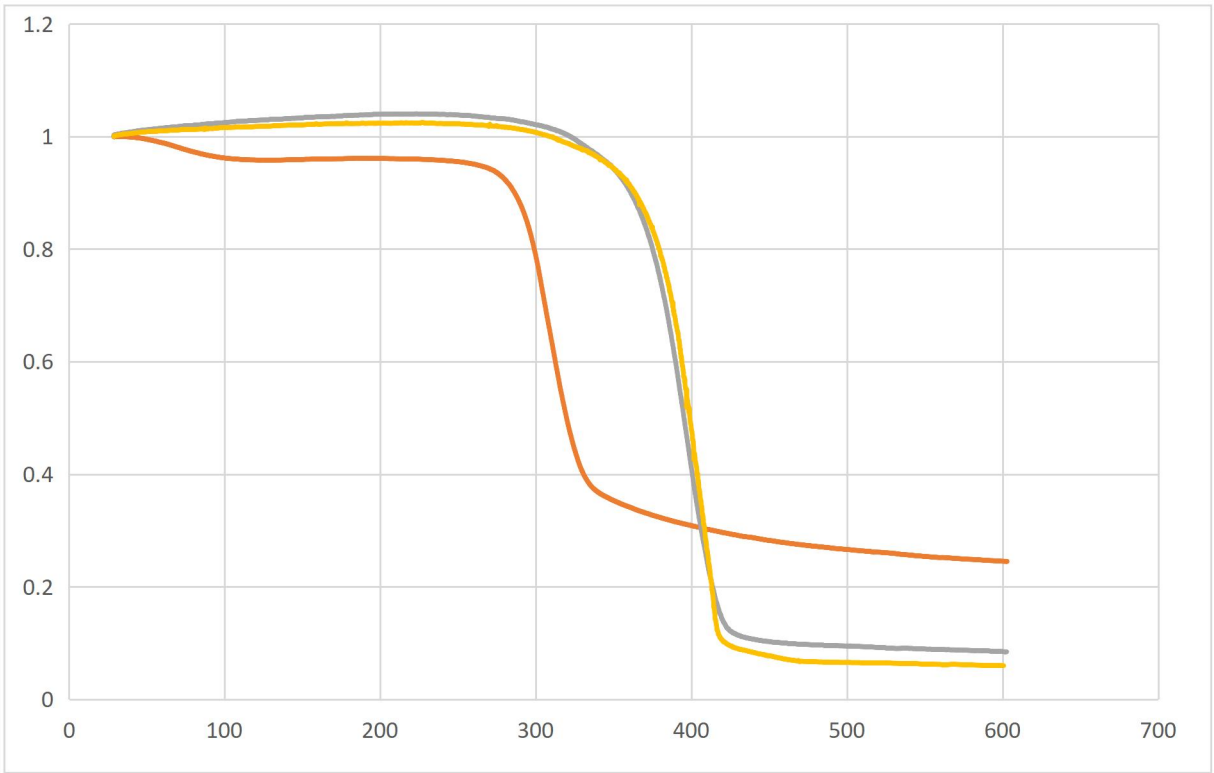

Fig. 4.9. TGA thermogram curves of curdlan (red), PCL-COOH (yellow) and PCL-curdlan (grey)

The resulting TGA thermogram of curdlan showed two weight losses as expected (Fig. 4.6). The first weight loss in the 50-150 °C ranges has been attributed to desorption and water loss, while the second weight loss in the 250-400 °C ranges can be associated with curdlan decomposition. As observed when curdlan-PLGA was analyzed, PCL-curdlan and PCL-COOH also showed a single weight loss curve (97). Like curdlan-PLGA, PCL-curdlan showed a slight increase in the rate of degradation with the highest weight loss observed at 397 °C (Fig. 4.8.), while the highest weight loss for PCL-COOH was observed at approximately 400 °C and 412 °C (Fig. 4.7.). This change was attributed to thermal instability caused by grafting/copolymerization, which was reported to introduce "weak links" which makes the graft susceptible to thermal degradation (278)(279). It was also worth noting that when a physical mixture of PCL-COOH and curdlan was prepared without using carbodiimide conjugation, its TGA thermogram (Fig. 4.7.) revealed two inflection points as observed in the thermogram of PCL-COOH alone. This was not the case when PCL-curdlan obtained through carbodiimide conjugation was analyzed. The thermogram of PCL-curdlan (Fig. 4.8.) reveals a single infection point, suggesting an interaction when carbodiimide conjugation was used.

4.4.1.2.4. HSM analysis of PCL-curdlan copolymer

HSM views and studies physical transitions compounds undergo as a function of temperature and time (233). HSM was used to investigate any visible changes following the subjection of the polymers and copolymer to various temperatures over time.

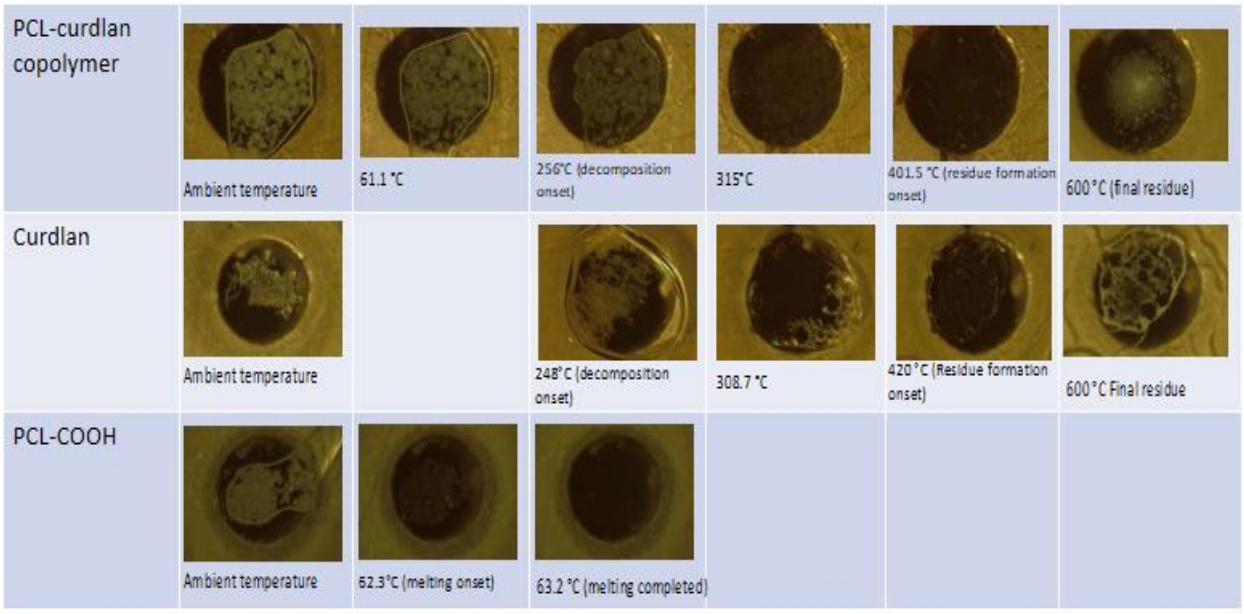

Fig. 4.10. HSM images of PCL-COOH, and PCL-curdlan copolymer.

The HSM results showed that PCL-COOH had completely melted at 62.3 °C. Had PCL-curdlan been a physical mixture of the two, it would be expected that a large mass loss would be observed since the PCL-COOH proportion is higher than that of curdlan. However, no melting of PCL-curdlan was observed at the same temperatures. The differences in physical changes between curdlan and PCL-curdlan were assessed as they were subjugated to various temperatures. It was noticed that the PCL-curdlan begins to decompose at 256 °C while curdlan begins at 248 °C. It was also noticed that residue formation started at about 401.5 °C for PCL-curdlan while it started at about 420 °C for curdlan. This difference in residue formation onset temperature is in keeping with the increased rate of degradation of the copolymer observed from the TGA results, supporting the introduction of 'weak links' as a result of polymer grafting that causes thermal instability. Finally, upon viewing the final residue of curdlan and PCL-COOH, it was clear that the two residues were notably different, also suggesting a form of interaction between PCL-COOH and curdlan when carbodiimide conjugation was used to form PCL-curdlan copolymer.

Taken together, all of the differences in physiochemical changes observed among PCL-COOH, curdlan and PCL-curdlan samples suggest formation of new chemical bonds. With the results from NMR indicating that only PCL-COOH and curdlan were present in the PCL-curdlan sample, it was concluded that a bond formed between PCL-COOH and curdlan through carbodiimide chemical conjugation. This bond was formed between the carboxyl

group of the PCL-COOH and the hydroxyl group of curdlan resulting in an ester bond that was responsible for all the observed changes.

Chapter 5: Synthesis and characterization of lipid-polymer hybrid NPs

5.1 Introduction

In addition to carefully considering possible controllable processes and parameters, NP characterization is essential. This chapter describes the synthesis and characterization of LPHNPs.

The lipid to polymer ratio has been shown to affect the properties of the resultant LPHNPs (146)(280). Therefore, the effect of various lecithin to PCL mass ratios on NP size, PDI, and zeta potential was investigated to determine the optimal ratio for NP synthesis from the most commonly reported % w/w mass ratio (10, 15, 20 and 25 % w/w of lecithin/PCL) (146)(280). This is because these properties determine the *in vitro* and *in vivo* properties of NPs such as stability, bioavailability, blood circulation, and excretion (146). Following the determination of the optimum % w/w mass ratio, different percentages of MA and curdlan were loaded onto lecithin/PCL LPHNPs. The functionalized NPs were thereafter characterized to study the effect of incorporation of MA and curdlan on the NP properties.

5.1.1. Aims and objectives

The aim of this part of the study was to synthesize and characterize LPHNPs including those containing MA and curdlan. The objective was to select the optimal % w/w mass ratio of lecithin/PCL from the most commonly reported ratios. A further objective was to use the determined ratio to synthesize and load LPHNPs with different percentages of MA and curdlan and to characterize the resulting NPs.

5.2. Materials

MA from *M. tuberculosis* (bovine strain), Lecithin (L-α-phosphatidylcholine from egg yolk (60 %)), curdlan from *Alcaligenes faecalis*, polycaprolactone (PCL) and chloroform were purchased from Sigma-Aldrich (St Louis, MO, United States). Chloroform was purchased from Merck KGaA (Darmstadt, German).

The equipment used included a probe sonicator (Sonoplus GM 2070, Bandelin, Germany), bath sonicator (Scientech, Ultrasonic Cleaners), magnetic stirrer (Kika Labortechnik, RCT Basic), thermometer (Brannan), Buchi rotary evaporator (Switzerland, RotavaporR11),

ZetaSizer, ZS-90 (Malvern, UK), analytical balance (Ohaus®, model GA 110), NMR spectrometer (Bruker Avance IIID Nanobay, Bruker BioSpin GmbH, Rheinstetten, Germany), UV-Visible spectrophotometer (Cintra 202, GBC Scientific Equipment, Australia) fluorescence micro-plate reader (Synergy Mx, BioTek Instruments, USA); Freezedryer (Virtis, freeze mobile model 125L),vacuum pump 4344 (Rocker, Singhla Scientific, Haryana, India); vortex mixer (VM-400, Gemmy Industrial Corp., Taiwan); water bath (Labcon®, model CDH 110 Maraisburg, South Africa), Centrifuge (Digicen 21, Orto Alresa, United Scientific) , rotary evaporator (Büchi, Labotec, South Africa), FEI Tecnai F20 transmission electron microscope (Thermo Fisher (FEI), Eindhoven, Netherlands), Tescan MIRA SEM, The EDS was done with the Thermo Fisher Nova NanoSEM230 using an Oxford X-max detector.

5.3. LPHNPs synthesis methods

5.3.1. Lecithin/PCL NP synthesis

The nanoprecipitation method was used to synthesize NPs of various ratios of lecithin/PCL. Four % w/w ratios namely 10 %, 15 %, 20 % and 25 % w/w of lecithin/PCL NPs were synthesized and characterized for size, PDI, and zeta potential. For a 15 % lecithin/PCL % w/w ratio, a 5 mg/mL concentration of lecithin in 5 mL water and a 25 mg/mL concentration of PCL in 6.67 mL chloroform were prepared under bath sonication. Table 1 shows all masses and volumes used to prepare NPs with various lecithin/PCL mass ratios (% w/w). The PCL solution was added dropwise (1 mL/min) to a lecithin/water solution with constant stirring (1000 rpm) on a magnetic stirrer. The resulting suspension was allowed to mix for 5 min with constant stirring (1000 rpm). It was then probe sonicated at 80 % power under ice for 2 min. After probe sonication, the product was placed on a rotary evaporator for approximately 1.5 h (until all organic solvent was completely evaporated). The resultant NPs were washed by placing the sample in a centrifuge for 10 min at 13 000 x *g*. The supernatant was then discarded and replaced with deionized water to redisperse the NPs. The suspension was then probe sonicated for 5 min. Thereafter, the NPs were characterized for size, PDI and zeta potential. Finally, after the addition of sucrose as a cryoprotectant at 0.125 % w/v in a ratio of 2:1 NP to sucrose, the NPs were lyophilized over three days.

Table 5.1. Required masses and volumes to prepare various lecithin/PCL ratios (% w/w) for the synthesis of LPHNPs. The concentration of lecithin and PCL remained constant throughout at 5 mg/mL (lecithin in water solution) and 25 mg/ mL (PCL in chloroform), respectively, however the mass of PCL was varied to yield different mass ratios (% w/w) while that of lecithin was kept constant.

% w/w ratio	10 %	15 %	20 %	25 %
PCL mass required (mg)	250	166.7	125	100
Lecithin mass (mg) required	25	25	25	25
Chloroform volume required (mL)	6.67	6.67	6.67	6.67
Water volume required (mL)	5	5	5	5

5.3.2. Lecithin/PCL/MA hybrid NP synthesis

Since it was determined that lecithin/PCL 15 % w/w was the optimal mass ratio (see section **5.5.**1), it was carried forward for further syntheses. PCL (166.7 mg), MA and lecithin were weighed depending on the percentage of MA required (see Table 2 for masses of lecithin and MA required for various % w/w incorporation of MA in the NPs). MA and PCL were dissolved in 6.67 mL of chloroform while lecithin was dissolved in 5 mL of water using a bath sonicator. MA-PCL solution was added dropwise (1 mL/min) to lecithin solution for about 5 min with constant stirring (1000 rpm) under a magnetic stirrer. The product was then probe sonicated at 80 % power for 2 min and then placed on a rotary evaporator for approximately 1 h for solvent evaporation (until all organic solvent was completely evaporated). The resultant NPs were washed by placing the sample in a centrifuge for 10 min at 13 000 x *g*. The supernatant was then discarded and replaced with deionized water to redisperse the NPs. The NPs were probe sonicated for 5 min and characterized for size, PDI, and zeta potential. Finally, after addition of sucrose as a cryoprotectant at 0.125 % w/v in a ratio of 2:1 NP to sucrose, the NPs were lyophilized over three days.

Table 5.2. Masses of lecithin and MA required for the synthesis of different percentages of MA. Due to its insolubility in water, MA was dissolved in chloroform while lecithin was dissolved in water. The mass of PCL remained constant (166.7 mg)

MA (% w/w)	2 %	5 %	8 %
Lecithin mass required (mg)	21.166	15.415	9.66
MA mass required (mg)	3.83	9.59	15.34
PCL mass required (mg)	166.7	166.7	166.7

5.3.3. PCL/ lecithin-curdlan NP synthesis

Briefly, 25 mg of lecithin, PCL and PCL-curdlan copolymer were weighed depending on the % w/w of curdlan required (Table 3). PCL and PCL-curdlan were dissolved in 6.67 mL of chloroform while lecithin was dissolved in 5 mL of water. PCL and PCL-curdlan solution was added dropwise (1 mL/min) to lecithin solution for about 5 min with constant stirring (1000 rpm) under a magnetic stirrer. The product was then probe sonicated at 80 % power for 2 min and then placed on a rotary evaporator for approximately 1 h for solvent evaporation (until all organic solvent was completely evaporated). The resultant NPs were washed by placing the sample in a centrifuge for 10 min at 13 000 x *g*. The supernatant was then discarded and replaced with deionized water to redisperse the NPs. The NPs were probe sonicated for 5 min and characterized for size, PDI, and zeta potential. Finally, after addition of sucrose as a cryoprotectant at 0.125 % w/v in a ratio of 2:1 NP to sucrose, the NPs were lyophilized over three days.

Table 5.3. Masses of curdlan and PCL required for various curdlan percentages. PCL and curdlan were dissolved in chloroform at a combined concentration of 25 mg/mL.

Curdlan (% w/w)	**2 %**	**5 %**	**10 %**
PCL mass required (mg)	141.14	102.8	38.9
PCL-curdlan mass required (mg)	25.56	63.9	127.8
Lecithin mass required (mg)	25	25	25

5.3.4. PCL/lecithin-MA-curdlan NPs synthesis

Briefly, it was found that 2 % w/w curdlan and 2 % w/w MA containing NPs were the highest non-toxic concentrations (see Chapter 6.) PCL (141.14 mg), PCL-curdlan copolymer (25.56 mg), lecithin (21.166 mg), and MA (3.834 mg) were weighed. PCL, PCL-curdlan, and MA were dissolved in 6.67 mL of chloroform while lecithin was dissolved in 5 mL of water. PCL, PCL-curdlan, and MA solution was added dropwise (1 mL/min) to the lecithin solution for about 7 min with constant stirring (1000 rpm) under a magnetic stirrer. The product was then probe sonicated at 80 % power for 2 min and then placed on a rotary evaporator for approximately 1 h (until all organic solvent was completely evaporated). The resultant NPs were washed by placing the sample in a centrifuge for 10 min at 13 000 x *g*. The supernatant was then discarded and replaced with deionized water to redisperse the NPs. The NPs were probe sonicated for 5 min and characterized for size, PDI, and zeta potential. Finally, after addition of sucrose as a cryoprotectant at 0.125 % w/v in a ratio of 2:1 NP to sucrose, the NPs were lyophilized over three days.

5.3.5. Determination cryoprotectant concentration

To determine the lowest sucrose concentration, serial dilutions of 1 % w/v were made to the lowest concentration of 0.0625 % w/v. NPs were lyophilized without cryoprotectant and with 0.0625 %, 0.125 %, 0.25 %, 0.5 % and 1 % w/v sucrose, over three days. NP suspension was mixed with sucrose solution in a ratio 2:1 (v/v). Size, PDI and zeta potential of the NPs

before and after lyophilization were measured and compared to determine the lowest sucrose concentration without significant effect on the NP properties.

5.4. LPHNPs characterization

5.4.1. LPHNPs characterization for size, PDI, and zeta potential

To determine the hydrodynamic size and the PDI, 1 mL of the suspension was added to a disposable polystyrene cuvette. The sample was analyzed at 25 °C with a minimum of three runs. Average size and PDI were reported. A DTS70 cell was used to determine the zeta potential. The NP suspension was injected into the cell until the electrodes were completely covered by the suspension medium. The sample was analyzed at 25 °C with a minimum of three runs and the average zeta potential was reported. Data were analyzed using Malvern Zeta Sizer software (version 8.00.4813) and statistical analysis was performed using GraphPad Prism 9.1.1 version (GraphPad software, San Diego, California, USA).

5.4.2. SEM and TEM analysis

TEM imaging was performed using a FEI Tecnai F20 transmission electron microscope (Thermo Fisher (FEI), Eindhoven, Netherlands) operated at 200 kV. Images were collected using a DE-16 camera (Direct Electron, USA). For negative staining TEM, carbon-coated copper grids (Agar Scientific, UK) were rendered hydrophilic using a EMS100 Glow Discharge Unit (Electron Microscopy Sciences, USA). Droplets of the sample were placed on the grids and negatively stained with 2 % uranyl acetate (SPI Supplies, USA).

SEM imaging was performed using a Tescan MIRA3 SEM (Tescan, Brno, Czech Republic), operated at an acceleration voltage of 5 kV with a magnification range of 20-100 000 times with in-Beam secondary electron detector. Energy disperse spectroscopy (EDS) was performed using a Thermo Fisher Nova NanoSEM230 using an Oxford X-max detector and INCA software. ImageJ software (National Institute of Health, USA) was used to analyze and process TEM and SEM images.

5.5. Results and discussion

5.5.1. LPHNPs size, PDI and Zeta potential characterization using dynamic light scattering

DLS was used to characterize the size of the four % w/w ratios of lipid to polymer. The results indicated that synthesized NPs of various ratios of lecithin/PCL ranged from 120-170 nm. For 10 % w/w lecithin/PCL, the size was 170.00 ± 63.97 nm; for 15 % w/w, the size was 120.16 ± 13.57 nm; for 20 %, the size was 166.14 ± 38.66 nm and for 25 % w/w, the size was 169.44 ± 49.53 nm, all of which were within nanometer range (134)(146)(149). Statistical analysis showed a statistically significant difference between the 15 % w/w ratio and the rest as shown in Fig. 5.1. (a). Previously, it has been reported that when PLGA and lecithin were used, a mass ratio of 10 % to 20 % w/w gave better LPHNP properties (149). A lipid to polymer mass ratio of 15 % w/w lecithin, PLGA and polyethylene glycol (PEG) has also been shown to provide the minimum lipid to polymer mass ratio to formulate NPs (lecithin/PCL-PEG) below 100 nm. A mass ratio of 15 % w/w was chosen as the optimal mass ratio as it provides sufficient lipid coverage of the PCL core and sufficient surface area for NP functionalization without significantly affecting their properties (149)(280). A higher lipid to polymer ratio provides excess lipid, which can lead to self-assembly of liposomes or increased viscosity of the dispersed phase, which in turn affects homogeneity efficiency and hence particle size (146)(149).

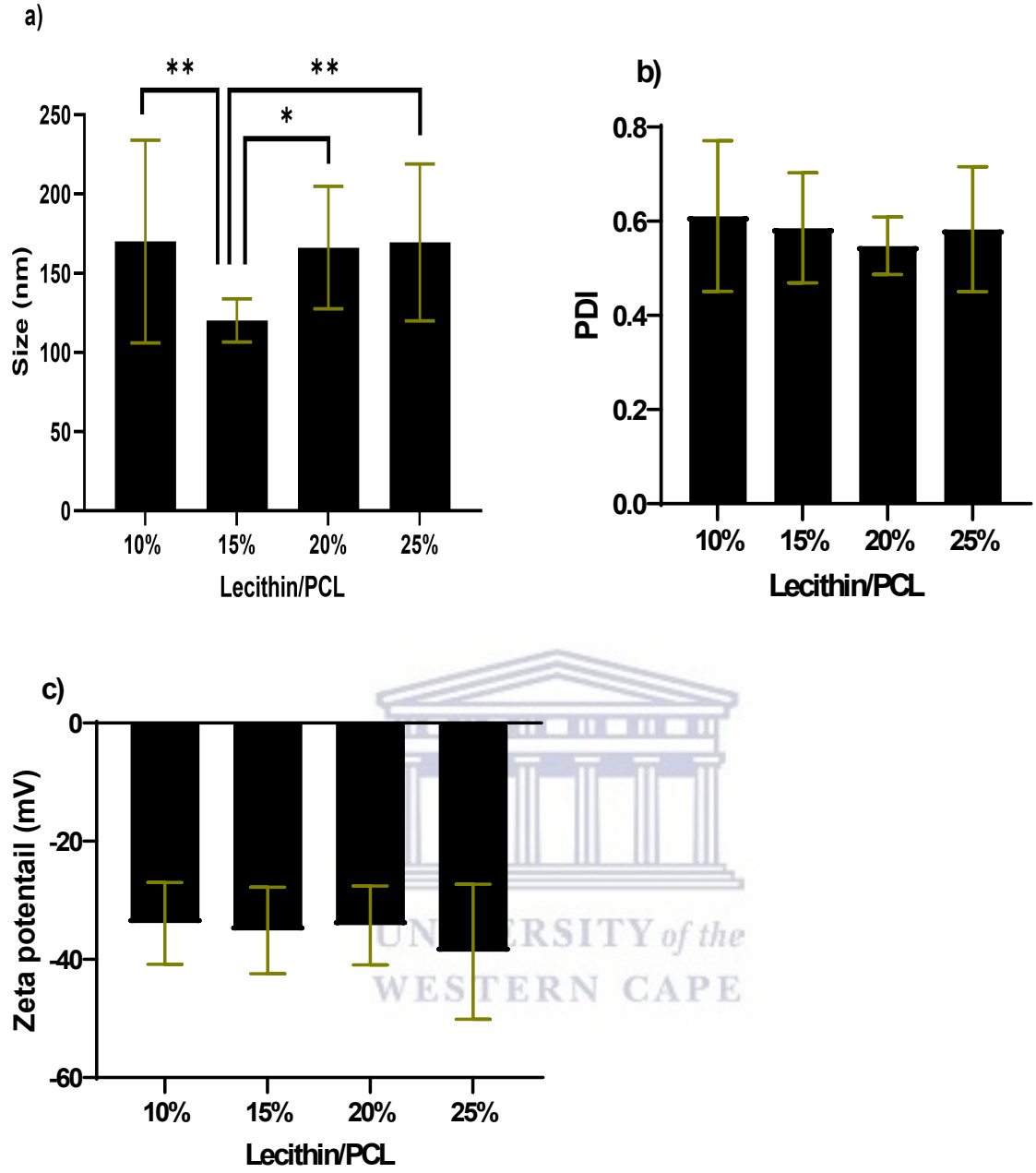

Fig. 5.1. Size, PDI and zeta potential comparison of various lecithin/PCL % w/w mass ratios after washing (n=8). (a) Size comparison of various % w/w mass ratios. The results showed that there was a statistically significant difference between the 15 % w/w and the rest. (b) PDI comparison of various % w/w mass ratios. The results showed no statistical significance between the ratios. (c) Zeta potential comparison of various % w/w mass ratios showing no statistical significance between the ratios. Statistical significance was indicated by not significant (ns) (p-value > 0.05), *: significant (p-value ≤ 0.05), **: very significant (p-value ≤ 0.01). T: standard deviation.

On the other hand, as shown in Fig. 5.1. (b) changes in the lipid/polymer % w/w mass ratio did not affect the PDI. The PDI ranged from 0.5 to 0.7, suggesting that the NPs were

polydisperse. This was speculated to be due to the use of PCL. PCL is a synthetic polymer and depending on the synthetic route and processes, some synthetic polymers such as PCL tend to be polydisperse in nature due to the polymerization reactions involved in its synthesis (281). Therefore, it was speculated that the polydispersity of PCL affected the PDI of NPs, yielding NPs with a slightly higher PDI.

The zeta potential, which represents the degree of repulsion between like-charged particles, is another crucial property that was characterized to predict the stability of NPs on storage. NPs with good stability have a zeta potential of ±30 mV (282). The zeta potential of the synthesized NPs ranged from -33.90 ± 6.93 mV to -38.70 ± 11.41 mV which were all less than -30 mV, which falls within the acceptable the range of less than -30 mV (149)(282). This suggests that NPs would exhibit good stability on storage as a suspension. The negative charge of NPs can be attributed to the carbonyl group of the PCL and phosphate groups of the lecithin (283)(284)(285)(286)(287). Statistical analysis showed no significant difference between the ratios, suggesting that various ratios did not significantly affect zeta potential. The negative charge of NPs suggests that they could be less toxic and more stable *in vivo* (146)(288).

In summary, the results showed no statistical significance in terms of their PDI and zeta potential. However, there was a statistically significant difference in size between the 15 % w/w ratio and the rest. Based on this difference, 15 % w/w was chosen as the optimal % w/w mass ratio to carry forward for further experiments.

After determining the optimal % w/w mass ratio of lecithin to PCL, other types of NPs were synthesized. MA and/or curdlan were conjugated to lecithin/PCL LPHNPs. MA conjugated LPHNPs ranged from 163.20 ± 31.11 nm to 225.10 ± 92.08 nm and showed no statistically significant difference between various MA loaded NPs in terms of their size, as indicated by Fig. 5.2. (a). There was also no statistically significant difference between various curdlan conjugated NPs as indicated by Fig. 5.3. (a). As indicated by the cytotoxicity studies, 2 % w/w mycolic and 2 % w/w curdlan loaded NPs were the highest non-toxic concentrations (see Section 6.4). Compared to 15 % lecithin/PCL NPs, it was observed that there was a statistically significant difference in size between unconjugated (lecithin/PCL only) (120.16 ± 13.57 nm) and MA (2 % w/w) (206.13 ± 66.37 nm), curdlan (2 % w/w) (327.85 ± 40.00 nm) and 2 % w/w (of each) MA-curdlan (269.13 ± 84.64 nm) loaded NPs. It was also observed that the difference between MA (2 % w/w) loaded NPs and curdlan (2 % w/w) was

statistically significant and it was speculated that this was due to the difference in their solubility in organic solvent. MA is fully soluble in chloroform (the organic solvent used in the synthesis of NPs), while curdlan, a linear polysaccharide, is not completely soluble in most organic solvents including chloroform used in the synthesis.

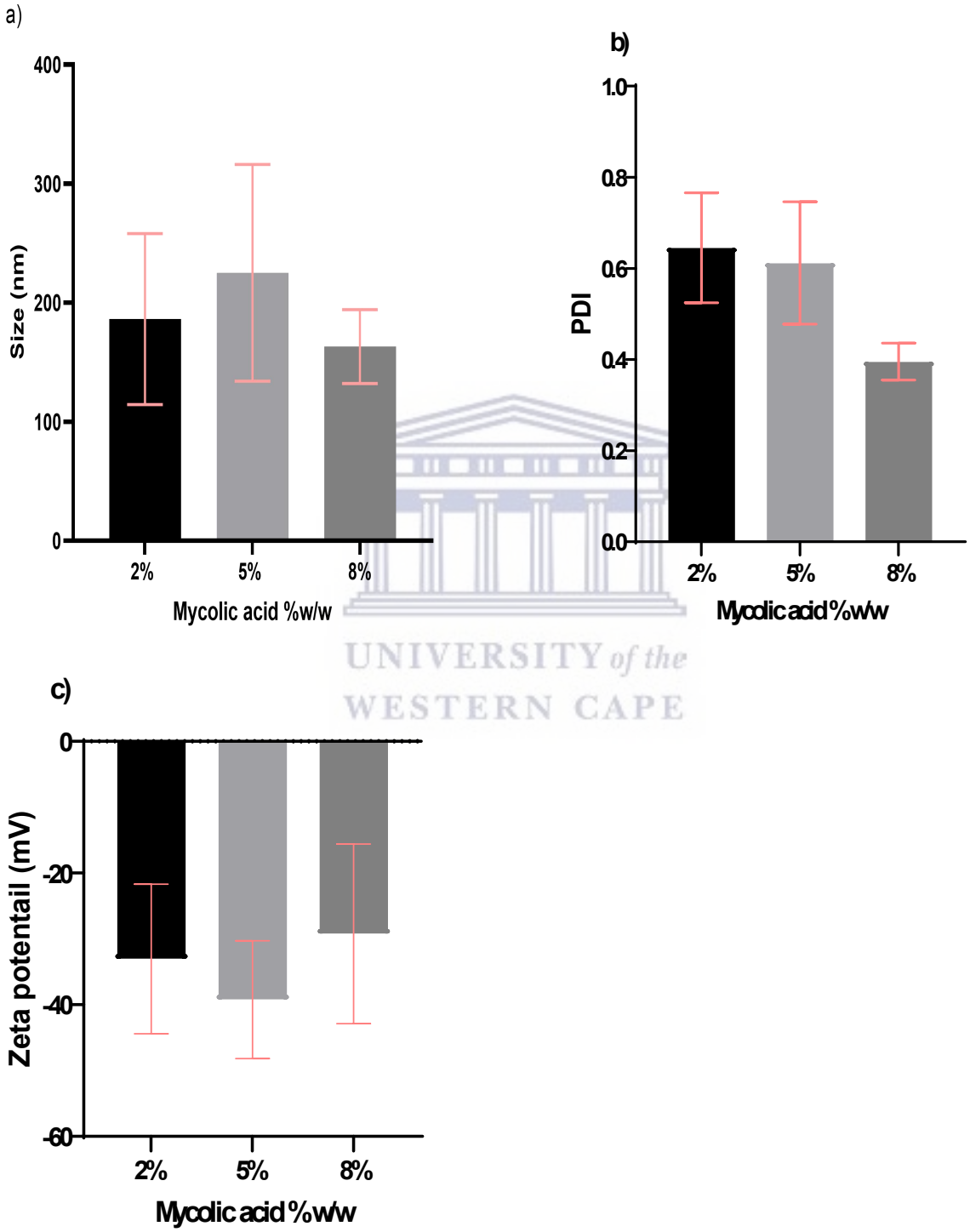

Fig. 5.2. Size, PDI and zeta potential comparison of NPs after conjugation of lecithin/PCL 15 % w/w ratio with various MA % w/w (n =3). (a) size comparison of various MA (% w/w) conjugated NPs. The results showed that there was no statistically significant difference between MA concentrations. (b) PDI comparison of various MA (% w/w) conjugated NPs. The results showed no statistical significance between the MA concentrations. (c) Zeta potential comparison of MA (% w/w) conjugated NPs showing no statistical significance between MA concentrations. Statistical significance was indicated by not significant (ns) (p-value > 0.05), *: significant (p-value ≤ 0.05), **: very significant (p-value ≤ 0.01). T: standard deviation.

It was also observed that after loading MA and curdlan, there was no statistically significant difference between various MA (% w/w) conjugated NPs, while there was a slight difference between 2 % w/w and 5 % w/w curdlan conjugated NPs in terms of their PDI. When compared to lecithin/PCL only LPHNPs, it was observed that there was no significant difference between curdlan and MA loaded NPs at 2 % w/w curdlan or MA, and lecithin/PCL NPs with respect their PDI (Fig. 5.4. (b)).

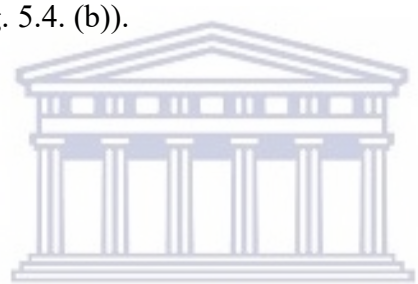

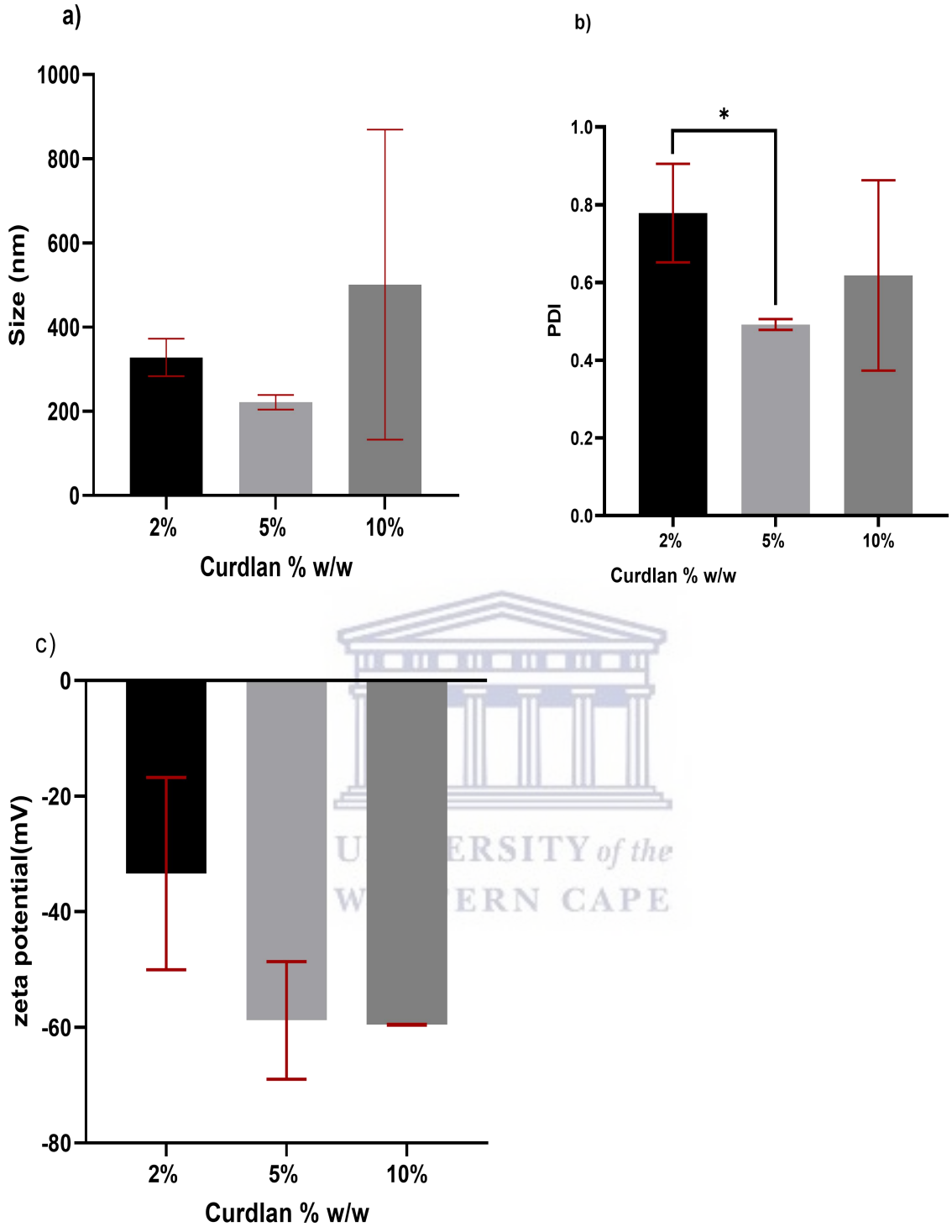

Fig. 5.3. Size, PDI and zeta potential comparison of NPs after conjugation of lecithin/PCL 15 % ratio (% w/w) with various curdlan % w/w (n=3). (a) PDI comparison of various curdlan (% w/w) conjugated NPs. The results showed that there was no statistically significant difference between the curdlan concentrations. (b) PDI comparison of various curdlan (% w/w) conjugated NPs. The results

showed no statistical significance between the curdlan concentrations. (c) Zeta potential comparison of curdlan (% w/w) conjugated NPs showing no statistical significance between curdlan concentrations. Statistical significance was indicated by not significant (ns) (p-value > 0.05), *: significant (p-value ≤ 0.05), **: very significant (p-value ≤ 0.01). T: standard deviation.

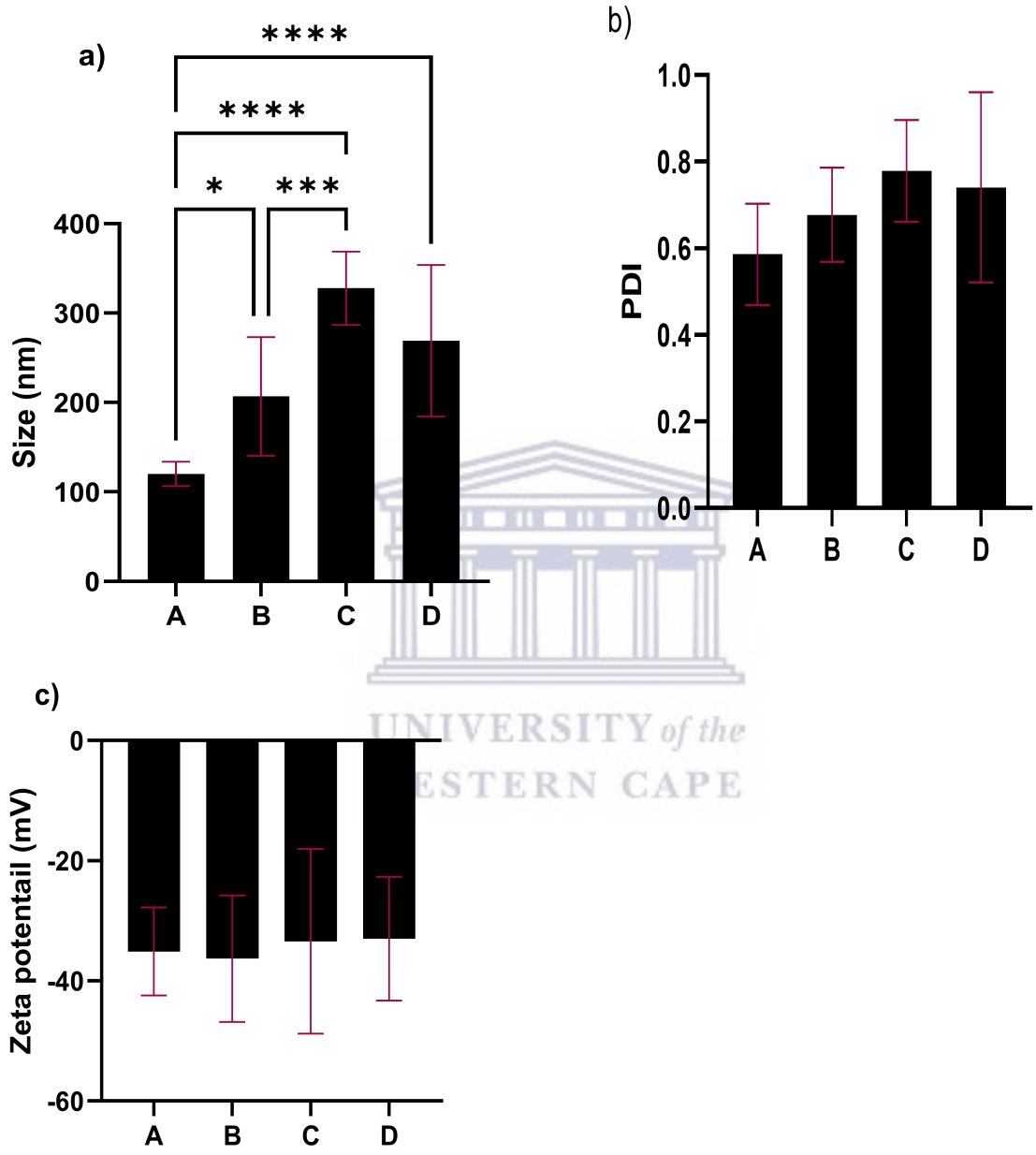

Fig. 5.4. Size, PDI and zeta potential comparison of the highest non-toxic concentrations of MA (2 % w/w) and Curdlan (2 % w/w) conjugated NPs with lecithin/PCL only (15 % w/w ratio) (n=3) (A: unconjugated 15 % w/w lecithin/PCL LPHNPs, B: conjugated MA 2 % w/w LPHNPs, C: conjugated curdlan 2 % w/w LPHNPs, D: 2 % w/w of each MA and curdlan conjugated LPHNPs. (a) Size

comparison of conjugated and unconjugated NPs. The results showed a statistically significant difference between unconjugated lecithin/PCL and MA (2 % w/w) or curdlan (2 % w/w) conjugated NPs. (b) PDI comparison of conjugated and unconjugated NPs. The results showed a statistically significant difference between curdlan conjugated and unconjugated NPs. (c) Comparison of the zeta potential of conjugated and unconjugated NPs. The results showed no statistically significant difference between conjugated and unconjugated NPs. Statistical significance was indicated by not significant (ns) (p-value > 0.05), *: significant (p-value ≤ 0.05), **: very significant (p-value ≤ 0.01), ***: extremely significant (p-value ≤ 0.001), ****: extremely significant (p-value ≤ 0.0001). T: standard deviation.

5.5.2. Determination of the concentration of the cryoprotectant sucrose

A sucrose concentration of 1 % (w/v) is often used as a cryoprotectant (289)(290). However, when it was attempted to use the same concentration after lyophilization, it was found that due to the low yield of NP synthesis, a relatively high concentration of sucrose was present, which could hamper accurate NP measurement and hence further experiments. It was also found that NPs lyophilized without sucrose showed a significant change in properties before and after lyophilization, confirming the necessity of the cryoprotectant (Fig. 5.5.). Following this observation, attempts were made to lower the sucrose concentration without affecting the stability of the NPs. Serial dilutions of 1 % w/v were made and used as cryoprotectants during lyophilization and the results are presented in Fig. 5.5. A comparison of size, PDI and zeta potential of different concentrations of cryoprotectants indicated that 0.25 % and 0.125 % sucrose concentration showed no change in these properties compared to the commonly used 1 % sucrose concentration. A comparison between sucrose 0.25 % w/v and 0.125 % w/v showed no statistically significant difference (Fig. 5.5.) in terms of size, PDI and zeta potential. Therefore, a sucrose concentration of 0.125 % was chosen as the lowest stable cryoprotectant concentration to be used throughout NP lyophilization, as it has the lowest sucrose concentration and still preserves the stability of NPs.

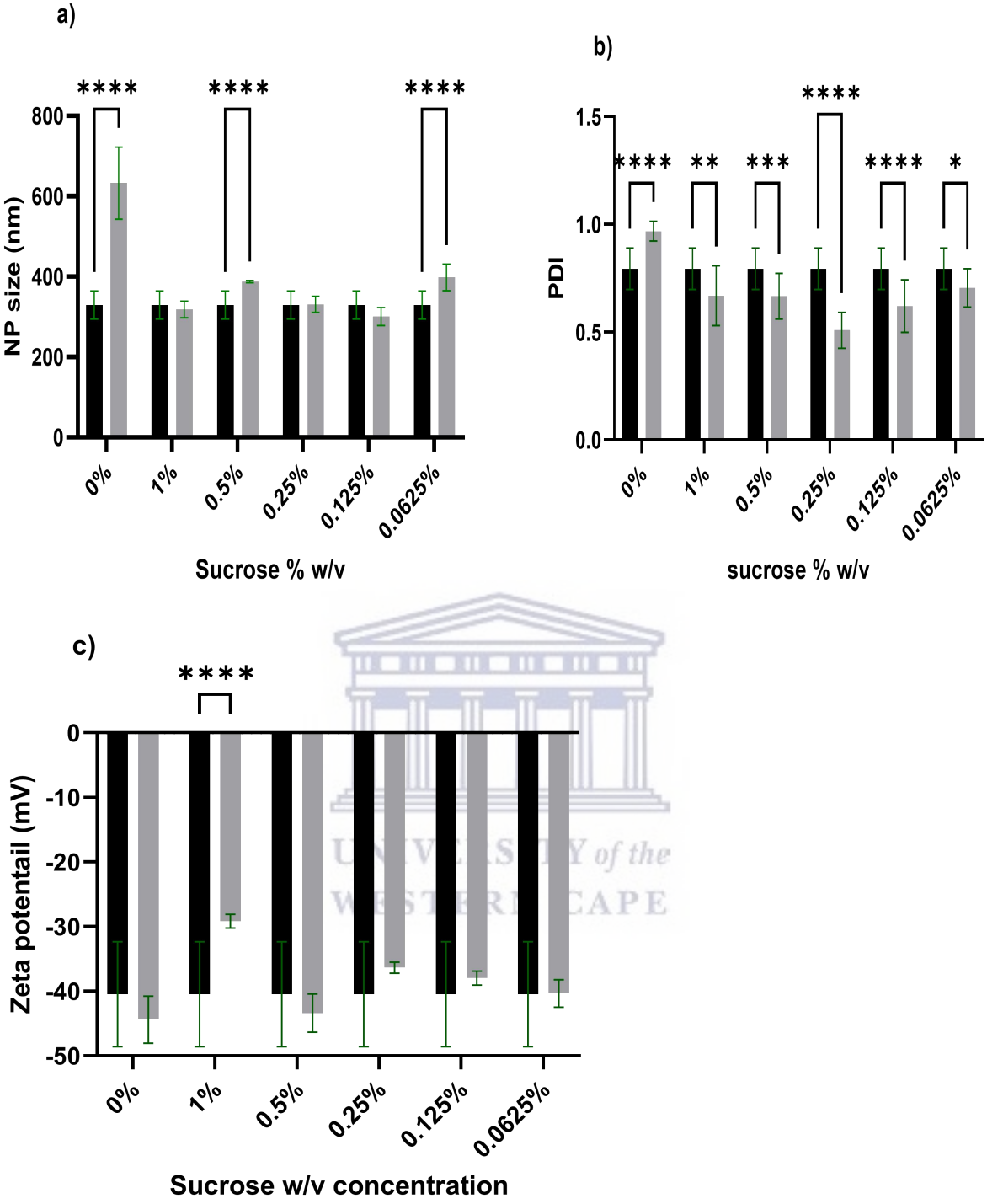

Fig. 5.5. NP size, PDI and zeta potential comparison of NPs before and after lyophilization with various sucrose concentrations (w/v) as cryoprotectants). 0 % w/v represent NPs lyophilized in the absence of sucrose. (n=3) (*: statistically significant, **: very significant, T: standard deviation, : before lyophilization, : after lyophilization). (a) Size comparison of various w/v concentrations of sucrose. The results showed that there was no statistically significant difference in size before and after lyophilization for concentrations of 0.125 % and 0.25 %. (b) PDI comparison showed various

differences between the concentrations. (c) Zeta potential comparison showed that it was not significantly affected by various sucrose concentrations. Statistical significance was indicated by not significant (ns) (p-value > 0.05), *: significant (p-value ≤ 0.05), **: very significant (p-value ≤ 0.01), ***: extremely significant (p-value ≤ 0.001), ****: extremely significant (p-value ≤ 0.0001). T: standard deviation.

5.5.3. SEM and TEM morphology assessment of LPHNPs

NPs were further characterized by SEM and TEM to study their surface morphology. SEM results showed that the NPs formed aggregates and had a rough inconsistent spherical shape (Fig. 5.6 (a)). It was speculated that excess lecithin, sometimes used as an emulsifier, and/or a binding agent caused the observed particle aggregation (291). However, upon close examination with HR TEM with uranyl acetate negative stain, the data revealed that the NPs were spherical in shape and formed small aggregates (Fig. 5.6 (b)). The differences between SEM and TEM with negative staining were therefore associated with sample preparation and handling for SEM and TEM with negative staining (240).

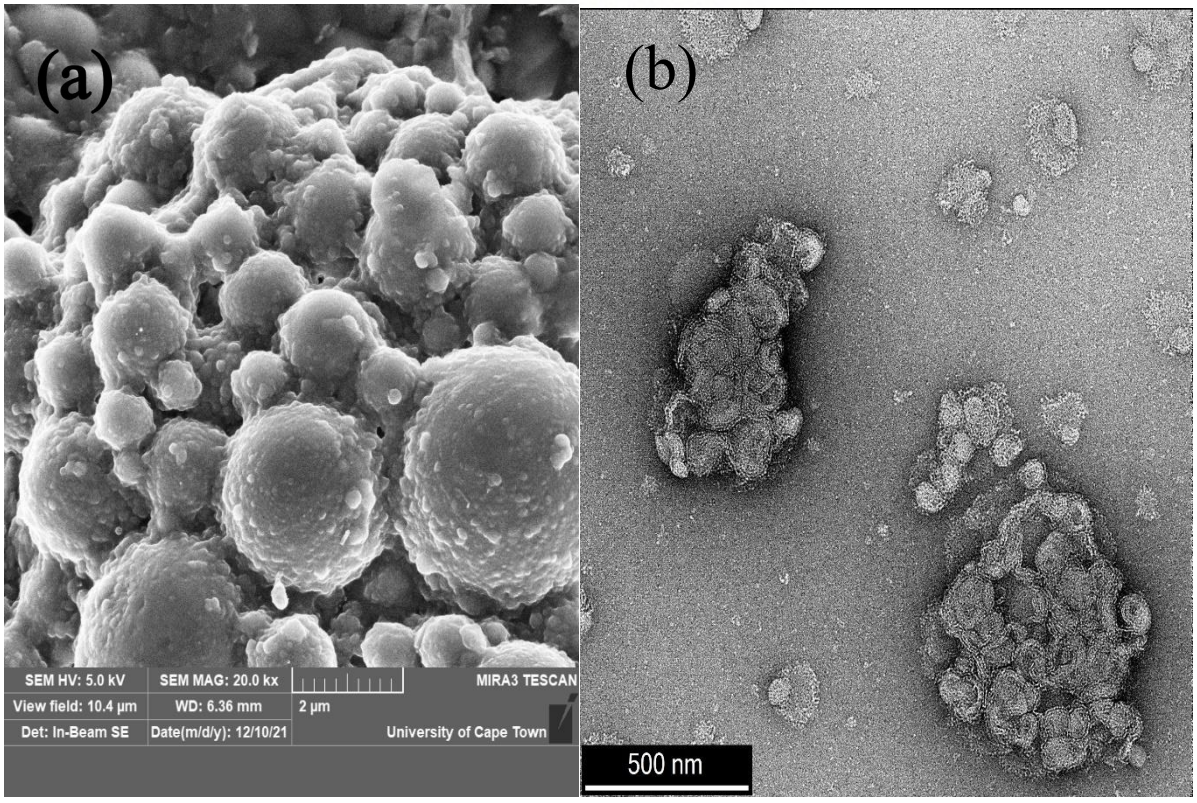

Fig. 5.6. (a) SEM images of lecithin/PCL LPHNPs. (b) uranyl acetate negative staining TEM images of lecithin/PCL NPs.

Taken together, 15 % w/w lipid/polymer was the optimal % w/w mass ratio for LPHNPs syntheses based on a statistically significant difference with the other ratios. According to the cytotoxicity study, 2 % w/w MA and/or curdlan conjugated NPs were the safest concentrations carried forward for the immunostimulatory effect. It was observed that there was a statistically significant difference between lecithin/PCL only NPs and 2 % MA and/or curdlan conjugated NPs, particularly with respect to size. For storage, a sucrose concentration of 0.125 % was determined as the lowest stable cryoprotectant concentration. The results of microscopic analysis revealed that the NPs were spherical and formed aggregates, which was speculated to be due to excess lecithin causing the NPs to agglomerate.

Chapter 6: Cytotoxicity and immune stimulation evaluation of the LPHNPs

6.1. Introduction

Cytotoxicity can be a major limiting factor to the application and clinical translation of NPs (292). The NP size to volume ratio provides excellent properties to the NPs as described in the literature review (see section 2.7). However, the change in properties associated with this ratio also raises cytotoxicity concerns and has been reported to cause toxicities such as those resulting from increased ROS production (293). Therefore, it is imperative to assess the safety of the NPs to ensure their use and safety. Lecithin and PCL NPs have been shown to be generally safe as all starting materials (lecithin and PCL) are FDA approved (217)(219)(294). Furthermore, literature has shown that LPHNPs are generally safe, including those containing lecithin and PCL (295). Regardless of the toxicity of the conjugate or the NPs, conjugation of NPs including addition of otherwise safe stabilizers, has been shown to affect NP toxicity (296). In this study, MTT was used to assess the toxicity of the newly formed NPs and to determine the highest non-toxic concentration of the NPs, which was further used to evaluate the immune modulation of the NPs. Loading NPs with MA and curdlan was hypothesized to confer immunomodulatory effect on the NPs. However, in immune modulation, a fine balance should be struck when administering immunomodulators to avoid excessive immune responses which can be deleterious to the host. An example of this can be a cytokine storm. On the other hand, some immunomodulators may lead to immune suppression as in the case of anti-inflammatory cytokine, therefore immune modulation of the newly synthesized NPs was evaluated by quantifying TNF-α and IL-10 cytokines produced by RAW 264.7 using an enzyme-linked immunoassay (ELISA) kits. This chapter describes the evaluation of cytotoxicity and immune modulation of the NPs.

6.1.1. Aims and objectives

The aim of this part of the study was to evaluate the cytotoxicity of various synthesized LPHNPs, including those containing MA and curdlan on RAW 264.7 macrophages. A further aim was to evaluate the immunomodulatory capabilities of the LPHNPs on RAW 264.7 macrophages. The objective of this part of the study was to determine the highest non-toxic concentration of various NPs on RAW macrophages. A further objective was to use the highest non-toxic concentration obtained from cytotoxicity studies to evaluate and compare the immune modulation of various LPHNPs on RAW 264.7 macrophages using ELISA kits.

6.2. Materials

Dulbecco's modified Eagle's medium (DMEM)-F12, Gentamycin, Glutamine, Foetal bovine serum (FBS), Trypsin, MTT (3- (4,5 dimethylthiazol-2-yl)-2,5-diphenyltetrazolium bromide), DMSO and Phosphate-Buffered saline (PBS) were purchased form Sigma-Aldrich (St Louis, MO, United States). Trypan blue stain, glutamax, gentamycin, penicillin-streptomycin were purchased from Gibco, Thermo Fisher Scientific, Inc (South Africa), cell scrapers were purchased from Whitehead Scientific (Pty) Ltd (South Africa).

The equipment used included a UV chamber (Ultra-violet products Inc, USA) which was used to sterilize the NPs and other materials used in the evaluation of cytotoxicity and immune modulation of the NPs. All the cellular work was conducted inside an ethanol sterilized Laminar Flow (Labotec, South Africa). POLARstar Omega plate reader (BMG LABTECH, Germany) was used for absorbance readings.

6.3. Seeding of RAW 264.7 macrophages and MTT assay procedure

Briefly, RAW 264.7 cells were seeded onto a 96-well plate at an initial density of 5 x 10^4 cells/well and incubated in supplemented DMEM-F12 at 37 °C for 24 h. The DMEM-F12 was then removed and replaced with 100 µL of media containing varying concentrations of LPHNPs. Four replicates of each concentration were used to determine cytotoxicity. The cells were then incubated for 24, 48 and 72 h. After incubation, the media containing NPs was replaced with 100 µL of DMEM-F12, followed by the addition of 20 µL of MTT (5 mg/mL) to each well and incubated at 37 °C for 2-4 h in the dark. After 2-4 h, DMEM-F12 and MTT were removed and 150 µL/well of DMSO was added to dissolve formazan crystals. Cell viability was determined by measuring absorbance at 570 nm on a POLARstar Omega plate reader (BMG LABTECH, Germany). The percentage viability was determined by comparing the viability of the treated cells to that of the untreated cells using Equation 1 (247). Statistical analyses were performed using GraphPad Prism 9.1.1 version (GraphPad Software, San Diego, California, USA).

Equation 1: % cell viability= [viability of treated cells] *100/ [viability of untreated cells]

6.4 Cytotoxicity evaluation of the LPHNPs

The *in vitro* cytotoxicity of LPHNPs was evaluated using MTT assay. The procedure followed for the MTT assay was adapted from Zhang *et al*. (2012) with some modifications

(247). First, the optimal concentration (µg/mL) of LPHNPs containing only lecithin and PCL was determined. This concentration was then used as the maximum concentration to assess the safety of LPHNPs containing different percentages and concentrations of curdlan. Once the optimal concentration and percentage of curdlan was obtained, the same concentration was used to assess the maximum concentration to evaluate the safety of MA LPHNPs. Finally, NPs containing both MA and curdlan at the identified optimal concentrations were evaluated to determine the safety of these LPHNPs. Statistical analyses were performed using GraphPad Prism 9.1.1 version (GraphPad Software, San Diego, California, USA).

6.5 Immune stimulation evaluation of the LPHNPs

To evaluate immunomodulation, supernatants of various LPHNPs at 25 µg/mL were collected following 24 h exposure of RAW 264.7 macrophages to the LPHNPs. The supernatants were centrifuged for 20 min at 1000 x *g* as per protocol of enzyme-linked immunoassay (ELISA) kit manufacturer (Elabscience Biotechnology Inc., Wuhan, China). Lipopolysaccharide (LPS) 10 ng/mL, as a positive control was used to induce cytokine production. Untreated cells were used as a negative control. The collected supernatants were then used for quantification of TNF-α and IL-10. Cytokines were quantified using an ELISA kit (Elabscience Biotechnology Inc., Wuhan, China) according to the manufacture's protocol. For TNF-α, the standard curve concentration range was 0 - 500 pg/mL, while for IL-10 the concentration range of the standard curve for IL-10 was 0 - 1000 pg/mL. Statistical analyses were performed using GraphPad Prism 9.1.1 version (GraphPad Software, San Diego, California, USA).

6.6. Results and discussion

6.6.1. Cytotoxicity evaluation of the NPs

6.6.1.1. Cytotoxicity of lecithin/PCL LPHNPs

The cytotoxicity of 4 different types of LPHNPs was evaluated at three different concentrations over a 72 h period. The experiment was set up to evaluate the toxicity of various concentrations of different the types of LPHNPs to determine the concentration and NP type that would be used to determine the cellular immune modulating activity of the NPs. NPs were considered safe if an average viability was maintained over 80 % (297)(298).

Initially, concentrations of 250, 500 and 1000 µg/mL of lecithin/PCL NPs were used to determine the highest non-toxic concentration (146). From Fig. 6.1. below, it can be seen that 250 µg/mL of lecithin/PCL NPs was the highest non-toxic concentration with a 94 ± 15.2 % viability. Statistical analysis showed no significant difference in cell viability at different time points measured at 250 µg/mL. Although previous works have shown that LPHNPs are generally safe, this work found that toxicity was concentration dependent.

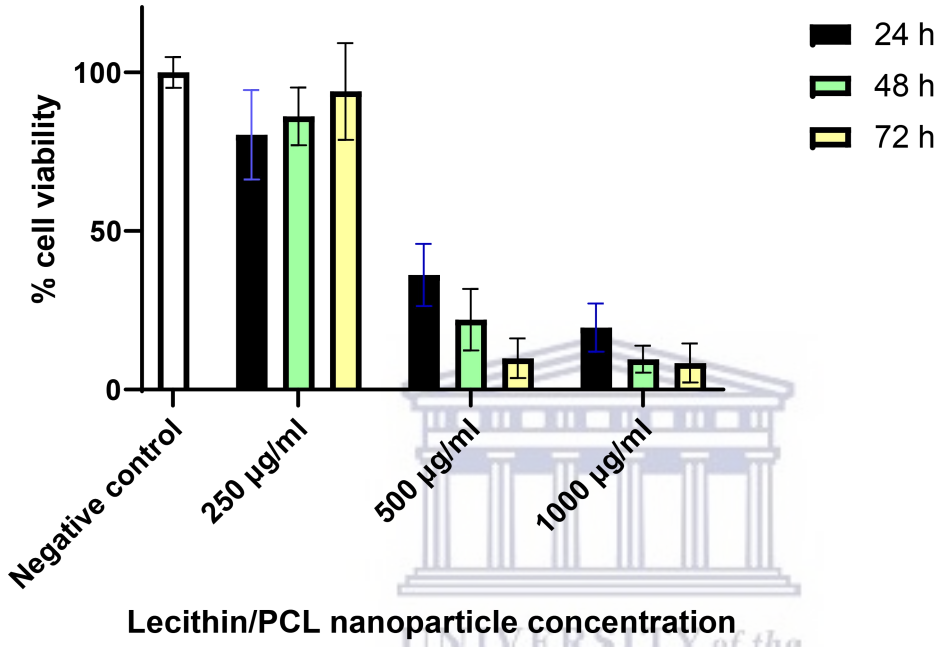

Fig. 6.1. Cytotoxicity measured by MTT (absorbance at 570 nm) following incubation of RAW 264.7 macrophages with lecithin/PCL LPHNPs for 72 h with an increasing concentration range of 250-1000 µg/mL to determine the highest non-toxic concentration. The negative control represents untreated cells. Data are expressed in mean ± SD (n=3). Statistical significance was indicated by not significant (ns) (p-value > 0.05), *: significant (p-value ≤ 0.05), **: very significant (p-value ≤ 0.01), ***: extremely significant (p-value ≤ 0.001), ****: extremely significant (p-value ≤ 0.0001). T: standard deviation.

6.6.1.2. Cytotoxicity of lecithin/PCL-curdlan LPHNPs

The determination of the highest non-toxic concentration of LPHNPs loaded with different percentages of curdlan, i.e. lecithin/PCL-curdlan LPHNPs 2, 5 and 10 % w/w curdlan was evaluated starting with the highest concentration of 250 µg/mL which was determined to be the highest non-toxic concentration of lecithin-PCL LPHNPs. NP concentrations of 50 and

100 µg/mL were also evaluated at the 2 %, 5 % and 10 % w/w curdlan levels. The results (Fig 6.2.) showed that 2 % w/w curdlan in lecithin/PCL-curdlan LPHNPs at 50 µg/mL was the highest non-toxic concentration over 72 h with 84 ± 4.7 % viability, while it was observed that at all concentrations toxicity showed a positive correlation with increased curdlan loading on the NPs i.e. NPs containing 10 % w/w curdlan were the most toxic at all concentrations, while those containing 2 % w/w curdlan appeared to be the least toxic at all concentrations (Fig. 6.2). Although the difference between different time points at 2 % w/w curdlan was significant, they all retained over 80 % viability. These results indicated that although curdlan is non-toxic, conjugation onto NPs can negatively affect NP toxicity, as demonstrated by other non-toxic conjugants (296).

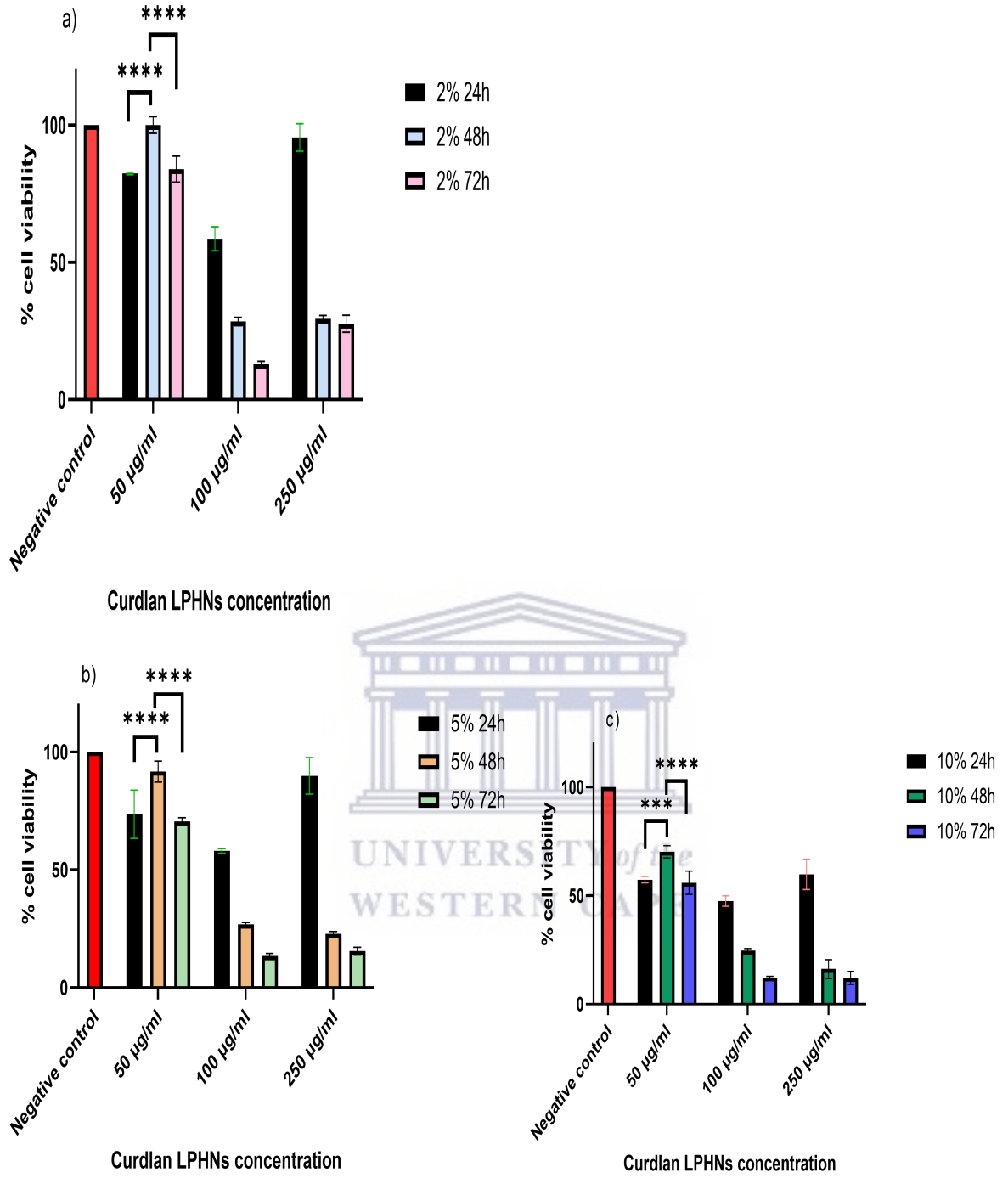

Fig. 6.2. Cytotoxicity measured by MTT (absorbance at 570 nm) following an incubation of RAW 264.7 macrophages with lecithin/PCL-curdlan LPHNPs for 72 h with an increasing concentration range of 50-250 µg/mL to determine the highest non-toxic concentration. (a) Incubation of RAW 264.7 macrophages with LPHNPs loaded with 2 % curdlan. (b) Incubation of RAW 264.7

macrophages with LPHNPs loaded with 5 % curdlan. (c) Incubation of RAW 264.7 macrophages with LPHNPs loaded with 10 % curdlan. The negative control represents untreated cells. Data are expressed in mean ± SD (n=3). Statistical significance was indicated by not significant (ns) (p-value > 0.05), *: significant (p-value ≤ 0.05), **: very significant (p-value ≤ 0.01), ***: extremely significant (p-value ≤ 0.001), ****: extremely significant (p-value ≤ 0.0001). T: standard deviation.

6.6.1.3. Cytotoxicity of lecithin/PCL-MA LPHNPs

The highest non-toxic concentration of NPs containing curdlan was carried forward to determine the highest non-toxic concentration of lecithin/PCL-MA LPHNPs containing 2, 5 and 8 % w/w of MA at a concentration of 50 µg/mL. The results showed that the 2 % w/w MA was non-toxic at a concentration of 50 µg/mL (Fig. 6.3) with a viability 85.8 ± 1.4 %. Statistical analysis showed no statistically significant difference in cell viability at this percentage at different time points evaluated. The results also showed a positive correlation between the amount of MA present on NPs and toxicity. As with curdlan, cytotoxicity increased with increasing MA concentration. Since 2 % w/w MA at a concentration of 50 µg/mL was the highest non-toxic concentration, it was carried forward to evaluate the safety of NPs containing both curdlan and MA.

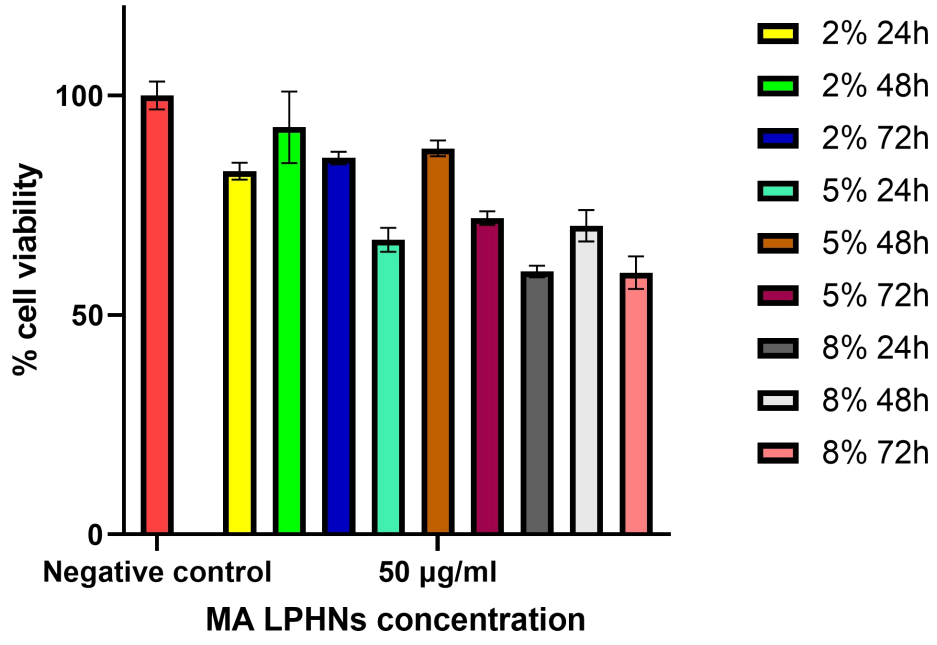

Fig. 6.3. Cytotoxicity measured by MTT (absorbance at 570 nm) following an incubation of RAW 264.7 macrophages with lecithin/PCL-MA LPHNPs for 72 h with an increasing MA percentage from 2 % to 8 % at a concentration of 50 µg/mL to determine the highest non-toxic concentration. The negative control represents untreated cells. Data are expressed in mean ± SD (n=3). Statistical significance was indicated by not significant (ns) (p-value > 0.05), *: significant (p-value ≤ 0.05), **: very significant (p-value ≤ 0.01). T: standard deviation.

6.6.1.4. Cytotoxicity of lecithin/PCL-curdlan-MA LPHINPs to RAW264.7 macrophages

The toxicity of LPHNPs containing 2 % w/w of both curdlan and MA at concentrations of 25 and 50 µg/mL was evaluated. The results (Fig. 6.4.) showed that the lower concentration of 25 µg/mL was non-toxic with a 100.1 ± 3.2 % viability while the higher concentration was slightly toxic (76. ± 0.4 % viability). No statistically significant difference was found at 25 µg/mL across various time points with respect to cellular viability. The toxicity results suggested that there was an additive effect on the toxicity of MA-curdlan containing LPHNPs due to the combination of both MA and curdlan, as an otherwise safe concentration of 50 µg at 2 % w/w MA-LPHNPs or 2 % w/w curdlan-LPHNPs become slightly toxic when both were combined, requiring a lower concentration to avoid toxicity.

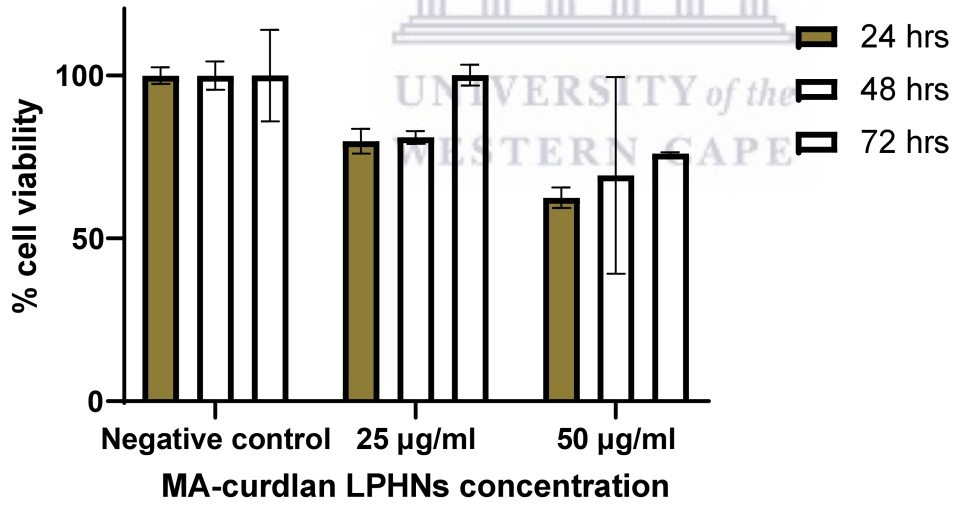

Fig. 6.4. Cytotoxicity measured by MTT (absorbance at 570 nm) following an incubation of RAW 264.7 macrophages with lecithin/PCL-curdlan-MA LPHNPs (at 2 % w/w of each MA and curdlan) for 72 h with an increasing concentration range of 25-50 µg/mL to determine the highest non-toxic concentration. The negative control represents untreated cells. Data are expressed in mean ± SD (n=3).

Statistical significance was indicated by not significant (ns) (p-value > 0.05), *: significant (p-value ≤ 0.05), **: very significant (p-value ≤ 0.01). T: standard deviation.

Taken together, different percentages (of curdlan and MA loaded onto LPHNPs) and concentrations of the various LPHNPs induced different levels of toxicity. Toxicity correlated positively with both NP concentration and percentage of either MA or curdlan present on the LPHNPs. The presence of both curdlan and MA on the NPs showed an additive effect on toxicity.

6.6.2. Immunostimulatory activity of the NPs

Activated macrophages are known to produce TNF-α, while IL-10 is produced to suppress immune responses (256)(299). Macrophage stimulation of various types of LPHNPs was assessed over a 24 h period using ELISA to quantify concentrations of TNF-α and IL-10. The highest non-toxic concentrations of LPHNPs (25 µg/mL) including those containing 2 % of both curdlan and MA, were used to stimulate macrophages. Results indicated that all LPHNPs, except lecithin/PCL-curdlan stimulated the production of TNF-α (lecithin/PCL produced 22.56 ± 1.65 pg/mL, lecithin/PCL-MA produced 25.76 ± 24.61 pg/mL, lecithin/PCL-curdlan-MA produced 51.16 ± 6.60 pg/mL. The positive control produced 68.10 ± 8.97 pg/mL while the negative control produced 17.00 ± 6.27 pg/mL) (Figure 6.5).

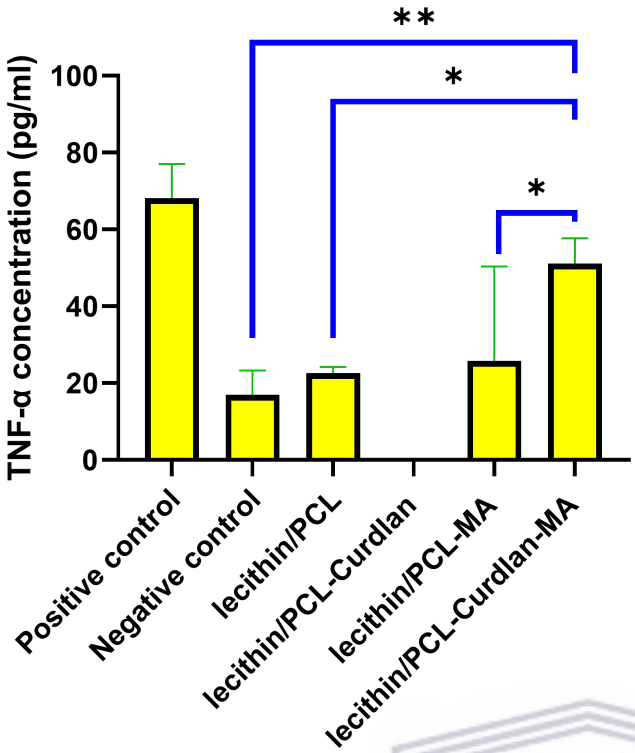

Fig. 6.5. TNF-α production by RAW 264.7 macrophages following exposure to various LPHNPs for 24h at a concentration of 25 µg/mL. The experiment was performed in triplicate. Results shown are the mean and standard deviation. LPS was used as a positive control while untreated NPs were used as a negative control. Statistical significance was indicated by not significant (ns) (p-value > 0.05), *: significant (p-value ≤ 0.05), **: very significant (p-value ≤ 0.01). T: standard deviation.

The results also showed that lecithin/PCL-curdlan-MA produced the highest amount of TNF-α. In fact, there was a statistically significant difference between lecithin/PCL-curdlan-MA NPs and the rest of the LPHNPs in relation to the amount of TNF-α produced (Fig. 6.5.). It was also noted that although the amount of TNF-α produced by both lecithin/PCL and lecithin/PCL-MA was slightly higher than that produced by the negative control (which consisted of untreated cells), the difference was not statistically significant. Unlike some other NPs containing curdlan, lecithin/PCL-curdlan did not elicit TNF-α synthesis. The result suggests that these NPs inhibit its synthesis, in fact, untreated cells produced a statistically significantly higher level of TNF-α than them. Interestingly, although there was no statistically significant difference between the negative control and lecithin/PCL-MA and while lecithin/PCL-curdlan did not produce TNF-α. When combined in lecithin/PCL-curdlan-MA, the amount of TNF-α produced was statistically significant from that of the negative control and from both lecithin/PCL-MA and lecithin/PCL-curdlan individually. In fact, there

was no statistically significant difference between lecithin/PCL-curdlan-MA and LPS, a known TNF-α inducer used as a positive control, suggesting a synergistic immunostimulatory effect when the two immunostimulants (MA and curdlan) were loaded together on the LPHNPs. Therefore, the results indicate that there was differential cytokine production that increases in the presence of both curdlan and MA.

In evaluating immunosuppression of LPHNPs, the highest concentrations of LPHNPs were used to quantify IL-10 (a potent immune suppressing cytokine). The results indicated that there was no IL-10 produced by any of the LPHNPs. This suggest that all LPHNPs i.e. lecithin/PCL, lecithin/PCL-curdlan, lecithin/PCL-MA and lecithin/PCL-curdlan-MA at 25 μg/mL did not induce immune response suppression. Together with the induction of TNF-α, this can serve as an indication of the immune modulatory capability of the NPs since they are able to induce immune stimulation through inducing the production of TNF-α without inducing the production of IL-10, a potent immune suppressing cytokine.

These data indicate that there is potential to develop the newly synthesized lecithin/PCL-curdlan-MA into a biomimetic immunotherapy against *M. tuberculosis* as indicated by differential cytokine production across various LPHNP formulations investigated. This is due to their ability to induce significantly high levels of TNF-α with no apparent effect on the induction of IL-10 levels. TNF-α is instrumental in fighting *M. tuberculosis* (258)(300), while the apparent lack of IL-10 is a good indication, as IL-10 is up-regulated by *M. tuberculosis* to inhibit phagosomal maturation, inhibit necessary cytokines and suppress antigen presentation, and inhibit apoptosis, all of which enhance *M. tuberculosis* survival, immune evasion, and persistence (77)(80)(81)(85). Therefore, lecithin/PCL-curdlan-MA has the potential to be used as a biomimetic immunostimulatory adjuvant to medicines to treat intracellular pathogens that inhibit the immune response to such pathogens and remain dormant, such as *M. tuberculosis* (97).

In summary, all LPHNPs except lecithin/PCL-curdlan NPs showed an immune stimulatory effect due to their ability to stimulate TNF-α production in RAW 264.7 macrophages. Lecithin/PCL-curdlan-MA stimulated the highest amount of TNF-α which was statistically significant compared to other LPHNPs. The results also indicated a synergistic effect in inducing TNF-α when both MA and curdlan were simultaneously conjugated onto the NPs.

Chapter 7: Conclusion

This work mainly aimed to synthesize and characterize LPHNPs and to load them with two immunomodulatory compounds, namely MA and curdlan. The NPs were characterized and evaluated for their cytotoxicity and immune modulation *in-vitro*.

For the synthesis of PCL-curdlan copolymer described in Chapter 4, an intermediate polymer named PCL-COOH was first synthesized from ε-caprolactone using a ring-opening method selected after attempting various methods. The synthesized PCL-COOH polymer was then conjugated with curdlan using the carbodiimide conjugation method to yield a PCL-curdlan copolymer. Following physiochemical characterizations of the polymers and the copolymer, it was concluded that the observed differences across those properties were due to the formation of a bond between curdlan and PCL-COOH which yielded a PCL-curdlan copolymer. The ratio (% w/w) of curdlan to PCL was determined to be 15 % w/w by NMR. The copolymer was used in subsequent experiments in the synthesis of curdlan loaded NPs.

Chapter 5 addressed the successful synthesis and characterization of various LPHNPs. Firstly, an optimal ratio of lecithin/PCL was determined to be 15 % w/w and this ratio was thereafter used in the synthesis of LPHNPs loaded with MA and curdlan. The loading proved to be successful and the results showed that it impacted the physiochemical properties of NPs such as size, PDI and zeta potential.

Chapter 6 reported the cytotoxicity and immune modulation of the newly synthesized LPHNPs. This chapter also aimed to report on the determination of the highest non-toxic concentration of the NPs, which was further used to evaluate the immune modulation of the NPs. Contrary to what was hypothesized, the LPHNPs showed some cytotoxicity towards RAW264.7. The toxicity was enhanced by loading NPs with curdlan and MA and the increase in toxicity was positively correlated with the amount of MA and curdlan loaded onto the NPs. The results also indicated an additive effect on toxicity when both MA and curdlan were loaded simultaneously onto the NPs. 25 μg /mL of LPHNPs loaded with both curdlan and MA was determined to be the highest non-toxic concentration and was therefore used to evaluate the immune modulation of the various NPs. The amount of TNF-α and IL-10 cytokines produced by RAW 264.7 macrophages were quantified. The results indicated that the NPs, with the exception of PCL/lecithin-curdlan NPs, possess an ability to induce TNF-α production. It was noted that lecithin/PCL-curdlan-MA NPs produced the highest amount of

TNF-α and the difference between the amount of TNF-α produced by these NPs was statistically significant from the rest. The results also indicated a synergistic effect in terms of TNF-α stimulation when both MA and curdlan were simultaneously loaded onto the NPs.

Overall, the aim of this study which was to synthesize and characterize LPHNPs including their *in-vitro* characterization to evaluate their cytotoxicity and immune modulation, was achieved. The preliminary data obtained suggest that lecithin/PCL-curdlan-MA NPs could potentially stimulate macrophages while inhibiting the immunosuppressive effect of IL-10, which supports survival of *M. tuberculosis*, suggesting the possibility to develop lecithin/PCL-curdlan-MA into a biomimetic immunotherapy against *M. tuberculosis.* Further studies are needed to further evaluate the immunomodulatory activity of the NPs and their anti-*M. tuberculosis* activity in both *in-vitro* and *in-vivo* models.

References

1. Organization WH. Global tuberculosis report 2021. Geneva PP - Geneva: World Health Organization; Available from: https://apps.who.int/iris/handle/10665/346387

2. Kamariza M, Shieh P, Ealand CS, Peters JS, Chu B, Rodriguez-Rivera FP, et al. Rapid detection of Mycobacterium tuberculosis in sputum with a solvatochromic trehalose probe. Sci Transl Med. 2018;10(430).

3. Pang Y, An J, Shu W, Huo F, Chu N, Gao M, et al. Epidemiology of extrapulmonary tuberculosis among inpatients, China, 2008-2017. Emerg Infect Dis. 2019;25(3):457–64.

4. Banta JE, Ani C, Bvute KM, Lloren JIC, Darnell TA. Pulmonary vs. extra-pulmonary tuberculosis hospitalizations in the US [1998–2014]. J Infect Public Health. 2019;13(1):131–9. Available from: https://doi.org/10.1016/j.jiph.2019.07.001

5. Singh P, Rameshwaram NR, Ghosh S, Mukhopadhyay S. Cell envelope lipids in the pathophysiology of Mycobacterium tuberculosis. Future Microbiol. 2018;13(6):689–710.

6. Cohen A, Mathiasen VD, Schön T, Wejse C. The global prevalence of latent tuberculosis: A systematic review and meta-analysis. Eur Respir J. 2019;54(3).

7. Qiu X, Tang Y, Zou R, Zeng Y, Yue Y, Li W, et al. Diagnostic accuracy of interferon-gamma-induced protein 10 for differentiating active tuberculosis from latent tuberculosis: A meta-analysis. Sci Rep. 2019;9(1):1–10.

8. Bhatt A, Fujiwara N, Bhatt K, Gurcha SS, Kremer L, Chen B, et al. Deletion of kasB in Mycobacterium tuberculosis causes loss of acid-fastness and subclinical latent tuberculosis in immunocompetent mice. 2007;

9. Maphasa RE, Meyer M, Dube A. The Macrophage Response to Mycobacterium tuberculosis and Opportunities for Autophagy Inducing Nanomedicines for Tuberculosis Therapy. 2021;10(February):1–22.

10. Pollara G, Turner CT, Rosenheim J, Chandran A, Bell LCK, Khan A, et al. Exaggerated IL-17A activity in human in vivo recall responses discriminates active tuberculosis from latent infection and cured disease. Sci Transl Med. 2021;13(592).

11. Talbot EA, Raffa BJ. Mycobacterium tuberculosis. Vol. 3, Molecular Medical Microbiology: Second Edition. Elsevier Ltd; 2014. 1637–1653 p. Available from: http://dx.doi.org/10.1016/B978-0-12-397169-2.00092-5

12. Queiroz A, Riley LW. Review Article Bacterial immunostat : Mycobacterium tuberculosis lipids and their role in the host immune response. 2017;50(1):9–18.

13. Spitaleri A, Ghodousi A, Miotto P, Cirillo DM. Whole genome sequencing in Mycobacterium tuberculosis. Ann Transl Med. 2019;7(S6):S197–S197.

14. Tiberi S, Plessis N, Walzl G, Vjecha MJ, Rao M, Ntoumi F, et al. Series Tuberculosis 1 Tuberculosis : progress and advances in development of new drugs , treatment regimens , and host-directed therapies. 2018;3099(18):1–16.

15. Aucamp M, Liebenberg W, Okaecwe T, Geldenhuys M, Stieger N. Compatibility between four anti-TB drugs and tablet excipients determined by microcalorimetry. Pharmazie. 2019;74(6):350–1.

16. Ghanizadeh Tabriz A, Nandi U, Hurt AP, Hui HW, Karki S, Gong Y, et al. 3D printed bilayer tablet with dual controlled drug release for tuberculosis treatment. Int J Pharm. 2021;593(December 2020):120147. Available from: https://doi.org/10.1016/j.ijpharm.2020.120147

17. Sharma A, Pandey R, Sharma S, Khuller GK. Chemotherapeutic efficacy of poly (dl - lactide-co-glycolide) nanoparticle encapsulated antitubercular drugs at sub-therapeutic dose against experimental tuberculosis. 2004;24:599–604.

18. Singh S, Mariappan TT, Sharda N, Singh B. Degradation of rifampicin, isoniazid and pyrazinamide from prepared mixtures and marketed single and combination products under acid conditions. Pharm Pharmacol Commun. 2000;6(11):491–4.

19. Ahmed S, Raqib R, Guðmundsson GH, Bergman P, Agerberth B, Rekha RS. Host-directed therapy as a novel treatment strategy to overcome tuberculosis: Targeting immune modulation. Antibiotics. 2020;9(1):1–19.

20. Gleeson LE, Sheedy FJ, Palsson-McDermott EM, Triglia D, O'Leary SM, O'Sullivan MP, et al. Cutting Edge: Mycobacterium tuberculosis Induces Aerobic Glycolysis in Human Alveolar Macrophages That Is Required for Control of Intracellular Bacillary Replication . J Immunol. 2016;196(6):2444–9.

21. Chuang YM, He L, Pinn ML, Tsai YC, Cheng MA, Farmer E, et al. Albumin fusion with granulocyte-macrophage colony-stimulating factor acts as an immunotherapy against chronic tuberculosis. Cell Mol Immunol. 2021;18(10):2393–401. Available from: http://dx.doi.org/10.1038/s41423-020-0439-2

22. Abreu R, Essler L, Loy A, Quinn F, Giri P. Heparin inhibits intracellular Mycobacterium tuberculosis bacterial replication by reducing iron levels in human macrophages. Sci Rep. 2018;8(1):1–12. Available from: http://dx.doi.org/10.1038/s41598-018-25480-y

23. Li W, Zhang X, Zhang C, Yan J, Hou X, Du S, et al. costimulatory receptors and enhance T cell. 2021;

24. Zhang Y, Cui Z, Kong H, Xia K, Pan L, Li J, et al. One-Shot Immunomodulatory Nanodiamond Agents for Cancer Immunotherapy. Adv Mater. 2016;28(14):2699–708.

25. GIOVANNI SOTGIU, GIORGIA SULIS and AM. A World Health Organization perspective. J Rheumatol Suppl. 2017;10:5–6.

26. Banta JE, Ani C, Bvute KM, Lloren JIC, Darnell TA. Pulmonary vs. extra-pulmonary tuberculosis hospitalizations in the US [1998–2014]. J Infect Public Health. 2020;13(1):131–9. Available from: https://doi.org/10.1016/j.jiph.2019.07.001

27. Houben RMGJ, Dodd PJ. The Global Burden of Latent Tuberculosis Infection: A Re-estimation Using Mathematical Modelling. PLoS Med. 2016;13(10):1–13.

28. Timothy R. Sterling M, Gibril Njie M, Dominik Zenner M, David L. Cohn M, Randall Reves M, Amina Ahmed M, et al. New guidelines for treatment of latent tuberculosis infection. Bull World Health Organ. 2020;78(5):710–1.

29. Organization WH. Global tuberculosis report 2020. Geneva PP - Geneva: World Health Organization; Available from: https://apps.who.int/iris/handle/10665/336069

30. Dube A, Lemmer Y, Hayeshi R, Balogun M, Labuschagne P, Swai H, et al. State of the art and future directions in nanomedicine for tuberculosis. 2014;1725–34.

31. Abdelwahab MT, Wasserman S, Brust JCM, Gandhi NR, Meintjes G, Everitt D, et al. Clofazimine pharmacokinetics in patients with TB: Dosing implications. J Antimicrob Chemother. 2020;75(11):3269–77.

32. Sileshi T, Tadesse E, Makonnen E, Aklillu E. The impact of first-line anti-tubercular drugs' pharmacokinetics on treatment outcome: A systematic review. Clin Pharmacol Adv Appl. 2021;13:1–12.

33. Schluger NW, Rom WN. State of the Art The Host Immune Response to Tuberculosis. (19).

34. Cambau E, Drancourt M. Steps towards the discovery of Mycobacterium tuberculosis by Robert Koch, 1882. Clin Microbiol Infect. 2014;20(3):196–201. Available from: http://dx.doi.org/10.1111/1469-0691.12555

35. Forrellad MA, Klepp LI, Gioffré A, García JS, Morbidoni HR, de la Paz Santangelo M, et al. Virulence factors of the mycobacterium tuberculosis complex. Virulence. 2013;4(1):3–66.

36. Sinha P, Gupta A, Prakash P, Anupurba S, Tripathi R, Srivastava GN. Differentiation of Mycobacterium tuberculosis complex from non-tubercular mycobacteria by nested multiplex PCR targeting IS6110, MTP40 and 32kD alpha antigen encoding gene fragments. BMC Infect Dis. 2016;16(1):1–10. Available from: http://dx.doi.org/10.1186/s12879-016-1450-1

37. G, Mercy Eleanor; T, Aditya; A, Kumar; M D. Review on Mycobacterium tuberculosis. Res Rev J Microbiol Biotechnol. 2016;2(1):9–18. Available from: http://www.rroij.com/open-access/review-on-mycobacterium-tuberculosis-.pdf%0Ahttps://www.rroij.com/open-access/review-on-mycobacterium-tuberculosis-.pdf

38. Rodriguez-rivera FP, Zhou X, Theriot JA, Bertozzi CR. Visualization of mycobacterial membrane dynamics in live cells. 2017;

39. Merget B, Zilian D, Mu T, Sotriffer CA. Structural bioinformatics MycPermCheck : the Mycobacterium tuberculosis permeability prediction tool for small molecules. 2013;29(1):62–8.

40. Augenstreich J, Haanappel E, Ferré G, Czaplicki G, Jolibois F, Destainville N, et al. The conical shape of DIM lipids promotes Mycobacterium tuberculosis infection of macrophages. Proc Natl Acad Sci U S A. 2019;116(51):25649–58.

41. Korf J, Stoltz A, Verschoor J, De Baetselier P, Grooten J. The Mycobacterium

tuberculosis cell wall component mycolic acid elicits pathogen-associated host innate immune responses. Eur J Immunol. 2005;35(3):890–900.

42. Alvarez-Jiménez VD, Leyva-Paredes K, García-Martínez M, Vázquez-Flores L, García-Paredes VG, Campillo-Navarro M, et al. Extracellular vesicles released from Mycobacterium tuberculosis-Infected neutrophils promote macrophage autophagy and decrease intracellular mycobacterial survival. Front Immunol. 2018;9(FEB):1–12.

43. Bickett TE, McLean J, Creissen E, Izzo L, Hagan C, Izzo AJ, et al. Characterizing the BCG Induced Macrophage and Neutrophil Mechanisms for Defense Against Mycobacterium tuberculosis. Front Immunol. 2020;11(June):1–13.

44. Braian C, Hogea V, Stendahl O. Mycobacterium tuberculosis-induced neutrophil extracellular traps activate human macrophages. J Innate Immun. 2013;5(6):591–602.

45. Lu Q, Zhang W, Fang J, Zheng J, Dong C, Xiong S. Mycobacterium tuberculosis Rv1096, facilitates mycobacterial survival by modulating the NF-κB/MAPK pathway as peptidoglycan N-deacetylase. Mol Immunol. 2020;127(December 2019):47–55. Available from: https://doi.org/10.1016/j.molimm.2020.08.005

46. Hinman AE, Jani C, Pringle SC, Zhang WR, Jain N, Martinot AJ, et al. Mycobacterium tuberculosis canonical virulence factors interfere with a late component of the TLR2 response. Elife. 2021;10.

47. Abel B, Thieblemont N, Quesniaux VJF, Brown N, Mpagi J, Miyake K, et al. Toll-Like Receptor 4 Expression Is Required to Control Chronic Mycobacterium tuberculosis Infection in Mice . J Immunol. 2002;169(6):3155–62.

48. Pahari S, Negi S, Aqdas M, Arnett E, Schlesinger LS, Agrewala JN. Induction of autophagy through CLEC4E in combination with TLR4: an innovative strategy to restrict the survival of Mycobacterium tuberculosis. Autophagy. 2020;16(6):1021–43. Available from: https://doi.org/10.1080/15548627.2019.1658436

49. Al-Bader T, Christodoulides M, Heckels JE, Holloway J, Semper AE, Friedmann PS. Activation of human dendritic cells is modulated by components of the outer membranes of Neisseria meningitidis. Infect Immun. 2003;71(10):5590–7.

50. Mogensen TH. Pathogen recognition and inflammatory signaling in innate immune defenses. Clin Microbiol Rev. 2009;22(2):240–73.

51. Pauwels A marie, Trost M, Beyaert R, Hoffmann E, Biosciences M. Patterns, Receptors, and Signals: Regulation of Phagosome Maturation. 2017;1–23.

52. Ahmad S. Pathogenesis , Immunology , and Diagnosis of Latent Mycobacterium tuberculosis Infection. 2011;2011.

53. Wang J, Li B xi, Ge P pu, Li J, Wang Q, Gao GF, et al. Mycobacterium tuberculosis suppresses innate immunity by coopting the host ubiquitin system. 2015;(January).

54. Carranza C, Chavez-galan L. Several Routes to the Same Destination: Inhibition of Phagosome-Lysosome Fusion by Mycobacterium tuberculosis. Am J Med Sci. 2018;357(3):184–94. Available from: https://doi.org/10.1016/j.amjms.2018.12.003

55. Vieira O V, Botelho RJ, Grinstein S. Phagosome maturation : aging gracefully. 2002;704:689–704.

56. Guo T, Gong L chen, Sui S fang. An Electrostatically Preferred Lateral Orientation of SNARE Complex Suggests Novel Mechanisms for Driving Membrane Fusion. 2010;1–11.

57. Sun J, Deghmane AE, Soualhine H, Hong T, Bucci C, Solodkin A, et al. Mycobacterium bovis BCG disrupts the interaction of Rab7 with RILP contributing to inhibition of phagosome maturation. J Leukoc Biol. 2007;82(6):1437–45.

58. Hashim S, Mukherjee K, Raje M, Basu SK, Mukhopadhyay A. Live Salmonella Modulate Expression of Rab Proteins to Persist in a Specialized Compartment and Escape Transport to Lysosomes *. 2000;275(21):16281–8.

59. Schekman WW and R. HHS Public Access. Physiol Behav. 2008;176(12):139–48.

60. Rene E. Harrison, Cecilia Bucci, Otilia V. Vieira, Trina A. Schroer and SG. Ethical, clinical, and social aspects of treatment of epilepsy in patients with comorbid depression. Epilepsia. 2003;23(18):6494–6506. Available from: http://www.embase.com/search/results?subaction=viewrecord&from=export&id=L613894118%0Ahttp://dx.doi.org/10.1111/epi.13609%0Ahttp://vb3lk7eb4t.search.serialssolutions.com?sid=EMBASE&issn=00139580&id=doi:10.1111%2Fepi.13609&atitle=Ethical%2C+clinical%2C+and

61. Roberts EA, Chua J, Kyei GB, Deretic V. Higher order Rab programming in phagolysosome biogenesis. 2006;174(7):923–9.

62. Queval CJ, Song O ryul, Carralot J philippe, Saliou J michel, Bongiovanni A, Deloison G, et al. Mycobacterium tuberculosis. 2017;1–28.

63. Wong D, Bach H, Sun J, Hmama Z, Av-gay Y. Mycobacterium tuberculosis protein tyrosine to inhibit phagosome acidi fi cation. 2011;(14).

64. Thompson CR, Iyer SS, Melrose N, Vanoosten R, Johnson K, Pitson SM, et al. Sphingosine Kinase 1 (SK1) Is Recruited to Nascent Phagosomes in Human Macrophages: Inhibition of SK1 Translocation by Mycobacterium tuberculosis. 2005;1.

65. Kusner DJ. Mechanisms of mycobacterial persistence in tuberculosis. Clin Immunol. 2005;114(3 SPEC. ISS.):239–47.

66. Vergne I, Chua J, Lee HH, Lucas M, Belisle J, Deretic V. Mechanism of phagolysosome biogenesis block by viable Mycobacterium tuberculosis. Proc Natl Acad Sci U S A. 2005;102(11):4033–8.

67. Jayachandran R, Sundaramurthy V, Combaluzier B, Mueller P, Korf H, Huygen K, et al. Survival of Mycobacteria in Macrophages Is Mediated by Coronin 1-Dependent Activation of Calcineurin. 2007;37–50.

68. Gatfield J, Albrecht I, Zanolari B, Steinmetz MO, Pieters J. Association of the Leukocyte Plasma Membrane with the Actin Cytoskeleton through Coiled Coil-mediated Trimeric Coronin 1 Molecules. 2005;16(June):2786–98.

69. Ferrari G, Langen H, Naito M, Pieters J. A Coat Protein on Phagosomes Involved in the Intracellular Survival of Mycobacteria. 1999;97:435–47.

70. Vergne I, Chua J, Deretic V. Tuberculosis Toxin Blocking Phagosome Maturation Inhibits a Novel Ca 2 ϩ / Calmodulin-PI3K hVPS34 Cascade. 2003;198(4).

71. Weiss G, Schaible UE. Macrophage defense mechanisms against intracellular bacteria. Immunol Rev. 2015;264(1):182–203.

72. Gengenbacher M, Kaufmann SHE. Mycobacterium tuberculosis : Success through dormancy. 2013;36(3):514–32.

73. Pieters J. Review Mycobacterium tuberculosis and the Macrophage : Maintaining a Balance. 2008;(June):399–407.

74. Duque GA, Descoteaux A. Macrophage cytokines : involvement in immunity and

infectious diseases. 2014;5(October):1–12.

75. Wang N, Liang H, Zen K. Molecular mechanisms that influence the macrophage M1-M2 polarization balance. Front Immunol. 2014;5(NOV):1–9.

76. Xin G, Zander R, Schauder DM, Chen Y, Weinstein JS, Drobyski WR, et al. Single-cell RNA sequencing unveils an IL-10-producing helper subset that sustains humoral immunity during persistent infection. Nat Commun. 2018;9(1):1–14. Available from: http://dx.doi.org/10.1038/s41467-018-07492-4

77. De Trez C, Stijlemans B, Bockstal V, Cnops J, Korf H, Van Snick J, et al. A Critical Blimp-1-Dependent IL-10 Regulatory Pathway in T Cells Protects From a Lethal Pro-inflammatory Cytokine Storm During Acute Experimental Trypanosoma brucei Infection. Front Immunol. 2020;11(June):1–15.

78. Niu Y, Chen Y, Sun P, Wang Y, Luo J, Ding Y, et al. Intragastric and atomized administration of canagliflozin inhibit inflammatory cytokine storm in lipopolysaccharide-treated sepsis in mice: A potential COVID-19 treatment. Int Immunopharmacol. 2021;96(January):107773. Available from: https://doi.org/10.1016/j.intimp.2021.107773

79. Meena SL, Rajni. Survival mechanisms of pathogenic Mycobacterium tuberculosis H 37 Rv. 2010;277:2416–27.

80. Patel NR, Swan K, Li X, Tachado SD, Koziel H. Impaired M. tuberculosis -mediated apoptosis in alveolar macrophages from HIV+ persons: potential role of IL-10 and BCL-3 . J Leukoc Biol. 2009;86(1):53–60.

81. Rodrigues MF, Barsante MM, Alves CCS, Souza MA, Ferreira AP, Amarante-Mendes GP, et al. Apoptosis of macrophages during pulmonary Mycobacterium bovis infection: Correlation with intracellular bacillary load and cytokine levels. Immunology. 2009;128(1 PART 2):691–9.

82. Parveen N, Varman R, Nair S, Das G, Ghosh S, Mukhopadhyay S. Endocytosis of Mycobacterium tuberculosis Heat Shock Protein 60 Is Required to Induce Interleukin-10 Production. 2013;288(34):24956–71.

83. Taylor P, Luo H, Zeng J, Huang Q, Liu M, Abdalla AE. Journal of Biomolecular Structure and Dynamics Mycobacterium tuberculosis Rv1265 Promotes Mycobacterial

Intracellular Survival and Alters Cytokine Profile of the Infected Macrophage Mycobacterium tuberculosis Rv1265 Promotes Mycobacterial Intracellular Su. 2015;(July).

84. Das S, Banerjee S, Majumder S, Chowdhury BP, Goswami A. Immune Subversion by Mycobacterium tuberculosis through CCR5 Mediated Signaling : Involvement of IL-10. 2014;9(4):1–11.

85. Redford PS, Boonstra A, Read S, Pitt J, Graham C, Stavropoulos E, et al. Enhanced protection to Mycobacterium tuberculosis infection in IL-10-deficient mice is accompanied by early and enhanced Th1 responses in the lung. Eur J Immunol. 2010;40(8):2200–10.

86. O'Leary S, Sullivan MPO, Keane J. IL-10 Blocks Phagosome Maturation in Mycobacterium tuberculosis – Infected Human Macrophages. 2011;1.

87. Miranda MS, Breiman A, Allain S, Deknuydt F, Altare F. The Tuberculous Granuloma : An Unsuccessful Host Defence Mechanism Providing a Safety Shelter for the Bacteria ? 2012;2012.

88. Cicchese JM, Dartois V, Kirschner DE, Linderman JJ. Both Pharmacokinetic Variability and Granuloma Heterogeneity Impact the Ability of the First-Line Antibiotics to Sterilize Tuberculosis Granulomas. Front Pharmacol. 2020;11(March):1–15.

89. Ernst JD. The immunological life cycle of tuberculosis. Nat Rev Immunol. 2012;12(August).

90. Palucci I, Delogu G. tuberculous granuloma an unsuccessful host defence mechanism providing a safety shelter for the bacteria.pdfculosis : Futures Strateg. 2018;172–80.

91. Kak V. Mediators of Systemic Inflammatory Response Syndrome and the Role of Recombinant Activated Protein C in Sepsis Syndrome. Infect Dis Clin North Am. 2011;25(4):835–50. Available from: http://dx.doi.org/10.1016/j.idc.2011.07.009

92. Kaufmann SHE, Dorhoi A, Hotchkiss RS, Bartenschlager R. Host-directed therapies for bacterial and viral infections. Nat Publ Gr. 2017;17(1):35–56. Available from: http://dx.doi.org/10.1038/nrd.2017.162

93. Delogu G, Goletti D, Delogu G, Goletti D. The Spectrum of Tuberculosis Infection :

New Perspectives in the Era of Biologics. 2014;91.

94. Garra AO, Redford PS, Mcnab FW, Bloom CI, Wilkinson RJ, Berry MPR. The Immune Response in Tuberculosis. 2013.

95. Neill JO'. Antimicrobial Resistance: Tackling a crisis for the health and wealth of nations The Review on Antimicrobial Resistance Chaired. 2014;(December).

96. Pulingam T, Parumasivam T, Gazzali AM, Sulaiman AM, Chee JY, Lakshmanan M, et al. Antimicrobial resistance: Prevalence, economic burden, mechanisms of resistance and strategies to overcome. Eur J Pharm Sci. 2022;170:106103. Available from: https://doi.org/10.1016/j.ejps.2021.106103

97. Tukulula M, Hayeshi R, Fonteh P, Meyer D, Ndamase A, Madziva MT, et al. Curdlan-Conjugated PLGA Nanoparticles Possess Macrophage Stimulant Activity and Drug Delivery Capabilities. 2015;2713–26.

98. Nahar A, Baker AL, Nichols DS, Bowman JP, Britz ML. Application of thin-layer chromatography-flame ionization detection (TLC-FID) to total lipid quantitation in mycolic-acid synthesizing Rhodococcus and Williamsia species. Int J Mol Sci. 2020;21(5).

99. Xiong L Bin, Liu HH, Zhao M, Liu YJ, Song L, Xie ZY, et al. Enhancing the bioconversion of phytosterols to steroidal intermediates by the deficiency of kasB in the cell wall synthesis of Mycobacterium neoaurum. Microb Cell Fact. 2020;19(1):1–11. Available from: https://doi.org/10.1186/s12934-020-01335-y

100. Groenewald W, Bulacu M, Croft A, Marrink S jan. Molecular Dynamics of Mycolic Acid Monolayers Molecular Dynamics of Mycolic Acid Monolayers. 2019;(2).

101. Ehtesham NZ, Grover S. Mycobacterium tuberculosis : Molecular Infection Biology , Pathogenesis , Diagnostics and New Interventions.

102. Brennan PJ, Nikaido H. The Envelope of Mycobacteria. Annu Rev Biochem. 1995 Jun;64(1):29–63.

103. Takayama K, Wang C, Besra GS. Pathway to Synthesis and Processing of Mycolic Acids in. Society. 2005;18(1):81–101. Available from: http://www.pubmedcentral.nih.gov/articlerender.fcgi?artid=544180&tool=pmcentrez&rendertype=abstract

104. Zhao J, Siddiqui S, Shang S, Bian Y, Bagchi S, He Y, et al. Mycolic acid-specific T cells protect against Mycobacterium tuberculosis infection in a humanized transgenic mouse model. Elife. 2015;4(DECEMBER2015):1–18.

105. Lemmer Y, Kalombo L, Pietersen RD, Jones AT, Semete-Makokotlela B, Van Wyngaardt S, et al. Mycolic acids, a promising mycobacterial ligand for targeting of nanoencapsulated drugs in tuberculosis. J Control Release. 2015;211:94–104.

106. Zhu Y, Delbianco M, Seeberger PH. Automated Assembly of Starch and Glycogen Polysaccharides. J Am Chem Soc. 2021;143(26):9758–68.

107. Ng JY, Obuobi S, Chua ML, Zhang C, Hong S, Kumar Y, et al. Biomimicry of microbial polysaccharide hydrogels for tissue engineering and regenerative medicine – A review. Carbohydr Polym. 2020;241(February):116345. Available from: https://doi.org/10.1016/j.carbpol.2020.116345

108. Waterschoot J, Gomand S V., Fierens E, Delcour JA. Starch blends and their physicochemical properties. Starch/Staerke. 2015;67(1–2):1–13.

109. Gatto F, Troncoso OP, Brunetti V, Malvindi MA, Pompa PP, Torres FG, et al. Human monocyte response to Andean-native starch nanoparticles. Starch/Staerke. 2016;68(9–10):1016–23.

110. Marques AP, Reis RL, Hunt JA. The biocompatibility of novel starch-based polymers and composites: In vitro studies. Biomaterials. 2002;23(6):1471–8.

111. Marques AP, Reis RL, Hunt JA. An in vivo study of the host response to starch-based polymers and composites subcutaneously implanted in rats. Macromol Biosci. 2005;5(8):775–85.

112. Li H, Wang D, Liu C, Zhu J, Fan M, Sun X, et al. Fabrication of stable zein nanoparticles coated with soluble soybean polysaccharide for encapsulation of quercetin. Food Hydrocoll. 2019;87(August 2018):342–51. Available from: https://doi.org/10.1016/j.foodhyd.2018.08.002

113. Wang N, Zhang X, Wang S, Guo Q, Li Z, Liu H, et al. Structural characterisation and immunomodulatory activity of polysaccharides from white asparagus skin. Carbohydr Polym. 2020;227(August 2019):115314. Available from: https://doi.org/10.1016/j.carbpol.2019.115314

114. Barbosa JR, Maurício MM, Oliveira LC, Luiza LH, Almada-Vilhena AO, Oliveira RM, et al. Obtaining extracts rich in antioxidant polysaccharides from the edible mushroom Pleurotus ostreatus using binary system with hot water and supercritical CO2. Food Chem. 2020;330:127173. Available from: https://doi.org/10.1016/j.foodchem.2020.127173

115. Bezerra I de L, Caillot ARC, Palhares LCGF, Santana-Filho AP, Chavante SF, Sassaki GL. Structural characterization of polysaccharides from Cabernet Franc, Cabernet Sauvignon and Sauvignon Blanc wines: Anti-inflammatory activity in LPS stimulated RAW 264.7 cells. Carbohydr Polym. 2018;186:91–9. Available from: http://dx.doi.org/10.1016/j.carbpol.2017.12.082

116. Marques AP, Reis RL, Hunt JA. Cytokine secretion from mononuclear cells cultured in vitro with starch-based polymers and poly-L-lactide. J Biomed Mater Res - Part A. 2004;71(3):419–29.

117. Xiong Q, Hao H, He L, Jing Y, Xu T, Chen J, et al. Anti-inflammatory and anti-angiogenic activities of a purified polysaccharide from flesh of Cipangopaludina chinensis. Carbohydr Polym. 2017;176(August):152–9.

118. Chan GCF, Chan WK, Sze DMY. The effects of beta-glucan on human immune and cancer cells. J Hematol Oncol. 2009;2:25.

119. Hetland G. L -1 , 3-Glucan reduces growth of Mycobacterium tuberculosis in macrophage cultures. 2002;33:41–5.

120. Tukulula M, Hayeshi R, Fonteh P, Meyer D, Ndamase A, Madziva MT, et al. Curdlan-conjugated PLGA nanoparticles possess macrophage stimulant activity and drug delivery capabilities. Pharm Res. 2015 Aug 1;32(8):2713–26.

121. Upadhyay TK, Fatima N, Sharma D, Saravanakumar V, Sharma R. Preparation and characterization of beta-glucan particles containing a payload of nanoembedded rifabutin for enhanced targeted delivery to macrophages. EXCLI J. 2017;16:210–28.

122. Goodridge HS, Wolf AJ, Underhill DM. B-Glucan Recognition By the Innate Immune System. Immunol Rev. 2009;230(1):38–50.

123. Taylor PR, Tsoni SV, Willment JA, Dennehy KM, Rosas M, Findon H, et al. Dectin-1 is required for β-glucan recognition and control of fungal infection. Nat Immunol.

2007;8(1):31–8.

124. Brown GD, Herre J, Williams DL, Willment JA, Marshall ASJ, Gordon S. Dectin-1 mediates the biological effects of β-glucans. J Exp Med. 2003;197(9):1119–24.

125. Brown GD, Taylor PR, Reid DM, Willment JA, Williams DL, Martinez-Pomares L, et al. Dectin-1 is a major β-glucan receptor on macrophages. J Exp Med. 2002;196(3):407–12.

126. Tukulula M, Gouveia L, Paixao P, Hayeshi R, Naicker B, Dube A. Functionalization of PLGA Nanoparticles with 1,3-β-glucan Enhances the Intracellular Pharmacokinetics of Rifampicin in Macrophages. Pharm Res. 2018;35(6).

127. Zhang R, Edgar KJ. Properties, chemistry, and applications of the bioactive polysaccharide curdlan. Biomacromolecules. 2014;15(4):1079–96.

128. Chaudhari V, Buttar HS, Bagwe-Parab S, Tuli HS, Vora A, Kaur G. Therapeutic and Industrial Applications of Curdlan With Overview on Its Recent Patents. Front Nutr. 2021;8(June).

129. Xu S, Huo J, Lee KG, Kurosaki T, Lam KP. Phospholipase Cγ2 is critical for Dectin-1-mediated Ca2+ flux and cytokine production in dendritic cells. J Biol Chem. 2009;284(11):7038–46. Available from: http://dx.doi.org/10.1074/jbc.M806650200

130. Liu F, Chen J, Wang P, Li H, Zhou Y, Liu H, et al. MicroRNA-27a controls the intracellular survival of Mycobacterium tuberculosis by regulating calcium-associated autophagy. Nat Commun. 2018;9(1). Available from: http://dx.doi.org/10.1038/s41467-018-06836-4

131. Westman J, Grinstein S, Maxson ME. Revisiting the role of calcium in phagosome formation and maturation. J Leukoc Biol. 2019;106(4):837–51.

132. Mansour MK, Tam JM, Khan NS, Seward M, Davids PJ, Puranam S, et al. Dectin-1 activation controls maturation of β-1,3-glucan-containing phagosomes. J Biol Chem. 2013;288(22):16043–54.

133. Soto E, Kim YS, Lee J, Kornfeld H, Ostroff G. Glucan Particle Encapsulated Rifampicin for Targeted Delivery to Macrophages. 2010;681–9.

134. Rauscher H, Roebben G, Mech A, Gibson N, Rauscher H, Gibson N. JRC SCIENCE

FOR POLICY REPORT An overview of concepts and terms used in the European Commission ' s definition of nanomaterial. 2019. 44 p.

135. Roduner E. Size matters: Why nanomaterials are different. Chem Soc Rev. 2006;35(7):583–92.

136. Almessiere MA, Slimani Y, Korkmaz AD, Taskhandi N, Sertkol M, Baykal A, et al. Sonochemical synthesis of Eu3+ substituted CoFe2O4 nanoparticles and their structural, optical and magnetic properties. Ultrason Sonochem. 2019;58(May):104621. Available from: https://doi.org/10.1016/j.ultsonch.2019.104621

137. Halwani AA. Development of Pharmaceutical Nanomedicines: From the Bench to the Market. Pharmaceutics. 2022;14(1):1–21.

138. Batista CAS, Larson RG, Kotov NA. Nonadditivity of nanoparticle interactions. Science (80-). 2015;350(6257).

139. Din F ud, W, Aman A, Ullah I, Qureshi OS, Mustapha O, et al. IJN-146315-effective-use-of-nano-carriers-as-drug-delivery-systems-for-. Int J Nanomedicine. 2017;7291–309.

140. Napier ME, DeSimone JM. Nanoparticle drug delivery platform. Polym Rev. 2007;47(3):321–7.

141. Lu J, Wang Y, Jin M, Yuan Z, Bond P, Guo J. Both silver ions and silver nanoparticles facilitate the horizontal transfer of plasmid-mediated antibiotic resistance genes. Water Res. 2020;169.

142. Li G, Chen X, Yin H, Wang W, Wong PK, An T. Natural sphalerite nanoparticles can accelerate horizontal transfer of plasmid-mediated antibiotic-resistance genes. Environ Int. 2020;136(January):105497. Available from: https://doi.org/10.1016/j.envint.2020.105497

143. Liu G, Zhou Y, Chen L. Intestinal uptake of barley protein-based nanoparticles for β-carotene delivery. Acta Pharm Sin B. 2019;9(1):87–96. Available from: http://dx.doi.org/10.1016/j.apsb.2018.10.002

144. Malgorzata Geszke-Moritz MM. Solid lipid nanoparticles as attractive drug vehicles : Composition , properties and therapeutic strategies. 2016;68:982–94.

145. Anselmo AC, Mitragotri S. Nanoparticles in the clinic: An update post COVID-19 vaccines. Bioeng Transl Med. 2021;6(3):1–20.

146. Devrim B, Kara A, Vural İ, Bozkır A. ST AC. 2016;9045(April).

147. Mandal B, Bhattacharjee H, Mittal N, Sah H, Balabathula P, Thoma LA, et al. Core-shell-type lipid-polymer hybrid nanoparticles as a drug delivery platform. Nanomedicine Nanotechnology, Biol Med. 2013;9(4):474–91. Available from: http://dx.doi.org/10.1016/j.nano.2012.11.010

148. Bobo D, Robinson KJ, Islam J, Thurecht KJ, Corrie SR, Corrie SR. Nanoparticle-Based Medicines : A Review of FDA-Approved Materials and Clinical Trials to Date. Pharm Res. 2016;2373–87. Available from: http://dx.doi.org/10.1007/s11095-016-1958-5

149. Zhang L, Chan JM, Gu FX, Rhee J wha, Wang AZ, Radovic-moreno AF, et al. HHS Public Access. 2015;2(8):1696–702.

150. Anselmo AC, Mitragotri S. Nanoparticles in the clinic : An update. 2019;(August):1–16.

151. Duncan R. Polymer therapeutics: Top 10 selling pharmaceuticals - What next? J Control Release. 2014;190:371–80. Available from: http://dx.doi.org/10.1016/j.jconrel.2014.05.001

152. Drahansky M, Paridah M., Moradbak A, Mohamed A., Owolabi F abdulwahab taiwo, Asniza M, et al. We are IntechOpen , the world ’ s leading publisher of Open Access books Built by scientists , for scientists TOP 1 %. Intech. 2016;i(tourism):13. Available from: https://www.intechopen.com/books/advanced-biometric-technologies/liveness-detection-in-biometrics

153. Sakla M, Breitinger U, Breitinger HG, Mansour S, Tammam SN. Delivery of trans-membrane proteins by liposomes; the effect of liposome size and formulation technique on the efficiency of protein delivery. Int J Pharm. 2021;606(July):120879. Available from: https://doi.org/10.1016/j.ijpharm.2021.120879

154. Sanches BCP, Rocha CA, Bedoya JGM, Da Silva VL, Da Silva PB, Fusco-Almeida AM, et al. Rhamnolipid-based liposomes as promising nano-carriers for enhancing the antibacterial activity of peptides derived from bacterial toxin-antitoxin systems. Int J

Nanomedicine. 2021;16:925–39.

155. Devrim B, Bozkır A. Biomolecular Research & Therapeutics Preparation and Characterization of Protein-loaded Lipid-polymer Hybrid Nanoparticles with Polycaprolactone as Polymeric Core Material. 2014;3(3):3–6.

156. Hadinoto K, Sundaresan A, Cheow WS. Lipid-polymer hybrid nanoparticles as a new generation therapeutic delivery platform: A review. Eur J Pharm Biopharm. 2013;85(3 PART A):427–43.

157. Christian A, Nkanga I, Krause RW, Noundou XS, Walker RB. Preparation and characterization of isoniazid-loaded crude soybean lecithin. Int J Pharm. 2017; Available from: http://dx.doi.org/10.1016/j.ijpharm.2017.04.074

158. Zeng C, Zheng R, Yang X, Du Y, Xing J, Lan W. Improved oral delivery of tilianin through lipid–polymer hybrid nanoparticles to enhance bioavailability. Biochem Biophys Res Commun. 2019;519(2):316–22. Available from: https://doi.org/10.1016/j.bbrc.2019.09.004

159. Rostamkalaei SS, Akbari J, Saeedi M, Morteza-Semnani K, Nokhodchi A. Topical gel of Metformin solid lipid nanoparticles: A hopeful promise as a dermal delivery system. Colloids Surfaces B Biointerfaces. 2019;175(November 2018):150–7. Available from: https://doi.org/10.1016/j.colsurfb.2018.11.072

160. Singh M, Guzman-Aranguez A, Hussain A, Srinivas CS, Kaur IP. Solid lipid nanoparticles for ocular delivery of isoniazid: Evaluation, proof of concept and in vivo safety & kinetics. Nanomedicine. 2019;14(4):465–91.

161. Sandri G, Motta S, Cristina M, Brocca P, Rossi S, Ferrari F, et al. European Journal of Pharmaceutics and Biopharmaceutics Chitosan-coupled solid lipid nanoparticles : Tuning nanostructure and mucoadhesion. 2017;110:13–8.

162. Nooli M, Chella N, Kulhari H, Shastri NR. Solid lipid nanoparticles as vesicles for oral delivery of olmesartan medoxomil : formulation , optimization and in vivo evaluation. 2017;9045.

163. Neves AR, Queiroz JF, Reis S. Brain - targeted delivery of resveratrol using solid lipid nanoparticles functionalized with apolipoprotein E. J Nanobiotechnology. 2016;1–11.

164. Rai R, Alwani S, Badea I. Polymeric nanoparticles in gene therapy: New avenues of

design and optimization for delivery applications. Polymers (Basel). 2019;11(4).

165. Bhattacharjee S. Polymeric Nanoparticles. Princ Nanomedicine. 2019;195–240.

166. Belbekhouche S, Bousserrhine N, Alphonse V, Floch F Le, Mechiche C, Menidjel I, et al. -chi + nanocapsules) in a liquid medium. Acridine orange staining demonstrated the bactericidal effect of chitosan- based capsules. These findings demonstrate that (chitosan/alginate). 2019;1–25.

167. Huo X, Zhang Y, Jin X, Li Y, Zhang L. A novel synthesis of selenium nanoparticles encapsulated PLGA nanospheres with curcumin molecules for the inhibition of amyloid β aggregation in Alzheimer's disease. J Photochem Photobiol B Biol. 2019;190:98–102. Available from: https://doi.org/10.1016/j.jphotobiol.2018.11.008

168. Yalcin TE, Ilbasmis-Tamer S, Takka S. Development and characterization of gemcitabine hydrochloride loaded lipid polymer hybrid nanoparticles (LPHNs) using central composite design. Int J Pharm. 2018;548(1):255–62. Available from: https://doi.org/10.1016/j.ijpharm.2018.06.063

169. Crucho CIC, Barros MT. Polymeric nanoparticles: A study on the preparation variables and characterization methods. Mater Sci Eng C. 2017;80:771–84. Available from: http://dx.doi.org/10.1016/j.msec.2017.06.004

170. Meyer RA, Sunshine JC, Green JJ. Biomimetic particles as therapeutics. Trends Biotechnol. 2015;33(9):514–24. Available from: http://dx.doi.org/10.1016/j.tibtech.2015.07.001

171. Fulgione A, Ianniello F, Papaianni M, Contaldi F, Sgamma T, Giannini C, et al. Biomimetic hydroxyapatite nanocrystals are an active carrier for salmonella bacteriophages. Int J Nanomedicine. 2019;14:2219–32.

172. Hwang J, Jeong Y, Park JM, Lee KH, Hong JW, Choi J. Biomimetics: Forecasting the future of science, engineering, and medicine. Int J Nanomedicine. 2015;10:5701–13.

173. Kennedy E, Fecheyr-Lippens D, Hsiung BK, Niewiarowski PH, Kolodziej M. Aktivisme Desain di Suatu Kampung Indonesia. 2015;31(3). Available from: www.magno-design.com.

174. Balmert SC, Little SR. Biomimetic Delivery with Micro- and Nanoparticles. 2012;3757–78.

175. Mancuso E, Tonda-Turo C, Ceresa C, Pensabene V, Connell SD, Fracchia L, et al. Potential of Manuka Honey as a Natural Polyelectrolyte to Develop Biomimetic Nanostructured Meshes With Antimicrobial Properties. Front Bioeng Biotechnol. 2019;7(December):1–13.

176. Makvandi P, Ali GW, Della Sala F, Abdel-Fattah WI, Borzacchiello A. Hyaluronic acid/corn silk extract based injectable nanocomposite: A biomimetic antibacterial scaffold for bone tissue regeneration. Mater Sci Eng C. 2020;107(June 2019):110195. Available from: https://doi.org/10.1016/j.msec.2019.110195

177. Ma J, Liu F, Sheu WC, Meng Z, Xie Y, Xu H, et al. Copresentation of Tumor Antigens and Costimulatory Molecules via Biomimetic Nanoparticles for Effective Cancer Immunotherapy. Nano Lett. 2020;20(6):4084–94.

178. Zhai Y, Ma Y, Pang B, Zhang J, Li Y, Rui Y, et al. A cascade targeting strategy based on modified bacterial vesicles for enhancing cancer immunotherapy. J Nanobiotechnology. 2021;19(1):1–18. Available from: https://doi.org/10.1186/s12951-021-01193-9

179. Lin H, Yang C, Luo Y, Ge M, Shen H, Zhang X, et al. Biomimetic Nanomedicine-Triggered in Situ Vaccination for Innate and Adaptive Immunity Activations for Bacterial Osteomyelitis Treatment. ACS Nano. 2022;16(4):5943–60.

180. Papa S, Vismara I, Mariani A, Barilani M, Rimondo S, De Paola M, et al. Mesenchymal stem cells encapsulated into biomimetic hydrogel scaffold gradually release CCL2 chemokine in situ preserving cytoarchitecture and promoting functional recovery in spinal cord injury. J Control Release. 2018;278(April):49–56. Available from: https://doi.org/10.1016/j.jconrel.2018.03.034

181. Oltolina F, Peigneux A, Colangelo D, Clemente N, D'urso A, Valente G, et al. Biomimetic magnetite nanoparticles as targeted drug nanocarriers and mediators of hyperthermia in an experimental cancer model. Cancers (Basel). 2020;12(9):1–25.

182. Özgür E, Topçu AA, Yılmaz E, Denizli A. Surface plasmon resonance based biomimetic sensor for urinary tract infections. Talanta. 2020;212(January):120778. Available from: https://doi.org/10.1016/j.talanta.2020.120778

183. Huang B, Almeida H, Bidanda B, Bártolo PJ. Additive Biomanufacturing Processes to

Fabricate Scaffolds for Tissue Engineering. Virtual Prototyp Bio Manuf Med Appl. 2021;95–124.

184. Moga A, Yandrapalli N, Dimova R, Robinson T. Optimization of the Inverted Emulsion Method for High-Yield Production of Biomimetic Giant Unilamellar Vesicles. ChemBioChem. 2019;20(20):2674–82.

185. Wang F, Fang RH, Luk BT, Hu C ming J, Thamphiwatana S, Dehaini D, et al. Nanoparticle-Based Antivirulence Vaccine for the Management of Methicillin-Resistant Staphylococcus aureus Skin Infection. 2016;1628–35.

186. Thamphiwatana S, Angsantikul P, Escajadillo T, Zhang Q, Olson J. Macrophage-like nanoparticles concurrently absorbing endotoxins and proinflammatory cytokines for sepsis management. 2017;114(43).

187. Maghrebi S, Jambhrunkar M, Joyce P, Prestidge CA. Engineering PLGA-Lipid Hybrid Microparticles for Enhanced Macrophage Uptake. ACS Appl Bio Mater. 2020;3(7):4159–67.

188. Abdel-Bar HM, Abdallah IA, Fayed MAA, Moatasim Y, Mostafa A, El-Behairy MF, et al. Lipid polymer hybrid nanocarriers as a combinatory platform for different anti-SARS-CoV-2 drugs supported by computational studies. RSC Adv. 2021;11(46):28876–91.

189. Liu J, Cheng H, Han L, Qiang Z, Zhang X, Gao W, et al. Synergistic combination therapy of lung cancer using paclitaxel- and triptolide-coloaded lipid-polymer hybrid nanoparticles. Drug Des Devel Ther. 2018;12:3199–209.

190. Jiang J, Liu W, Xiong Z, Hu Y, Xiao J. Biomaterials Advances Effects of biomimetic hydroxyapatite coatings on osteoimmunomodulation. Biomater Adv. 2022;134(December 2021):112640. Available from: https://doi.org/10.1016/j.msec.2021.112640

191. Guo P, Buttaro BA, Xue HY, Tran NT, Wong HL. Lipid-polymer hybrid nanoparticles carrying linezolid improve treatment of methicillin-resistant Staphylococcus aureus (MRSA) harbored inside bone cells and biofilms. 2020;

192. Dobreva M, Stefanov S, Andonova V. Natural Lipids as Structural Components of Solid Lipid Nanoparticles and Nanostructured Lipid Carriers for Topical Delivery.

Curr Pharm Des. 2020 May 14;26.

193. Pei Y, Bao Y, Sacchetti C, Brady J, Gillard K, Yu H, et al. Synthesis and bioactivity of readily hydrolysable novel cationic lipids for potential lung delivery application of mRNAs. Chem Phys Lipids. 2022;243(February):105178. Available from: https://doi.org/10.1016/j.chemphyslip.2022.105178

194. Souto EB, Baldim I, Oliveira WP, Rao R, Yadav N, Gama FM, et al. SLN and NLC for topical, dermal, and transdermal drug delivery. Expert Opin Drug Deliv. 2020;17(3):357–77. Available from: https://doi.org/10.1080/17425247.2020.1727883

195. Achouak M, Mazouni N, Nedjhioui M. Plants' Bioactive Metabolites and Extraction Methods. In: Mazouni N, editor. Rijeka: IntechOpen; 2021. p. Ch. 3. Available from: https://doi.org/10.5772/intechopen.96698

196. Anthony A, Mumuni A, Philip F. Lipid Nanoparticulate Drug Delivery Systems: A Revolution in Dosage Form Design and Development. Recent Adv Nov Drug Carr Syst. 2012;

197. Duque L, Körber M, Bodmeier R. Impact of change of matrix crystallinity and polymorphism on ovalbumin release from lipid-based implants. Eur J Pharm Sci. 2018;117(November 2017):128–37. Available from: https://doi.org/10.1016/j.ejps.2018.02.019

198. Severino P, Pinho SC, Souto EB, Santana MHA. Polymorphism, crystallinity and hydrophilic-lipophilic balance of stearic acid and stearic acid-capric/caprylic triglyceride matrices for production of stable nanoparticles. Colloids Surfaces B Biointerfaces. 2011;86(1):125–30.

199. Cholakova D, Glushkova D, Tcholakova S, Denkov N. Nanopore and Nanoparticle Formation with Lipids Undergoing Polymorphic Phase Transitions. ACS Nano. 2020;14(7):8594–604.

200. Gomes da Silva M, Ramponi Rodrigues de Godoi K, Pavie Cardoso L, Paula Badan Ribeiro A. Effect of stabilization and fatty acids chain length on the crystallization behavior of interesterified blends during storage. Food Res Int. 2022;157(December 2021):111208. Available from: https://doi.org/10.1016/j.foodres.2022.111208

201. Bertoni S, Passerini N, Albertini B. Liquid lipids act as polymorphic modifiers of

tristearin-based formulations produced by melting technologies. Pharmaceutics. 2021;13(7).

202. Zielinska A, Nowak I. Solid lipid nanoparticles and nanostructured lipid carriers as novel carriers for cosmetic ingredients. Nanobiomaterials Galen Formul Cosmet Appl Nanobiomaterials. 2016;231–55.

203. Beloqui A, Solinís MÁ, Rodríguez-Gascón A, Almeida AJ, Préat V. Nanostructured lipid carriers: Promising drug delivery systems for future clinics. Nanomedicine Nanotechnology, Biol Med. 2016;12(1):143–61. Available from: http://dx.doi.org/10.1016/j.nano.2015.09.004

204. Jun SH, Kim H, Lee H, Song JE, Park SG, Kang NG. Synthesis of retinol-loaded lipid nanocarrier via vacuum emulsification to improve topical skin delivery. Polymers (Basel). 2021;13(5).

205. Ezequiel P, Yamila G, Adriana M, Gonz L, Turyn D, Bregni C. In Vitro Evaluation of Lecithin-Based Nanoparticles for siRNA Delivery. 2012;2012.

206. Li J, Wang X, Zhang T, Wang C, Huang Z. ScienceDirect A review on phospholipids and their main applications in drug delivery systems. 2015;0(103).

207. Haider A, Wei Y chen, Lim K, Hardie RC, Siniossoglou S, Savage DB, et al. PCYT1A Regulates Phosphatidylcholine Homeostasis from the Inner Nuclear Membrane in Response to Membrane Stored Curvature Elastic Article PCYT1A Regulates Phosphatidylcholine Homeostasis from the Inner Nuclear Membrane in Response to Membrane Stored Curva. 2018;481–95.

208. Norris GH, Milard M, Michalski MC, Blesso CN. Protective properties of milk sphingomyelin against dysfunctional lipid metabolism, gut dysbiosis, and inflammation. J Nutr Biochem. 2019;73:108224. Available from: https://doi.org/10.1016/j.jnutbio.2019.108224

209. Casares D, Escribá P V., Rosselló CA. Membrane lipid composition: Effect on membrane and organelle structure, function and compartmentalization and therapeutic avenues. Int J Mol Sci. 2019;20(9).

210. Alhajj MJ, Montero N, Yarce CJ, Salamanca CH. Lecithins from vegetable, land, and marine animal sources and their potential applications for cosmetic, food, and

pharmaceutical sectors. Cosmetics. 2020;7(4):1–19.

211. Nara E, Miyashita K, Ota T. Oxidative stability of liposomes prepared from soybean PC, chicken egg PC, and salmon egg PC. Biosci Biotechnol Biochem. 1997;61(10):1736–8.

212. Sharma P, Sharma N, Kaur S, Singh P. Synthesis, self-assembly and biolabeling of perylene diimide-tyrosine alkyl amide based amphiphiles: nanomolar detection of AOT surfactant. New J Chem. 2022 Jun 22;46(19):9280–9. Available from: https://app.dimensions.ai/details/publication/pub.1146969754

213. Baccile N, Seyrig C, Poirier A, Alonso-De Castro S, Roelants SLKW, Abel S. Self-assembly, interfacial properties, interactions with macromolecules and molecular modelling and simulation of microbial bio-based amphiphiles (biosurfactants). A tutorial review. Green Chem. 2021;23(11):3842–944.

214. Yanasarn N, Sloat RB, Cui Z. Potential Delivery System for Docetaxel. 2010;379(1):174–80.

215. Behl A, Parmar VS, Malhotra S, Chhillar AK. Biodegradable diblock copolymeric PEG-PCL nanoparticles: Synthesis, characterization and applications as anticancer drug delivery agents. Polymer (Guildf). 2020;207(August):122901. Available from: https://doi.org/10.1016/j.polymer.2020.122901

216. Acik G. Bio-based Poly(ε-caprolactone) from Soybean-Oil Derived Polyol via Ring-Opening Polymerization. J Polym Environ. 2020;28(2):668–75. Available from: https://doi.org/10.1007/s10924-019-01597-7

217. Bartnikowski M, Dargaville TR, Ivanovski S, Hutmacher DW. Degradation mechanisms of polycaprolactone in the context of chemistry, geometry and environment. Prog Polym Sci. 2019;96:1–20.

218. Hajiali F, Tajbakhsh S, Shojaei A. Fabrication and Properties of Polycaprolactone Composites Containing Calcium Phosphate-Based Ceramics and Bioactive Glasses in Bone Tissue Engineering: A Review. Polym Rev. 2018;58(1):164–207. Available from: https://doi.org/10.1080/15583724.2017.1332640

219. Mondal D, Griffith M, Venkatraman SS. Polycaprolactone-based biomaterials for tissue engineering and drug delivery: Current scenario and challenges. Int J Polym

Mater Polym Biomater. 2016;65(5):255–65. Available from: http://dx.doi.org/10.1080/00914037.2015.1103241

220. Sánchez-González S, Diban N, Urtiaga A. Hydrolytic degradation and mechanical stability of poly(ε-Caprolactone)/reduced graphene oxide membranes as scaffolds for in vitro neural tissue regeneration. Membranes (Basel). 2018;8(1).

221. Woodruff MA, Hutmacher DW. The return of a forgotten polymer - Polycaprolactone in the 21st century. Prog Polym Sci. 2010;35(10):1217–56.

222. Dwivedi R, Kumar S, Pandey R, Mahajan A, Nandana D, Katti DS, et al. Polycaprolactone as biomaterial for bone scaffolds: Review of literature. J Oral Biol Craniofacial Res. 2020;10(1):381–8.

223. Mukherjee A, Waters AK, Kalyan P, Achrol AS, Kesari S, Yenugonda VM. Lipid-polymer hybrid nanoparticles as a nextgeneration drug delivery platform: State of the art, emerging technologies, and perspectives. Int J Nanomedicine. 2019;14:1937–52.

224. Hitzman CJ, Elmquist WF, Wattenberg LEEW, Wiedmann TS. Development of a Respirable , Sustained Release Microcarrier for 5-Fluorouracil I : In Vitro Assessment of Liposomes , Microspheres , and Lipid Coated Nanoparticles. 2006;95(5):1114–26.

225. Hasan W, Chu K, Gullapalli A, Dunn SS, Elizabeth M, Enlow Φ, et al. Nanoparticles for Treatment of Prostate Cancer. Nano Lett. 2012;12(1):287–92.

226. Wang Y, Kho K, Cheow WS, Hadinoto K. A comparison between spray drying and spray freeze drying for dry powder inhaler formulation of drug-loaded lipid-polymer hybrid nanoparticles. Int J Pharm. 2012;424(1–2):98–106. Available from: http://dx.doi.org/10.1016/j.ijpharm.2011.12.045

227. Shah S, Famta P, Raghuvanshi RS, Singh SB, Srivastava S. Lipid polymer hybrid nanocarriers: Insights into synthesis aspects, characterization, release mechanisms, surface functionalization and potential implications. Colloids Interface Sci Commun. 2022;46:100570. Available from: https://doi.org/10.1016/j.colcom.2021.100570

228. Sengel-turk CT, Gumustas M, Uslu B, Ozkan SA. Chapter 3. A novel approach for drug targeting: Core-shell type lipid-polymer hybrid nanocarriers. Design of Nanostructures for Theranostics Applications. Elsevier Inc.; 2018. 69–108 p. Available from: http://dx.doi.org/10.1016/B978-0-12-813669-0.00003-8

229. Li X, Anton N, Arpagaus C, Belleteix F, Vandamme TF. Nanoparticles by spray drying using innovative new technology: The Büchi Nano Spray Dryer B-90. J Control Release. 2010;147(2):304–10. Available from: http://dx.doi.org/10.1016/j.jconrel.2010.07.113

230. Abdul-Karim R, Hameed A, Malik MI. Ring-opening polymerization of propylene carbonate: Microstructural analysis of the polymer and selectivity of polymerization by 2D-NMR techniques. Eur Polym J. 2018;105(May):95–106. Available from: https://doi.org/10.1016/j.eurpolymj.2018.05.028

231. Kaur A, Bhardwaj N, Kaur A, Nagaraja TP, Ali A, Prakash R. Proton NMR based method for the quantification of epoxidized methyl oleate. 2020;1–10.

232. Thomas LC, Schmidt SJ. Thermal Analysis BT - Food Analysis. In: Nielsen SS, editor. Cham: Springer International Publishing; 2017. p. 529–44. Available from: https://doi.org/10.1007/978-3-319-45776-5_30

233. Kumar A, Singh P, Nanda A. Hot stage microscopy and its applications in pharmaceutical characterization. Vol. 50, Applied Microscopy. 2020.

234. Stetefeld J, McKenna SA, Patel TR. Dynamic light scattering: a practical guide and applications in biomedical sciences. Biophys Rev. 2016;8(4):409–27. Available from: http://dx.doi.org/10.1007/s12551-016-0218-6

235. Falke S, Betzel C. Dynamic Light Scattering (DLS). Springer International Publishing; 2019. 173–193 p. Available from: http://dx.doi.org/10.1007/978-3-030-28247-9_6

236. Valiño V, San Román MF, Ibáñez R, Benito JM, Escudero I, Ortiz I. Accurate determination of key surface properties that determine the efficient separation of bovine milk BSA and LF proteins. Sep Purif Technol. 2014;135:145–57. Available from: http://dx.doi.org/10.1016/j.seppur.2014.07.051

237. Berg JM, Romoser A, Banerjee N, Zebda R, Sayes CM. The relationship between pH and zeta potential of ~ 30 nm metal oxide nanoparticle suspensions relevant to in vitro toxicological evaluations. Nanotoxicology. 2009;3(4):276–83.

238. Tantra R, Schulze P, Quincey P. Effect of nanoparticle concentration on zeta-potential measurement results and reproducibility. Particuology. 2010;8(3):279–85. Available from: http://dx.doi.org/10.1016/j.partic.2010.01.003

239. Méndez-Vilas A. Current microscopy contributions to advances in science and technology. 2012;2(July):6002.

240. Renz P, Kokkinopoulou M, Landfester K, Lieberwirth I. Imaging of Polymeric Nanoparticles: Hard Challenge for Soft Objects. Macromol Chem Phys. 2016;217(17):1879–85.

241. Pal SL, Jana U, Manna PK, Mohanta GP, Manavalan R. Nanoparticle: An overview of preparation and characterization. J Appl Pharm Sci. 2011;1(6):228–34.

242. Sun X, Shi J, Fu X, Yang Y, Zhang H. Long-Term in vivo biodistribution and toxicity study of functionalized near-infrared persistent luminescence nanoparticles. Sci Rep. 2018;8(1):1–11.

243. Guerreiro JCM, Ochoa-Rodrígez VM, Rodrigues EM, Chavez-Andrade GM, Tanomaru-Filho M, Guerreiro-Tanomaru JM, et al. Antibacterial activity, cytocompatibility and effect of Bio-C Temp bioceramic intracanal medicament on osteoblast biology. Int Endod J. 2021;54(7):1155–65.

244. Vernazza S, Tirendi S, Scarfi S, Passalacqua M, Oddone F, Traverso CE, et al. 2D-A nd 3D-cultures of human trabecular meshwork cells: A preliminary assessment of an in vitro model for glaucoma study. PLoS One. 2019;14(9):1–16.

245. Pintor AVB, Queiroz LD, Barcelos R, Primo LSG, Maia LC, Alves GG. MTT versus other cell viability assays to evaluate the biocompatibility of root canal filling materials: a systematic review. Int Endod J. 2020;53(10):1348–73.

246. Benov L. Improved Formazan Dissolution for Bacterial MTT Assay. Microbiol Spectr. 2021;9(3):1–9.

247. Zhang Y, Ma P, Wang Y, Du J, Zhou Q, Zhu Z, et al. Biocompatibility of Porous Spherical Calcium Carbonate Microparticles on Hela Cells. World J Nano Sci Eng. 2012;02(01):25–31.

248. Gomez Perez M, Fourcade L, Mateescu MA, Paquin J. Neutral Red versus MTT assay of cell viability in the presence of copper compounds. Anal Biochem. 2017;535:43–6. Available from: http://dx.doi.org/10.1016/j.ab.2017.07.027

249. Wang P, Henning SM, Heber D. Limitations of MTT and MTS-based assays for measurement of antiproliferative activity of green tea polyphenols. PLoS One.

2010;5(4).

250. Jaszcyszyn A, Gasiorowski K. Limitations of the MTT Assay in Cell Viability Testing Ograniczenia testu MTT w ocenie żywotności komórek. Adv Clin Exp Med. 2008;17(5):525–9.

251. Peng L, Wang B, Ren P. Reduction of MTT by flavonoids in the absence of cells. Colloids Surfaces B Biointerfaces. 2005;45(2):108–11.

252. Weyermann J, Lochmann D, Zimmer A. A practical note on the use of cytotoxicity assays. Int J Pharm. 2005;288(2):369–76.

253. García-Martínez E, Smith M, Buqué A, Aranda F, Peña FA de la, Ivars A, et al. Trial Watch: Immunostimulation with recombinant cytokines for cancer therapy. Oncoimmunology. 2018;7(6):1–16. Available from: https://doi.org/10.1080/2162402X.2018.1433982

254. Agache I, Akdis CA. Precision medicine and phenotypes, endotypes, genotypes, regiotypes, and theratypes of allergic diseases. J Clin Invest. 2019;129(4):1493–503.

255. Breiteneder H, Diamant Z, Eiwegger T, Fokkens WJ, Traidl-Hoffmann C, Nadeau K, et al. Future research trends in understanding the mechanisms underlying allergic diseases for improved patient care. Allergy Eur J Allergy Clin Immunol. 2019;74(12):2293–311.

256. Josephs SF, Ichim TE, Prince SM, Kesari S, Marincola FM, Escobedo AR, et al. Unleashing endogenous TNF-alpha as a cancer immunotherapeutic. J Transl Med. 2018;16(1):1–8. Available from: https://doi.org/10.1186/s12967-018-1611-7

257. Ribeiro CM, Oliveira SR, Alfieri DF, Flauzino T, Kaimen-Maciel DR, Simão ANC, et al. Tumor necrosis factor alpha (TNF-α) and its soluble receptors are associated with disability, disability progression and clinical forms of multiple sclerosis. Inflamm Res. 2019;68(12):1049–59. Available from: https://doi.org/10.1007/s00011-019-01286-0

258. Jacobs M, Togbe D, Fremond C, Samarina A, Allie N, Botha T, et al. Tumor necrosis factor is critical to control tuberculosis infection. Microbes Infect. 2007;9(5):623–8.

259. Yasui K. Immunity against mycobacterium tuberculosis and risk of biological anti-rheumatic agents. Japanese J Clin Immunol. 2015;37(5):423–9.

260. Ouyang W, O'Garra A. IL-10 Family Cytokines IL-10 and IL-22: from Basic Science to Clinical Translation. Immunity. 2019;50(4):871–91. Available from: https://doi.org/10.1016/j.immuni.2019.03.020

261. Sabat R. IL-10 family of cytokines. Cytokine Growth Factor Rev. 2010;21(5):315–24. Available from: http://dx.doi.org/10.1016/j.cytogfr.2010.11.001

262. Akdis CA, Akdis M. Mechanisms of allergen-specific immunotherapy and immune tolerance to allergens. World Allergy Organ J. 2015;8(1):1–12. Available from: ???

263. O'Leary S, O'Sullivan MP, Keane J. IL-10 blocks phagosome maturation in Mycobacterium tuberculosis-infected human macrophages. Am J Respir Cell Mol Biol. 2011;45(1):172–80.

264. Thibodeau J, Bourgeois-Daigneault MC, Huppé G, Tremblay J, Aumont A, Houde M, et al. Interleukin-10-induced MARCH1 mediates intracellular sequestration of MHC class II in monocytes. Eur J Immunol. 2008;38(5):1225–30.

265. Richardson ET, Shukla S, Sweet DR, Wearsch PA, Tsichlis PN, Henry Boom W, et al. Toll-like receptor 2-dependent extracellular signal-regulated kinase signaling in Mycobacterium tuberculosis-infected macrophages drives anti-inflammatory responses and inhibits Th1 polarization of responding T cells. Infect Immun. 2015;83(6):2242–54.

266. McNab FW, Ewbank J, Howes A, Moreira-Teixeira L, Martirosyan A, Ghilardi N, et al. Type I IFN Induces IL-10 Production in an IL-27–Independent Manner and Blocks Responsiveness to IFN-γ for Production of IL-12 and Bacterial Killing in Mycobacterium tuberculosis –Infected Macrophages . J Immunol. 2014;193(7):3600–12.

267. Giacomini E, Iona E, Ferroni L, Miettinen M, Fattorini L, Orefici G, et al. Infection of Human Macrophages and Dendritic Cells with Mycobacterium tuberculosis Induces a Differential Cytokine Gene Expression That Modulates T Cell Response . J Immunol. 2001;166(12):7033–41.

268. Huynh JP, Lin CC, Kimmey JM, Jarjour NN, Schwarzkopf EA, Bradstreet TR, et al. Bhlhe40 is an essential repressor of IL-10 during Mycobacterium tuberculosis infection. J Exp Med. 2018;215(7):1823–38.

269. Verbon A, Juffermans N, Van Deventer SJH, Speelman P, Van Deutekom H, Van Der Poll T. Serum concentrations of cytokines in patients with active tuberculosis (TB) and after treatment. Clin Exp Immunol. 1999;115(1):110–3.

270. Liu J, Liu X. Nanoparticles Prepared by Blending of Carboxylic Acid Terminated Poly (e -caprolactone) and L -Phenylalanine Substituted Dextran. 2010;

271. Zhang Y, Zhao Q, Shao H, Zhang S, Han X. Synthesis and characterization of star-shaped block copolymer sPCL-b-PEG-GA. Adv Mater Sci Eng. 2014;2014.

272. Maafi EM, Malek F, Tighzert L, Laoutid F, Dubois P. Synthesis and thermal properties of new copolyesters based on polycaprolactone. E-Polymers. 2012;(027):1–13.

273. Bharti SK, Roy R. Quantitative 1H NMR spectroscopy. TrAC - Trends Anal Chem. 2012;35:5–26. Available from: http://dx.doi.org/10.1016/j.trac.2012.02.007

274. Hrkach JS, Peracchia MT, Domb A, Lotan N, Langer R. Nanotechnology for biomaterials engineering: Structural characterization of amphiphilic polymeric nanoparticles by 1H NMR spectroscopy. Biomaterials. 1997;18(1):27–30.

275. Báez JE, Martínez-Richa A, Marcos-Fernández A. One-step route to α-hydroxyl-ω-(carboxylic acid) polylactones using catalysis by decamolybdate anion. Macromolecules. 2005;38(5):1599–608.

276. Wang T, Rong F, Tang Y, Li M, Feng T, Zhou Q, et al. Targeted polymer-based antibiotic delivery system: A promising option for treating bacterial infections via macromolecular approaches. Prog Polym Sci. 2021;116:101389. Available from: https://doi.org/10.1016/j.progpolymsci.2021.101389

277. Zeng Q. End-capping Star-like Polycaprolactone with Different Functional Groups and the Interaction with Smooth Muscle Cells. 2017;

278. Khayet M, Nasef MM, Mengual JI. Radiation grafted poly(ethylene terephthalate)-graft-polystyrene pervaporation membranes for organic/organic separation. Vol. 263, Journal of Membrane Science. 2005. p. 77–95.

279. Shi L. Characterization of the flame retardancy of EVA copolymer by plasma grafting of acrylic acid. Eur Polym J. 2000;36(12):2611–5.

280. Chan JM, Zhang L, Yuet KP, Liao G, Rhee J wha, Langer R, et al. Biomaterials PLGA

– lecithin – PEG core – shell nanoparticles for controlled drug delivery. Biomaterials. 2009;30(8):1627–34. Available from: http://dx.doi.org/10.1016/j.biomaterials.2008.12.013

281. Gong C, Li J, Yi C, Qu S. Catalytic Regulation of Oligomers in Polycaprolactone. Mol Catal. 2021;508(May):111594. Available from: https://doi.org/10.1016/j.mcat.2021.111594

282. Kumar A, Dixit CK. Methods for characterization of nanoparticles. Adv Nanomedicine Deliv Ther Nucleic Acids. 2017;44–58.

283. Murthy A, Ravi PR, Kathuria H, Vats R. Self-assembled lecithin-chitosan nanoparticles improve the oral bioavailability and alter the pharmacokinetics of raloxifene. Int J Pharm. 2020;588(August):119731. Available from: https://doi.org/10.1016/j.ijpharm.2020.119731

284. Dong W, Ye J, Wang W, Yang Y, Wang H, Sun T, et al. Self-assembled lecithin/chitosan nanoparticles based on phospholipid complex: A feasible strategy to improve entrapment efficiency and transdermal delivery of poorly lipophilic drug. Int J Nanomedicine. 2020;15:5629–43.

285. Ajiboye AL, Trivedi V, Mitchell JC. Preparation of polycaprolactone nanoparticles via supercritical carbon dioxide extraction of emulsions. Drug Deliv Transl Res. 2018;8(6):1790–6.

286. Jardim KV, Siqueira JLN, Báo SN, Sousa MH, Parize AL. The role of the lecithin addition in the properties and cytotoxic activity of chitosan and chondroitin sulfate nanoparticles containing curcumin. Carbohydr Polym. 2020;227(February 2019):115351. Available from: https://doi.org/10.1016/j.carbpol.2019.115351

287. Tavares MR, Menezes LR de, Dutra Filho JC, Cabral LM, Tavares MIB. Surface-coated polycaprolactone nanoparticles with pharmaceutical application: Structural and molecular mobility evaluation by TD-NMR. Polym Test. 2017;60:39–48.

288. Shao XR, Wei XQ, Song X, Hao LY, Cai XX, Zhang ZR, et al. Independent effect of polymeric nanoparticle zeta potential/surface charge, on their cytotoxicity and affinity to cells. Cell Prolif. 2015;48(4):465–74.

289. D'Souza S, Du Plessis SM, Egieyeh S, Bekale RB, Maphasa RE, Irabin AF, et al.

Physicochemical and Biological Evaluation of Curdlan-Poly(Lactic-Co-Glycolic Acid) Nanoparticles as a Host-Directed Therapy Against Mycobacterium Tuberculosis. J Pharm Sci. 2022;111(2):469–78. Available from: https://doi.org/10.1016/j.xphs.2021.09.012

290. Tukulula M, Hayeshi R, Fonteh P, Meyer D, Ndamase A, Madziva MT, et al. Curdlan-conjugated PLGA nanoparticles possess macrophage stimulant activity and drug delivery capabilities. Pharm Res. 2015;32(8):2713–26.

291. Zaitoun B, Palmer N, Amamcharla J. Characterization of a Commercial Whey Protein Hydrolysate and Its Use as a Binding Agent in the Whey Protein Isolate Agglomeration Process. Kansas Agric Exp Stn Res Reports. 2020;7(3).

292. Das SS, Bharadwaj P, Bilal M, Barani M, Rahdar A, Taboada P, et al. Stimuli-responsive polymeric nanocarriers for drug delivery, imaging, and theragnosis. Polymers (Basel). 2020;12(6).

293. Ribeiro APC, Anbu S, Alegria ECBA, Fernandes AR, Baptista P V., Mendes R, et al. Evaluation of cell toxicity and DNA and protein binding of green synthesized silver nanoparticles. Biomed Pharmacother. 2018;101(February):137–44. Available from: https://doi.org/10.1016/j.biopha.2018.02.069

294. Li X, Yang X, Deng H, Guo Y, Xue J. Gelatin films incorporated with thymol nanoemulsions: Physical properties and antimicrobial activities. Int J Biol Macromol. 2020;150:161–8. Available from: https://doi.org/10.1016/j.ijbiomac.2020.02.066

295. Devrim B, Kara A, Vural İ, Bozkır A. Lysozyme-loaded lipid-polymer hybrid nanoparticles: preparation, characterization and colloidal stability evaluation. Drug Dev Ind Pharm. 2016;42(11):1865–76.

296. Grabowski N, Hillaireau H, Vergnaud J, Tsapis N, Pallardy M, Kerdine-Römer S, et al. Surface coating mediates the toxicity of polymeric nanoparticles towards human-like macrophages. Int J Pharm. 2015;482(1–2):75–83. Available from: http://dx.doi.org/10.1016/j.ijpharm.2014.11.042

297. Iwasawa A, Ayaki M, Niwano Y. Cell viability score (CVS) as a good indicator of critical concentration of benzalkonium chloride for toxicity in cultured ocular surface cell lines. Regul Toxicol Pharmacol. 2013;66(2):177–83. Available from:

http://dx.doi.org/10.1016/j.yrtph.2013.03.014

298. Souza SD, Plessis SM Du, Egieyeh S, Bekale RB, Maphasa RE, Irabin AF, et al. Physicochemical and biological evaluation of curdlan-poly(lactic-co-glycolic acid) nanoparticles as a host-directed therapy against Mycobacterium tuberculosis. J Pharm Sci. 2021; Available from: https://doi.org/10.1016/j.xphs.2021.09.012

299. Sanin DE, Prendergast CT, Mountford AP. IL-10 Production in Macrophages Is Regulated by a TLR-Driven CREB-Mediated Mechanism That Is Linked to Genes Involved in Cell Metabolism. J Immunol. 2015;195(3):1218–32.

300. Quesniaux VFJ, Jacobs M, Allie N, Grivennikov S, Nedospasov SA, Garcia I, et al. TNF in host resistance to tuberculosis infection. Curr Dir Autoimmun. 2010;11:157–79.